Power System Mode Estimation

Using Associate Hermite Expansion

by

Barrie Lee Kokanos

A Dissertation Presented in Partial Fulfillment
of the Requirements for the Degree
Doctor of Philosophy

ARIZONA STATE UNIVERSITY

December 2010

Power System Mode Estimation

Using Associate Hermite Expansion

by

Barrie Lee Kokanos

has been approved

October 2010

Graduate Supervisory Committee:

George Karady, Chair
Richard Farmer
Raja Ayyanar
Gerald Heydt
Lina Karam

ACCEPTED BY THE GRADUATE COLLEGE

ABSTRACT

Many methods have been proposed to estimate power system small signal stability, for either analysis or control, through identification of modal frequencies and their damping levels. Generally, estimation methods have been employed to assess small signal stability from collected field measurements. However, the challenge to using these methods in assessing field measurements is their ability to accurately estimate stability in the presence of noise.

In this thesis a new method is developed which estimates the modal content of simulated and actual field measurements using orthogonal polynomials and the results are compared to other commonly used estimators. This new method estimates oscillatory performance by fitting an associate Hermite polynomial to time domain data and extrapolating its spectrum to identify small signal power system frequencies. Once the frequencies are identified, damping assessment is performed using a modified sliding window technique with the use of linear prediction (LP). Once the entire assessment is complete the measurements can be judged to be stable or unstable. Collectively, this new technique is known as the associate Hermite expansion (AHE) algorithm.

Validation of the AHE method versus results from four other spectral estimators demonstrates the method's accuracy and modal estimation ability with and without the presence of noise. A Prony analysis, a Yule-Walker autoregressive algorithm, a second sliding window estimator and the Hilbert-Huang Transform method are used in comparative assessments in support of this

thesis. Results from simulated and actual field measurements are used in the comparisons, as well as artificially generated simple signals. A search for actual field testing results performed by a utility was undertaken and a request was made to obtain the measurements of a brake insertion test. Comparison results show that the AHE method is accurate as compared to the other commonly used spectral estimators and its predictive capability exceeded the other estimators in the presence of Gaussian noise. As a result, the AHE method could be employed in areas including operations and planning analysis, post-mortem analysis, power system damping scheme design and other analysis areas.

ACKNOWLEDGMENTS

I would like to thank Dr. George Karady for my thesis and post-graduate work. He challenged and guided me while remaining patient and providing encouragement throughout my time in the engineering college. I will remember always his enthusiasm and ingenuity. I also would like to thank my supervisory committee, Dr. Raja Ayyanar, Dr. Lina Karam, Prof. Richard Farmer and Dr. Gerald Heydt, for their patience and support throughout my time at the university and within the program. Assistance from Mr. Donald Davies, Mr. Branden Sudduth and Mr. Kent Bolton from the Western Electricity Coordinating Council (WECC) was invaluable in my thesis work. I would like to also thank Mr. Brian Moore for his assistance. I want to thank Mr. Scott Waples for his leadership and friendship throughout the years. Finally, I must thank Mr. Bill Mittelstadt, Mr. Jim Burns and Dr. Lei Wang for their suggestions, perspective and advice regarding studying small signal stability phenomenon.

TABLE OF CONTENTS

Page

LIST OF TABLES

Table Page

LIST OF FIGURES

Figure Page

Figure Page

Figure Page

NOMENCLATURE

ACS	autocorrelation sequence
AESOPS	Analysis of Essentially Spontaneous Oscillations in Power Systems
$\underline{a_f}$	linear predictor model parameters
AHE	associate Hermite expansion
AR	autoregression
ARMA	autoregression moving average
ANN	artificial neural network
ARYW	autoregression Yule-Walker
d	shift index
EMD	empirical mode decomposition
EPRI	Electric Power Research Institute
ESPRIT	Estimation of Signal Parameters by Rotational Invariance Techniques
FFT	fast Fourier transform
FIR	finite impulse response
f_i	ith estimated frequency
f_j	jth estimated frequency from eigenvalue analysis
f_{id}	ith estimated downshifted frequency
f_{iu}	ith estimated upshifted frequency
f_w	frequency window or bandwidth

GUI	graphical user interface
HHT	Hilbert-Huang Transform
$H_m(t)$	mth order Hermite polynomial
$h_m(f,\mu)$	mth order frequency domain associate Hermite polynomial
$h_m(t,\lambda)$	mth order time domain associate Hermite polynomial
$\underline{h}_f$	frequency domain associate Hermite matrix
$\underline{h}_t$	time domain associate Hermite matrix
IMF	intrinsic mode function
l	linear predictor order
LP	linear prediction
LMS	least mean square
M	initial AHE polynomial order
MANSTAB	Machine and Network Stability Program
MAM	modified Arnodi method
MASS	Multi-Area Small Signal Stability Program
MLP	multi-layer perceptron
MP	Matrix Pencil
N	number of time samples
n_d	sliding window shift length
P	number of frequency samples
PEALS	Program for Eigenvalue Analysis of Large Systems
PMU	phasor measurement unit

POSSIM	Power System Simulator
P_{ref}	reference load setting
PSD	power spectral density
PSS	power system stabilizer
RLS	recursive least square
SNR	signal-to-noise ratio
SSSP	Small Signal Stability Program
SVC	static var compensator
SVD	singular value decomposition
T_s	sampling period
t_w	time window
V_{ref}	reference voltage setting
WAMS	wide area measurement system
WECC	Western Electricity Coordinating Council
$y(t)$	initial measurements
$\hat{y}(t)$	approximated measurements
$y_d(t)$	downshifted measurements
$\lvert\hat{Y}_{f0}\rvert$	magnitude of the downshifted estimated associate Hermite spectrum
$\hat{Y}(f)$	Fourier transform of the time domain associate Hermite expansion

$\hat{Y}_I(f)$	imaginary component of the estimated associate Hermite spectrum
$\hat{Y}_R(f)$	real component of the estimated associate Hermite spectrum
α_i	*i*th estimated damping factor
α_j	*j*th estimated damping factor from eigenvalue analysis
λ	time scale factor
μ	frequency scale factor
σ_i	*i*th singular value
σ_{Max}	maximum singular value
$\Psi_I\{\ldots\}$	imaginary component of the Fourier transform
$\Psi_R\{\ldots\}$	real component of the Fourier transform

Chapter 1

SMALL SIGNAL STABILITY ESTIMATION IN POWER SYSTEMS

1.1 Overview

As early as the 1920's, small signal or electromechanical mode analysis in power systems was performed due to a phenomenon referred to as hunting [80] causing synchronous generator rotor speeds to oscillate about an operating point. Engineers discovered that the problem was the result of excessive transmission line reactances and found the solution was to add amortisseur windings to the affected generator rotors. Excessive transmission line reactances are still recognized today as factor in affecting damping torques within generators.

Today as was probably the case in the 1920's, small signal oscillations often are initiated by random changes in loads causing local oscillations in generators. Oscillations could also occur between clusters of generators. Occasionally these oscillations were further aggravated by high-speed excitation controls with large voltage regulator gains and small time constants [1-3]. The resulting oscillations could potentially become negatively damped affecting the security and reliability of the power system. High real power loading and high var absorption in generators have also been identified with reducing damping torques in generators [62] Unacceptable oscillations may occur between a load center and one or more local generators. The exchanges of power between load centers and remote generators can also manifest itself in power transfer oscillations across transmission lines or paths resulting in interarea oscillations. Researchers and engineers [80] have loosely classified the different types of

oscillations into three groups based on where the problem occurs and its frequency range:

- Interarea oscillations which occur between groups of generators and generally have the lowest frequency range of .2 to .7 Hz.
- Local oscillations which occur between a generator or groups of generators and the electrically adjacent power system with a frequency range of .8 to 1.5 Hz.
- Intraplant oscillations which occur within a generating station or cogeneration plant with a frequency range of 2 to 3 Hz.

In this thesis, only interarea and local oscillations were studied since they generally have a direct impact on the interconnected transmission system.

All types of power system oscillations can potentially affect protection systems producing miss-operations, poor coordination or false tripping. Mitigation measures can include adding power system stabilizers (PSS), retuning existing PSS, adding compensation to high voltage DC converter controls, adding or retuning an existing static var compensator (SVC), retuning exciter regulators or reducing flows on transmission lines. Fig. 1.1 shows a typical small signal event of a simulated growing oscillation in the rotor angle of a generator caused by a slight perturbation near the generator.

Over the years engineers have employed many tools and test procedures for the analysis of these interarea and local oscillations. Since the resulting oscillations are thought to be small deviations about an operating point, the

methods employed to study small signal stability events are typically linear techniques. Some of the methods currently used are appropriate for off-line analysis while others are applicable for on-line monitoring. The tools could be further characterized by their processing capabilities. For example, some analysis methods are more accurate for use in field testing environments while others show greater efficacy using ambient measurements. Certain techniques are more accurate in the presence of noise than other methods.

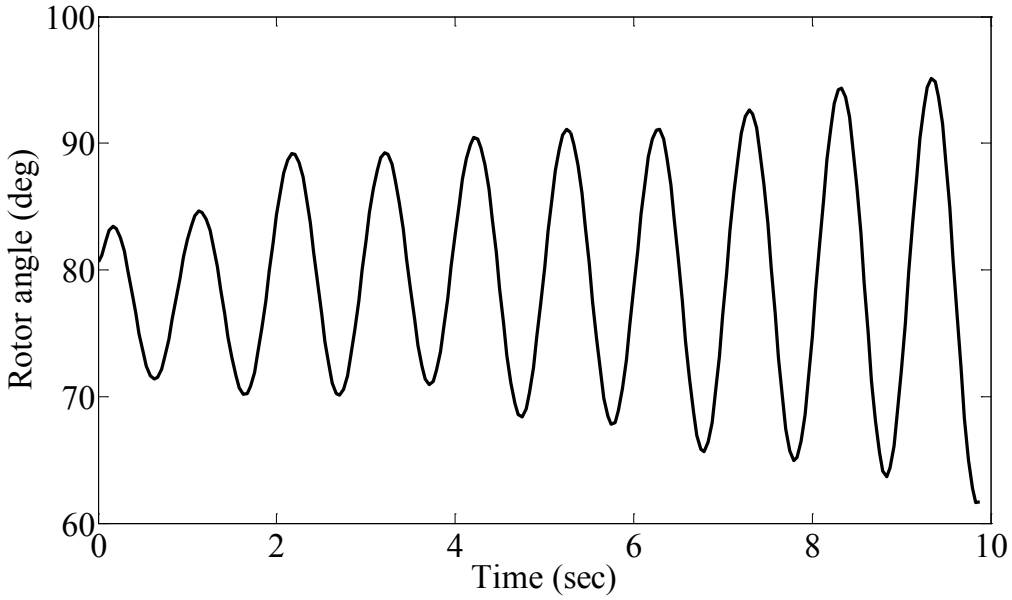

Fig. 1.1. Typical generator rotor angle small signal event response.

Recently an increasing number of state governments in the United States of America are adopting mandatory renewable portfolio standards for jurisdictional utilities [4] with the potential of future federal regulations being mandated for all utilities. Some proposed wind and solar generation facilities are approaching 1000 MW in size [5] and do not anticipate having damping mitigation equipment such as PSS. Complicating this fact is a United States

Department of Energy report [6] recommending that new wind generation stations locate away from population centers using existing transmission lines for delivery to customers thereby increasing congestion. The combination of size and location of large wind farms allows them to have a potentially adverse effect on power system modes, which could require additional scrutiny by power system engineers.

The need to continue to develop new tools for estimating modes and their damping levels and to design mitigating measures within the power system is important for the following reasons:

- To identify potentially negatively damped local and interarea modes.
- To prevent relay miss-operation resulting from lightly damped modes.
- To aid in the mitigation of lightly damped modes by adding or retuning damping mitigation devices.

1.2 Small signal stability estimation problem

Although many methods have been proposed and are actively employed to calculate electromechanical modes in power systems, new methods are continually being sought out for their unique capabilities or to complement existing methods. Some successful methods possess two important characteristics in their estimating ability: linearity and orthogonality. One of the most well known tools for estimating periodic signals is the Fourier series. The Fourier

series is a linear representation of orthogonal functions that are also harmonically related. Key metrics such as accuracy in the presence of noise and measurement window length are also important for any effective mode estimator. This thesis introduces a new method for identifying modes and their respective damping levels. The method uses an orthogonal polynomial for estimating the spectrum from measurements. Once the frequencies of the modes are identified, a modified sliding window technique is used to estimate the damping level of each mode. Damping levels are calculated by downshifting the original measurement and solving a linear prediction routine by using the estimated frequency spectrum. Together, both assessments are referred to as the associate Hermite expansion (AHE) method.

1.3 Small signal estimation methods

One of the earliest tools for identification of power system modes was the use of eigenvalue analysis. Eigenvalue analysis begins with assembling the differential and algebraic equations of a study system (1.1)

$$\begin{aligned} \underline{\dot{x}} &= \underline{A}\underline{x} + \underline{B}\underline{u} \\ \underline{y} &= \underline{C}\underline{x} + \underline{D}\underline{u} \end{aligned} \tag{1.1}$$

where $\underline{x}$ is the vector of state variables, $\underline{y}$ is the vector of output variables, $\underline{u}$ is the vector of input variables, $\underline{A}$ is the linearized state matrix, $\underline{B}$ is the input matrix, $\underline{C}$ is the output matrix, and $\underline{D}$ is the algebraic input-output matrix. If the Laplace transform is taken of state equation of (1.1), the frequency domain expression is given as

$$\underline{x}(s) = (s\underline{I} - \underline{A})^{-}[\underline{x}(0) + \underline{B}\underline{u}(s)] \tag{1.2}$$

where s is the continuous generalized frequency variable, $\underline{I}$ is the identify matrix and $\underline{x}(0)$ is the set of initial conditions. The eigenvalues of (1.2) are the roots of (1.3). The generalized frequency variable s can be broken down into the components in (1.4), where α represents the damping factor and f represents the frequency. Using the values of α and f, the damping ratio ζ is calculated in (1.5). The relations in (1.4) and (1.5) are used repeatedly in the following chapters.

$$\det(s\underline{I} - \underline{A}) = 0 \tag{1.3}$$

$$s = \alpha \pm j2\pi f \tag{1.4}$$

$$\zeta = \frac{-\alpha}{\sqrt{\alpha^2 + (2\pi f)^2}} \tag{1.5}$$

To determine the eigenvalues of the state matrix $\underline{A}$, the state equations are linearized about an operating point. For example in the case of an induction motor, the operating point may include the quadrature axis stator terminal voltage and the direct axis rotor voltage. The state matrix $\underline{A}$ associated is decomposed to provide the eigenvalues of the study system. With the eigenvalues known, the eigenvectors can be calculated.

In eigenvalue analysis, the eigenvectors provide important diagnostic information about modes and states that is a direct result of being a model-based analysis tool. The relationships in (1.1) represent a system under a forced input. If (1.1) is rewritten to represent a system with only initial conditions to provide a response its state representation is shown in (1.6).

$$\dot{\underline{x}} = \underline{\underline{A}}\,\underline{x} \tag{1.6}$$

Decomposing the state matrix in (1.6) using eigenvalue analysis can take two forms.

$$\begin{aligned} \underline{\underline{\Gamma}}\,\underline{\underline{A}} &= \underline{\underline{\Lambda}}\,\underline{\underline{\Gamma}} \\ \underline{\underline{A}}\,\underline{\underline{\Xi}} &= \underline{\underline{\Xi}}\,\underline{\underline{\Lambda}} \end{aligned} \tag{1.7}$$

where $\underline{\underline{\Gamma}}$ is a matrix of left eigenvectors of $\underline{\underline{A}}$ and $\underline{\underline{\Xi}}$ is a matrix of right eigenvectors of $\underline{\underline{A}}$. The right and left eigenvector matrices have been shown [3] to provide a mapping between the actual states $\underline{x}$ in the system to a set of states $\underline{z}$ that are only related to a single mode as given in (1.8) and (1.9).

$$\underline{x} = \underline{\underline{\Xi}}\,\underline{z} \tag{1.8}$$

$$\underline{z} = \underline{\underline{\Gamma}}\,\underline{x} \tag{1.9}$$

In (1.8) the right eigenvectors determine the mode shape or the amount of activity in the system states if a certain mode is excited. Alternately, the relationship in (1.9) identifies the weighted combination of system states that contributes to a single mode. A more useful relationship that is widely used in current software tools is the participation factor P (1.10), which also relies on the eigenvectors of $\underline{\underline{A}}$

$$P_{jm} = \gamma_{jm}\chi_{mj} \tag{1.10}$$

where γ is the right eigenvector of the j state of the m mode and χ is the left eigenvector of the m state of the j mode.

The participation factor is a per unit metric that defines the amount of activity of one selected system state in one selected mode and can be interpreted in the reverse order.

A power flow program is used to provide the initial conditions for eigenvalue analysis. Fig. 1.2 shows the flowchart for a typical eigenvalue analysis algorithm. To determine which modes are affected by which states, participation factors are computed using the modes eigenvectors. For small signal stability problems, complex eigenvalues indicate an oscillatory response to a perturbation. Eigenvalues also contain the frequency of the modes along with their damping levels.

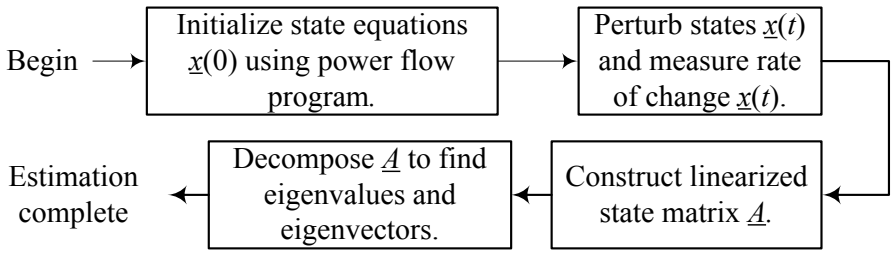

Fig. 1.2. Example algorithm for eigenvalue estimation.

Some of the tools to perform eigenvalue analysis have been used to identify power system modes since the 1970's. Two programs were developed by General Electric for the estimation of eigenvalues from a linearized state matrix: Power System Simulator (POSSIM) and the Machine and Network Stability (MANSTAB) routine [7]. Both programs follow the general eigenvalue analysis routine of Fig. 1.2. However, MANSTAB utilizes a dynamic model of the system as opposed to an algebraic representation found in POSSIM. As a result, MANSTAB has the ability to be used for sub-synchronous resonance analysis where as POSSIM is typically used for small signal stability assessments.

Another eigenvalue analysis package was developed through a joint effort between the Electric Power Research Institute (EPRI) and Ontario Hydro

resulting in the development of the Multi-Area Small Signal Stability Program (MASS) and the Program for Eigenvalue Analysis of Large Systems (PEALS) [8]. MASS was initially used to study detailed models such as a power plant or small power system representations. In such models little sparsity exists in the linearized state matrix. The PEALS tool, on the other hand, was designed to identify the system's eigenvalues for a limited number of modes and is generally used for large scale analysis. Within the PEALS tool, two algorithms can be selected: Analysis of Essentially Spontaneous Oscillations in Power Systems (AESOPS) algorithm and the modified Arnodi method (MAM). Both MASS and PEALS were later made available in a single package referred to as the Small Signal Stability Program (SSSP) [9].

An improvement to the AESOPS algorithm has been proposed by Martins [10]. Due to the large amount of sparsity that exists in the linearized state matrix $\underline{A}$, techniques are employed to create a reduced version of this matrix prior to factorization. Another complication to working with large power system state matrices is they are usually highly asymmetric. Reducing the sparsity of the state matrix resulted in reduced computation time for determining the eigenvalues. Overall, the modified AESOPS method required a longer computation time than the original AESOPS algorithm. Kundur et al [11] examined the accuracy of the MASS and the two PEALS algorithms given the same study system. A review of the two PEALS algorithms shows that the AESOPS algorithm is computationally faster than the modified Arnodi technique. A comparison of each algorithms

performance shows all three methods reported essentially the same modal estimates.

At present, new tools are being developed utilizing PC based platforms in lieu of mainframe applications for eigenvalue analyses. Small signal stability analysis is being performed using MATLAB and Simulink software for designing and implementing devices to improve damping levels [12-14]. Due to its multi-function capability, PC tools offer various abilities to design eigenvalue-based controllers that would have been more difficult using mainframe tools.

In the 1795, a method to identify the relationship between the pressure and volume of gases was developed. Gaspard Riche Baron de Prony proposed fitting an exponential model to equally spaced data points and then using another exponential model to calculate the intervening points [15]. Today the basic Prony analysis typically fits data through a least squares process to obtain a linear predictor model. A simple forward predictor is generally used however more sophisticated linear predictors can be applied. Roots are extracted from this finite impulse response (FIR) filter and inserted within an exponential model along with complex weights. A flowchart for the modern basic Prony algorithm is shown in Fig. 1.3. Prony's method was recognized in the 1950's by spectral analysis researchers as an effective means to obtain spectral estimates [16]. In the 1980's different versions of Prony's method began to appear [17] as well as greater use as an identification tool in lieu of other established spectral methods [18]. In addition, researchers in the western United States began to use Prony's method to

investigate oscillatory phenomenon that were occurring during day-to-day power system operations [19].

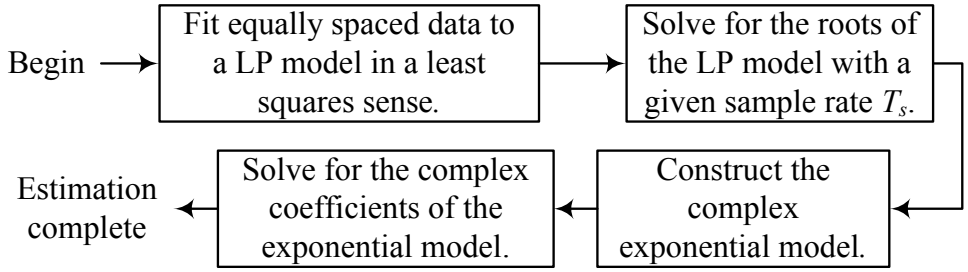

Fig. 1.3. Basic Prony algorithm for estimating modes.

Unike eigenvalue analysis, Prony's method estimates the modes and the associated damping levels through a least squares curve fit using measurements. Prony's method also provides phase information as well as the strength of the individual modes. In addition to studying small signal phenomenon, Prony's method has also been used to assess large signal disturbances in the conjunction with a time domain sliding window [20]. Because it can estimate phase angles associated with modes, Prony's method can be used as a tool for coherency identification either from separated generation clusters or between measurements separated spatially [21].

Because of its applicability to field measurements and model development, Prony analysis has been deployed for the tuning and design of power system devices to improve small signal damping. In one research example, engineers and researchers developed test systems with dynamics similar to those found in actual practice for the tuning process. Next, a Prony analysis along with a root locus method was then used to derive PSS model which subsequently

demonstrated damping improvements [22]. In another case, researchers have used the identification capability available in Prony's method to help design a controller for a SVC [23]. With the help of Prony's method, model validation and analysis was also performed in the design of a controller at the site of a DC converter station [24]. In this case, both disturbance and ambient data were collected for the project.

One of the principal uses of Prony analysis is to process data from different types of field tests for either identification purposes or, as explained before, to assemble models. One type of field test is the staged field test. This may include either the insertion of the brake [25], the intentional tripping of a line or an abrupt change in the reference of an exciter's voltage regulator. The purpose here is to provide an input to the power system large enough to excite modes yet small enough not to create a non-stationary event. Another related measurement event is the unintentional yet opportunistic disturbance event. Again, the only critical issue here is that the disturbance be not too large or extreme so as to create a non-stationary response from the power system. A third type of staged field test is the injection of a small signal into a controller producing a modulated signal in the power system. An example of this type of test was mentioned earlier regarding a DC line converter. As for the type of signal, the injection could either be a low level white noise signal, a square wave [26] or sinusoid. Another type of analysis is the collection and processing of ambient data from a convenient location, such as a potential or current

transformer at a substation or power plant. It is assumed that the naturally occurring noise that exists in the power system would excite modes without the need to either inject a signal or stage a non-destructive disturbance. This type of analysis has the obvious advantage of avoiding the need to coordinate a staged test making it cost effective and reasonably secure. In any case, monitoring is required for all the tests and analyses described here. Also, the more monitors recording these events insure that the failure of one unit to operate correctly will not jeopardize the entire test. As a consequence, a wide area measurement system (WAMS) can play a key role in collecting data for use in a Prony analysis or any other small signal assessment.

Use of Prony analysis has some disadvantages in the estimation of electromechanical modes in power systems. Basic Prony analysis requires the user to choose the order of the approximation. A typical recommendation is to select the order to exceed the number of complex modes thought to exist in the data set using a range between N/3 and N/2 [27-28], where N represents the length of the data block. If the size of the data set is for example 240, then a reasonable order could vary from 80 to 120. Some researchers have proposed setting the order equal to N to improve resolution between closely spaced modes [17] and to mitigate noise effects. However, selecting too high an order can produce spurious complex modes, oscillatory behavior and excessive computational effort. Fortunately, an outcome of a Prony analysis provides the user the means to quickly sift through the results by examining the amplitude of

the complex exponentials. In general, Prony analysis compares well with eigenvalue analysis in that both can accommodate multiple signal systems [29] and the accuracy has been found to be similar using identical test scenarios [30]. In [29], the authors were able to add additional signals to the linear prediction model while holding the model order constant.

A Prony analysis is the application of a deterministic parametric spectral analysis method. However, Prony analysis is not the only parametric method that has been employed for the detecting of electromechanical power system modes. Researchers have noted that parametric methods, in general, produce high resolution spectral results with relative short data records [31] as compared to non-parametric methods. Some of the most recent research has focused on the use on autoregressive methods to extract electromechanical frequency and damping information. However unlike the Prony analysis discussed previously, autoregression methods use a time-series model that can represent a stochastic process using autocorrelation sequence estimates. Equation (1.11) shows the general structure of the model, where $\hat{y}[n]$ is the approximated function, $x[n]$ is the output of the process, $u[n]$ is the input to the process, $\underline{a}$ are the model output parameters, $\underline{b}$ are the model input parameters, and p and q are the model orders.

$$\hat{y}[n] = \sum_{k=1}^{p} a[k]x[n-k] + \sum_{k=0}^{q} b[k]u[n-k] \tag{1.11}$$

Autoregressive techniques attempt to model the poles and zeros of the data record usually assuming the input is stationary. To solve for the model parameters, the autocorrelation sequence (ACS) estimate is calculated directly

from the data record. The system matrix is symmetric so that fast algorithms can be applied to quickly calculate the $\underline{a}$ and $\underline{b}$ coefficients. The resulting system matrix has a Toeplitz and Hermitian structure. If only the output is modeled (q=0), the autoregression method referred to as the autoregressive Yule-Walker (ARYW) normal method. Other autoregression (AR) methods besides the ARYW method are possible. The relationship in (1.12) shows the ARYW normal equations that are solved for the $\underline{a}$ model parameters

$$\begin{matrix}\begin{bmatrix} \\ \underline{r} \\ \\ \end{bmatrix} \\ m\times 1\end{matrix} = -\begin{matrix}\begin{bmatrix} \\ \underline{R} \\ \\ \end{bmatrix} \\ m\times m\end{matrix} \begin{matrix}\begin{bmatrix} \\ \underline{a} \\ \\ \end{bmatrix} \\ m\times 1\end{matrix} \tag{1.12}$$

where $\underline{r}$ is the ACS estimate vector, $\underline{R}$ is the ACS system matrix and $\underline{a}$ is the output coefficient vector. Fig. 1.4 provides a flowchart for the ARYW estimation method.

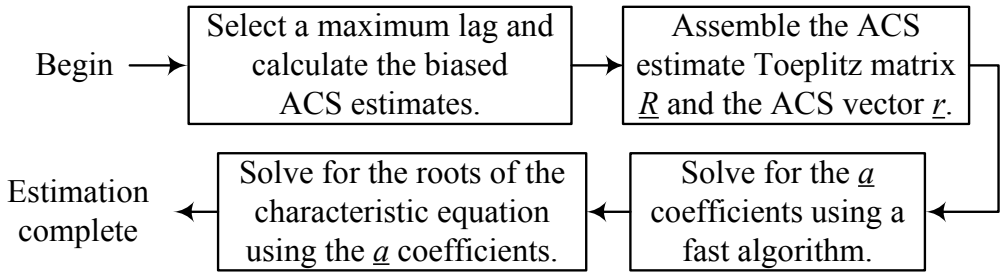

Fig. 1.4. AR Yule-Walker autoregression estimation method.

If both the output and input is used to approximate the process (p≠0, q≠0) the resulting technique is the autoregression moving average (ARMA) Yule-

Walker normal method. However because the true relationship between the input parameters b and the actual ACS values is non-linear, special methods must be introduced to solve for both input and output ARMA model parameters. The authors in [18, 31] propose generating an ARMA model by filtering the original data record with a created AR filter and estimating the $\underline{b}$ coefficients from the residuals. Even though this sequential process is sub-optimal it has the advantage of not requiring iterations which allows ARMA models to be used in on-line power system applications.

In the 1990's power system researchers began to assess the effectiveness of autoregressive methods as compared to existing Prony and state space methods [32]. It was found that the ARMA technique compared favorably to other methods in terms of accuracy without the presence of noise. However in this case, the researchers used the data directly instead of calculating the ACS estimates to solve for the $\underline{a}$ coefficients in (1.12). As a result, the accuracy of the ARMA method suffered when white or colored noised was introduced as compared to the state space method.

Other researchers have found that ARMA methods employing the ACS estimates were effective in improving damping in the case of tuning damping devices [33]. These researchers used an ARMA algorithm for tuning a PSS using global signals as opposed to local inputs. Other researchers have compared the accuracy of AR, ARMA and Prony methods in identifying modes from field tests and ambient measurements [34]. In the case of using these three parametric

methods, researchers varied the model order and gauged the accuracy of the mode identification and damping levels. Frequency estimates from the AR and ARMA methods were insensitive to changes in order. However, damping estimates from the AR method approached those obtained from the ARMA method as the pole order increased. In nearly all cases, the ARMA method was found to be superior to the AR method when using the same number of poles. ARMA was also found to be essentially equivalent to the Prony results if the numerator and denominator orders were allowed to be sufficiently large. A variation on the ARMA method has been used with ambient measurements [35]. In this case, models are generated with simple pole-zero transfer functions that enable the user to determine the modal content from ambient data.

Adaptive filtering has been investigated by researchers and the results compared with an AR method for identification of modes. Researchers have used the least mean square (LMS) adaptive algorithm with the AR method providing an initial starting point versus just using the AR method alone, and found both techniques gave acceptable results [36]. However, the step size selection in the adaptive algorithm was a critical decision in how the method converged. In this case the investigators assumed a linear method for use on a linear process. Some researchers have developed a modified AR method that is applicable to non-linear modal behavior [37]. A method was created that used higher order statistics to characterize and detect higher order nonlinearities. The consequence of this

modified AR method is that large signal disturbances with non-linear effects can also be assessed to determine their modal content along with damping levels.

Investigators have used a two-variable ARMA technique that not only identifies modes but also provides an indication of the coherency between generators or groups of generators [38]. The cross spectrum is calculated on-line from time series data to determine the eigenvector associated with modes common to generators from different groups. The results show the researchers not only successfully identified the modes but the strength of the relationships between generators.

Research as early as the 1990's began to focus on using an artificial neural network (ANN) to identify electromechanical modes. Unlike the other identification methods described before, the application of neural networks requires training to determine the appropriate weights for linkages, also known as neurons, for the correct output function. Once the training session is completed a test session is typically performed to gauge the accuracy of the ANN and to make any final adjustments to the weights. Learning is sometimes improved through the use of feedback loops to accelerate convergence of the weights to their final values. An ANN also has the ability to take either continuous or discrete inputs and generate either continuous or discrete outputs. Fig. 1.5 shows a general structure for a feed-forward multilayer ANN.

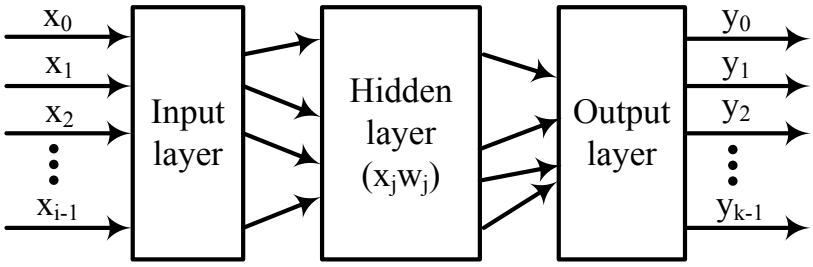

Fig. 1.5. Generalized ANN representation.

Examination of Fig. 1.4 shows that the input layer receives inputs *x* from 0 to *i* while the hidden layer screens and applies weights *w* to the inputs. Finally, the output layer neurons produce one or more output *y*'s using the hidden layer neuron decisions.

Researchers have proposed a multilayer ANN which produces a single analog output representing the real portion of the most lightly damped system eigenvalues [39]. However, the authors wanted to use as many of the power system variables that they believed affected the lightly damped eigenvalues. As a result, they constructed a second clustering ANN to select the most effective input variables from the initial larger set. Reducing the number of input variables reduces the training time for the multilayer ANN. But in this case the consequence of using fewer input variables was found to reduce the accuracy of the multilayer ANN. The researchers found the computation time of 50 ms gave an acceptable level of accuracy for their ANN, which may allow them to employ their device for on-line estimation. However, only one mode was modeled in the study. Also, no consideration was taken for line-out or other network changes

which are common in operations analysis and which would require additional training.

Some researchers have studied an adaptive scheme that can learn while the ANN is operating on-line in a modal identification role. The adaptive approach is achieved using a Kalman filtering scheme to minimize the output variance of the ANN [40]. In this case, outputs and inputs are analog quantities. The authors successfully demonstrated that their method can accurately predict power system variables in an on-line setting. Unfortunately, few documented results were provided that demonstrated whether the modified ANN could be employed to predict the damping of eigenvalues as originally intended.

Many ANN schemes have been proposed for use as an adaptively tuned PSS to improve power system damping. A multi-layer perceptron (MLP) is proposed by some authors to be used as an adaptive analog PSS since it has the advantage of changing control capabilities as a result of changing stochastic operating conditions and non-linear effects in the power system [41]. The authors argue that conventional stabilizers do not have this capability which puts them at a disadvantage as compared to an adaptive PSS. In this research, the MLP PSS is trained using a conventional adaptive PSS. Later the authors train the MLP PSS using the input-output relationships of a synchronous generator [42]. With inverse mapping, the product of the synchronous machine and the adaptive MLP PSS should ideally provide unity output. Up until this point the authors have only tested their proposed MLP PSS on a single machine infinite bus system. In [43],

the authors test their device on a small test system and simulated different operating conditions and disturbances. The researchers demonstrated that either operating alone, with another adaptive MLP PSS or in combination with convention PSS their proposed device adds positive damping to the test model for different operating conditions. However, no measurements were given regarding the computation time or accuracy of the MLP PSS and its left to the reader to assess whether the test system had replicated a real world scenario to an adequate degree.

Researchers have further improved on the adaptive MLP PSS design by splitting the MLP unit into two interconnected neural networks [44]. One unit operates by identifying the plant characteristics using speed deviation as the generator output and the PSS output as the generator input. The second unit acts as a controller for the first unit to damp out plant oscillations. Input of the controller is accelerating power from the generator and the output is the actual output from the adaptive MLP PSS. Learning is achieved for both the identifier and the controller through a single error vector for each unit while on-line. Simulations on a single machine system shows damping is improved using the split MLP PSS design. In [45] the authors applied the improved adaptive MLP design to a multi-machine system with the same results. Finally, the authors hard wired their adaptive MLP PSS to a motherboard and used a laboratory facility to test the operation on a small synchronous machine [46]. Once again the results were successful. However like the previous study, few metrics were provided to

gauge the speed and accuracy of the new design. Also, the physical tests had difficulty mimicking outage conditions that would be seen in a field setting.

The Matrix Pencil (MP) method was previously used in electromagnetic field analysis but has been recently applied to the identification of electromechanical modes. Similar to other subspace analyses, the MP estimator calculates the complex modes using a single measurement and is related to the Estimation of Signal Parameters by Rotational Invariance Techniques (ESPRIT) spectral method [47]. From the measurements, two matrices ($\underline{Y}_1$ and $\underline{Y}_2$) are constructed using vectors with a length of L (1.13), where L spans the entire subspace.

$$\underline{Y}_1 = \begin{bmatrix} y[1] & y[2] & \cdots & y[L] \\ y[2] & y[3] & \cdots & y[L+1] \\ \vdots & \vdots & & \vdots \\ y[N-L] & y[N-L+1] & \cdots & y[N-1] \end{bmatrix}_{(N-L)xL}$$
$$\underline{Y}_2 = \begin{bmatrix} y[0] & y[1] & \cdots & y[L-1] \\ y[1] & y[2] & \cdots & y[L] \\ \vdots & \vdots & & \vdots \\ y[N-L-1] & y[N-L] & \cdots & y[N-2] \end{bmatrix}_{(N-L)xL} \quad (1.13)$$

It is assumed that the number of signal modes M in the measurement is less than L, and $\underline{Y}_1$ and $\underline{Y}_2$ can be factored using the relationships in (1.14).

$$\underline{Z}_1 = \begin{bmatrix} 1 & 1 & \cdots & 1 \\ z_1 & z_2 & \cdots & z_M \\ \vdots & \vdots & & \vdots \\ z_1^{N-L-1} & z_2^{N-L-1} & \cdots & z_M^{N-L-1} \end{bmatrix}_{(N-L)xM}$$

$$\underline{Z}_2 = \begin{bmatrix} 1 & z_1 & \cdots & z_1^{L-1} \\ 1 & z_2 & \cdots & z_2^{L-1} \\ \vdots & \vdots & & \vdots \\ 1 & z_M & \cdots & z_M^{L-1} \end{bmatrix}_{MxL}$$

$$\underline{Z}_0 = diag\left[z_1, z_2, \cdots, z_M\right]$$

$$\underline{R} = diag\left[R_1, R_2, \cdots, R_M\right] \qquad (1.14)$$

Fig. 1.6 shows the basic steps of the MP analysis method. Note that the values of the matrix $\underline{R}$ in (1.14) are residues of the roots of the $\underline{Z}_0$ matrix.

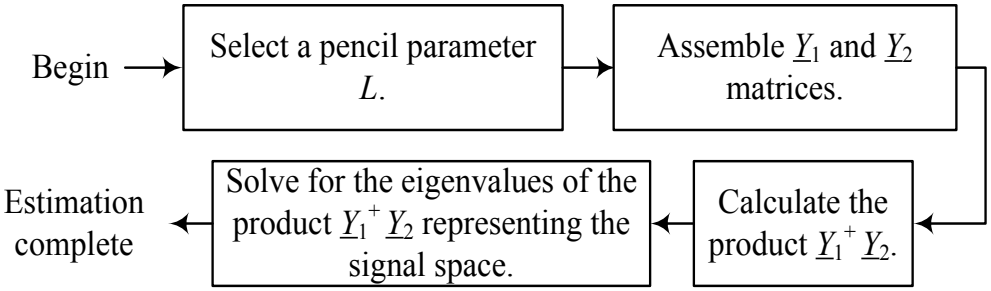

Fig. 1.6. MP analysis technique for the non-noise case.

Next, the pencil relationship (1.15) is formulated and the eigenvalues of the product $\underline{Y}_2^{+}\underline{Y}_1$ are the eigenvalues of the signal space [48], where $^{+}$ is the Moore-Penrose inverse. In the presence of noise, the $\underline{Y}_1$ and $\underline{Y}_2$ matrices are combined and singular value decomposition (SVD) is used to isolate and remove the smallest singular values and thus the noise subspace [49]. Use of SVD also allows a rational selection of M. The obvious disadvantage of a MP analysis, like the Prony and ESPRIT analyses, is that the selection of the value of M requires a

priori knowledge of the number of signal modes contained in the measurement which is not always possible.

$$\underline{Y}_1 - \lambda \underline{Y}_2 = \underline{Z}_1 \underline{R}(\underline{Z}_0 - \lambda \underline{I})\underline{Z}_2 \qquad (1.15)$$

The application of MP analysis to electromechanical mode extraction in power systems has already been performed [50] for a theoretical controller design. However, the authors had difficulty selecting the order even after examining the measurements' singular values. A comparison with Prony's method using field measurements reveals that the MP analysis gave very similar results. On the other hand, the MP method demonstrated that, like Prony analysis, assessing non-stationary disturbances produced erroneous results [51]. A more thorough comparison with Prony's method and the Hankel Total Least Squares method shows the MP analysis is less sensitive to noise than the Prony analysis [52]. Computational speed between MP and Prony analyses was dependent on how the inverse is calculated either by SVD or QR factorization. The authors in [52] also used the scheme to dampen lightly damped oscillations through modulation of the Pacific DC Intertie.

Besides MP and general eigenvalue assessments, researchers have used other subspace methods for small signal analysis in power systems. Some authors have found that reduced order models can be obtained by separating eigenvectors and their associated eigenvalues into smaller subspaces [53]. Other researchers have used iterative methods and focused on calculation of only one complex eigenvalue in lieu of the conjugate pair. In addition, the authors have only

calculated the most lightly damped eigenvalues which usually garner the most interest [54]. To avoid use of models and to be able to use real measurements, the researchers in [55] have proposed a stochastic subspace method to calculate the modes. Hankel matrices were constructed using past and present measurements. Next, projection and observability matrices are formed after an SVD assessment selects the order and removes the unwanted noise. Finally, the eigenvalues of the reduced measurement matrix are found. Advantages of this method include working exclusively with data measurements in lieu of models or ACS matrices. Also since the technique uses only ambient data, the method of [55] can be implemented in an on-line setting. A comparison from the results of the method in [55] was made with ARMA and state space methods. The ARMA estimation was found to be more accurate with shorter data records than the other two methods. However, the stochastic subspace method was as accurate as the other techniques for longer data records and provided higher levels of certainty in the results. In [56], the same authors studied estimating confidence intervals which provided more dependable results in modal identification and damping estimates.

Very recently some researchers have employed adaptive filtering techniques for the estimation of power system modes. One of these methods was described earlier in [36] working in conjunction with an AR estimator that provided initial weight vector estimates. Fig. 1.7 shows the components of the general LMS adaptive algorithm [57].

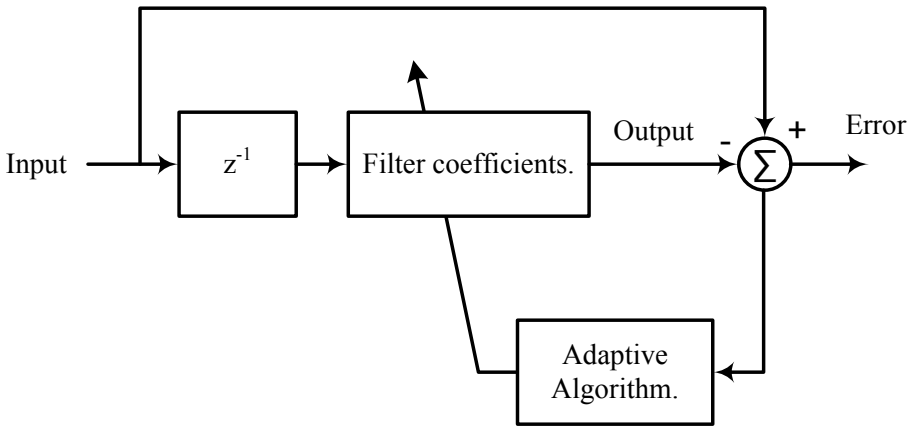

Fig. 1.7. Generalized LMS adaptive algorithm [57].

The researchers' results indicate the convergence time was highly related to the step size and the initial values of the weight vector. Other researchers have used variations on the recursive least square (RLS) adaptive algorithm to predict power system modes. RLS algorithms essentially solve for the model coefficients $\underline{a}$ in the AR problem in Fig. 1.4 by calculating the ACS estimate vector $\underline{r}$ and the ACS estimate matrix $\underline{R}$ at every time step but with actual data measurements. Researchers have found the RLS methods are quicker to converge to a solution than LMS methods but at a higher computational cost [58-59]. However, it has also been shown that RLS methods can accommodate outlier and missing data situations successfully while still accurately predicting electromechanical modes. Both LMS and RLS methods are time recursive which allows both methods to be used in on-line or mode meter applications. Another potential benefit of these time recursive methods is the ability to estimate non-linear modes resulting from large signal disturbances. As the mode changes in time the adaptive algorithms can move and track the mode as it changes. A potential disadvantage of adaptive

measures is that they are iterative, unlike model based methods, and they require additional time to reach a solution for each time step. In addition, selection of the size of the time step for these methods is also a critical decision in terms of accuracy and speed.

A variety of other methods have been proposed to detect and estimate small signal power system modes that are worth mentioning here. The authors in [60] have demonstrated use of the Hilbert transform to identify low frequency modes. An interesting outcome of the research is that the method calculates the instantaneous modal estimates per step making it applicable to non-stationary signal analysis. The paper contains a comparison of the proposed method to Prony's method.

Many researchers have used newly proposed electromechanical estimation methods to create stability indices resulting from small signal stability assessments. These assessments are generally intended to be used in on-line applications using ambient data so as to give power system operators a continuous assessment of the power system state. This is the case in [61] where a parametric framework based on the Box-Jenkins model is implemented. For this application, the Box-Jenkins model represents the errors separately from the estimator. The authors then estimate a stability index based on an adjustment to the classical damping factor α. Results show the Box-Jenkins model provided statistically better results than the ordinary least squares method and the modified damping factor proved to be a reasonable indicator of proximity to instability.

In [63] the Heffron-Phillips model for an induction machine is used to assess the machine modes and their effects on other induction machines as well as synchronous machines. Although the model is linearized about an operating point as in the case of previous discussed methods [7-14], use of the Heffron-Phillips model allowed easy computation of the induction machines eigenvalues. In addition, the assessment showed that the induction machine eigenvalues were typically damped. Results also revealed that the critical model components for motors are inertial and the rotor open circuit time constant. However more importantly, the design of damping control devices is directly affected by the load dynamic representation and thus accurate representation of induction machines is critical for the estimation of damping in a power system.

For [64], the researcher used non-parametric methods to estimate the power spectral density (PSD) of measured data. The tool the author used was the Welch periodogram. Essentially, the Welch periodogram calculates an average fast Fourier transform (FFT) using multiple FFTs' from successive time windows to obtain a high resolution estimate of the PSD. Among non-parametric estimators, the Welch PSD method is one of the most accurate. However like other non-parametric methods, the Welch PSD method's accuracy is a function of the record length. Consequently the greater the number of FFTs' used and the larger the length of the time window, the more accurate the spectral estimate. However, increasing both the number of windows and the length of the data record comes with a higher computational cost for this method.

1.4 Small signal estimation using associate Hermite expansion

From the brief review presented in the last section, various methods have been proposed and tested in the attempt to identify electromechanical modes in power systems. Estimation methods can be categorized as either model based or measurement based. Some techniques are described as non-parametric methods while others are parametric or curve fitting techniques. Still other estimators are learning algorithms and other methods are purely subspace estimators. Most of these techniques assume the measurements are stationary and can be represented by a linear process.

As was stated earlier, the method used in this thesis to estimate modes and their damping levels utilizes an orthogonal polynomial that is fitted in a least squares sense to power system measurements. Order of the estimation is achieved through relationships involving time and frequency windows and the time scale factor, which also gives the process a degree of noise mitigation capability by maintaining a low condition number for the system matrix. Use of this polynomial as a harmonic analysis tool was first suggested by [65] due to its isomorphic nature, orthogonal structure and ease of calculating higher ordered polynomials. However, the AHE functions have only recently been proposed to be used in the power system field of small signal stability assessment [66].

Once the fit with the observations is complete using the AHE polynomials, the time domain model parameters are used to extrapolate the Fourier spectrum of the initial window and the mode estimates are identified. Next, the original

measurement is downshifted to the baseband for each identified mode. Several sliding windows are constructed and individual spectrums are calculated for each mode. For a particular frequency in a given window, the magnitude of the demodulated spectrum is recorded. The spectrum samples are then used in a LP or FIR filter. The LP filter assumes the spectrum samples are from an autoregressive process and provides both frequency and damping factor information about the original mode. This process is repeated for all the significant modes that were identified from the initial extrapolated spectrum.

1.5 Organization of the thesis

A literature summary of recently proposed small signal stability estimation methods is provided in Chapter 1 along with a description of the identification estimation problem and a brief outline of the proposed new method. Chapter 2 describes the proposed AHE algorithm used to estimate electromechanical mode frequencies and their respective damping levels. Prony's method, a Yule-Walker autoregressive method, another sliding window technique and the Hilbert-Huang Transform method are describe in detail in Chapter 3 for their subsequent use in this thesis. In Chapter 4, the results from AHE method are compared to results from other widely used estimation methods to gauge the limitations and benefits of the AHE method using artificially generated signals as well as a field measurement case. In Chapter 5, simulations from a commercial transient stability program were generated by applying an approximated impulse to either a specific generator's reference load or voltage setting. The responses were

assessed using the AHE algorithm and the other four estimators. Results from these assessments were compared to results obtained from an eigenvalue small signal analysis program. Using simulations from Chapter 5, a PSS was added to three generators to improve damping performance in Chapter 6. The AHE algorithm, Prony's method and eigenvalue analysis were used to determine the modal content prior to using the PSS and to verify the damping improvement after the PSS was added. A four example involved retuning a PSS to improve performance from a growing small signal oscillation to a damped stable result. Chapter 6 demonstrated the ability of the AHE algorithm to be used as a potential design tool for damping mitigation devices. Chapter 7 summarizes the results found from the new method and suggests future work and applications for the new procedure.

Chapter 2

ASSOCIATE HERMITE EXPANSION STABILITY ESTIMATION

2.1 AHE time domain approximation

This chapter provides the development of the AHE algorithm for the estimation of electromechanical modes from power system measurements. The algorithm is composed of two parts. The first part of the algorithm is the use of the AHE polynomials to fit the time domain observations to an approximate model. Using the modeling parameters from the time domain fit, an approximation of the Fourier spectrum is generated and from which the modes are identified. For the second part of the algorithm, an established sliding window technique is modified and is used to estimate the damping associated with each previously identified mode. A general outline of the AHE algorithm is shown in Fig. 2.1 and its components are explained hereafter.

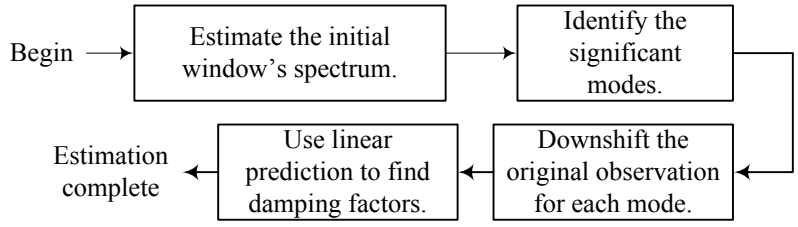

Fig. 2.1. Overview of the AHE estimation algorithm.

The heart of the estimation routine is a polynomial that approximates the original signal $y(t)$. If it can be assumed that the signal $y(t)$ is stationary, then it can be represented by a linear combination of orthogonal functions. One such representation is the Fourier series that is comprised of orthogonal set of

harmonically related sine and cosine terms. An alternative to the Fourier series could include another orthogonal expandable function or series.

Hermite polynomials constitute a set of functions having infinite time support with higher ordered terms calculated recursively (2.1). This form of the Hermite polynomial is not orthogonal and requires a modification to become orthogonal [81].

$$\begin{aligned} H_0(t) &= 1 && m = 0 \\ H_1(t) &= 2t && m = 1 \\ H_m(t) &= 2tH_{m-1}(t) - 2(m-1)H_{m-2}(t), && m \geq 2 \end{aligned} \tag{2.1}$$

A definition of orthogonality is given in (2.2)

$$\int_a^b z_m(t) z_n(t) dt = \begin{cases} 0, & for\ m \neq n \\ 1, & for\ m = n \end{cases} \tag{2.2}$$

where $z_m(t)$ and $z_n(t)$ are two real-valued functions that exist on an interval from a to b. As a simple example to test orthogonality, two Hermite polynomials over the interval from 2 to 5 are examined using (2.2).

$$\begin{aligned} m &= 1; \qquad H_1(t) = 2t \\ m &= 2; \qquad H_2(t) = 4t^2 - 2 \end{aligned}$$

$$\begin{aligned} \int_a^b H_1(t) H_2(t) dt &= \int_a^b 2t\left(4t^2 - 2\right) dt \\ &= 2t^4 - 2t^2 \Big|_2^5 \\ &\neq 0 \end{aligned}$$

Unlike the Hermite polynomials of (2.1), the associate Hermite polynomials in (2.3) can be shown to demonstrate orthogonality, where π is the geometric constant, λ is the time scale factor and ! is the factoral operator. As

was the case with the original Hermite polynomials in (2.1), the time domain associate Hermite polynomials $h_m(t,\lambda)$ also have an order recursive form (2.4).

$$h_m(t,\lambda)=\frac{H_m\left(t/\lambda\right)e^{-.5\left(t/\lambda\right)^2}}{\sqrt{2^m m!\lambda\sqrt{\pi}}}, \qquad m=0,1,2,\cdots,M \qquad (2.3)$$

$$h_0(t,\lambda)=\frac{H_0\left(t/\lambda\right)e^{-.5\left(t/\lambda\right)^2}}{\sqrt{\lambda}\pi^{.25}} \qquad m=0$$

$$h_1(t,\lambda)=\frac{H_1\left(t/\lambda\right)e^{-.5\left(t/\lambda\right)^2}}{\sqrt{2\lambda}\pi^{.25}} \qquad m=1$$

$$h_m(t,\lambda)=\frac{1}{\sqrt{m}}\left\{\sqrt{2}\ t/\lambda\ h_{m-1}\left(t/\lambda\right)-\sqrt{m-1}\,h_{m-2}\left(t/\lambda\right)\right\}, \qquad m\geq 2 \qquad (2.4)$$

Using the same example before but this time using the associate Hermite polynomials over the interval from -∞ to ∞, λ=1, and with the help of l'Hospital's Rule and integration by parts,

$$m=1; \qquad h_1(t,\lambda)=\frac{2t}{\sqrt{2}\pi^{.25}}e^{-.5t^2}$$

$$m=2; \qquad h_2(t,\lambda)=\frac{4t^2-2}{2\sqrt{2}\pi^{.25}}e^{-.5t^2}$$

$$\begin{aligned}\int_{-\infty}^{\infty}h_1(t,\lambda)h_2(t,\lambda)dt &= \frac{1}{\sqrt{2}\pi^{.25}}\int_{-\infty}^{\infty}\frac{2t\left(4t^2-2\right)e^{-t^2}}{2}dt\\ &= \frac{1}{\sqrt{2}\pi^{.25}}\int_{-\infty}^{\infty}2t\left(2t^2-1\right)e^{-t^2}dt\\ &= \frac{1}{\sqrt{2}\pi^{.25}}\left(-\left(2t^2-1\right)e^{-t^2}\Big|_{-\infty}^{\infty}+\int_{-\infty}^{\infty}4te^{-t^2}dt\right)\\ &= 0\end{aligned}$$

Consequently, the two associate Hermite polynomials are orthogonal to one another [67].

To identify the modes in the signal $y(t)$ and assess the level of damping, an estimate of the spectrum must be determined. With the assumption that the AHE polynomials can be used to approximate the original signal, the linear time domain expansion model of (2.5) is employed,

$$\hat{y}(t) = a_0 h_0(t,\lambda) + a_1 h_1(t,\lambda) + \cdots + a_m h_m(t,\lambda), \qquad m = 0,1,2,\cdots M$$

$$\hat{y}(t) = \sum_{m=0}^{M} a_m h_m(t,\lambda), \qquad 0 \le t \le t_w \qquad (2.5)$$

where t_w represents length of the time domain window and M is the order of the approximation. The matrix representation of (2.5) is shown in (2.6) where N is the number of time samples,

$$\underline{h}_t = \begin{bmatrix} h_0(t_1,\lambda) & h_1(t_1,\lambda) & \cdots & h_{M-1}(t_1,\lambda) & h_M(t_1,\lambda) \\ h_0(t_2,\lambda) & h_1(t_2,\lambda) & \cdots & h_{M-1}(t_2,\lambda) & h_M(t_2,\lambda) \\ \vdots & \vdots & \vdots & \vdots & \vdots \\ h_0(t_{N-1},\lambda) & h_1(t_{N-1},\lambda) & \cdots & h_{M-1}(t_{N-1},\lambda) & h_M(t_{N-1},\lambda) \\ h_0(t_N,\lambda) & h_1(t_N,\lambda) & \cdots & h_{M-1}(t_N,\lambda) & h_M(t_N,\lambda) \end{bmatrix}_{N\times(M+1)}$$

$$\underline{\hat{y}} = \begin{bmatrix} \hat{y}(t_1) & \hat{y}(t_2) & \cdots & \hat{y}(t_{N-1}) & \hat{y}(t_N) \end{bmatrix}^T \qquad N\times 1$$

$$\underline{a} = \begin{bmatrix} a_0 & a_1 & \cdots & a_{M-1} & a_M \end{bmatrix}^T \qquad (M+1)\times 1 \qquad (2.6)$$

Since usually $N>M+1$ in (2.6), $\underline{h}_t$ is overdetermined. As a result, the solution of the model parameters $\underline{a}$ in (2.6) is obtained through a least squares normal fit using the actual observations $y(t)$ and the time domain AHE matrix $\underline{h}_t$ from (2.5-6) in (2.7).

$$\underline{a} = \left(\underline{h}_t^T \underline{h}_t\right)^{-} \underline{h}_t^T \underline{y} \tag{2.7}$$

As an example of the time domain AHE polynomials, Fig. 2.2 show a set of curves generated by (2.5-6) with λ=1 and $\underline{a}$=1. Note that the time support increases as the order increases. This is in addition to the support provided by the time scale factor λ. The relationship between the time support required by the model and the model's order M is not only important for accuracy of the algorithm estimation of modes but also the degree to which $\underline{h}_t$ is well conditioned. A well conditioned $\underline{h}_t$ matrix allows the AHE estimator to successfully identify modes in low signal-to-noise ratio (SNR) measurements.

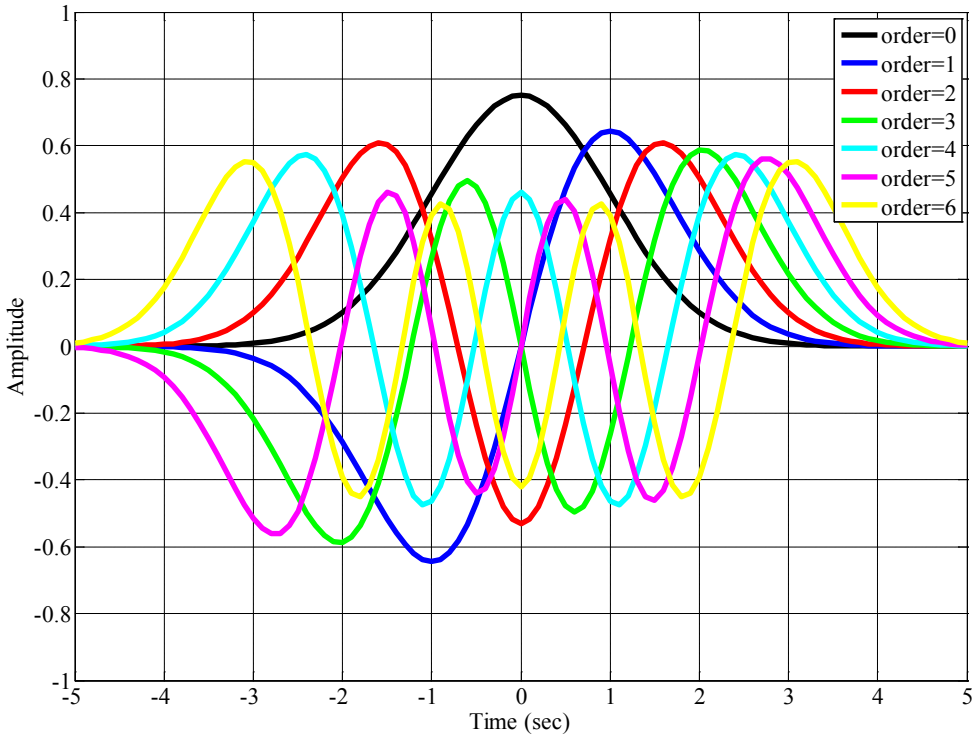

Fig. 2.2. Time domain AHE polynomials (2.5-6) with lambda=1.

2.2 AHE frequency domain approximation

With the model parameters $\underline{a}$ calculated using (2.7), all that is needed to estimate the spectrum of $y(t)$ is the Fourier transform of $\underline{h}_t$. In [65] the Fourier transform of (2.5-6) is computed with the relationship in (2.8)

$$\Psi\left(h_m(t,\lambda)\right) = \int_{-\infty}^{\infty} \left(h_m(t,\lambda)\right) \exp\left(-j2\pi f\right) dt$$

$$\Psi\left(h_m(t,\lambda)\right) = \int_{-\infty}^{\infty} \left(\frac{H_m\left(t/\lambda\right) \exp\left(-.5\left(t/\lambda\right)^2\right)}{\sqrt{2^m m!\lambda\sqrt{\pi}}} \right) \exp\left(-j2\pi f\right) dt$$

$$\Psi\left(h_m(t,\lambda)\right) = (-j)^m h_m(f,\mu) \tag{2.8}$$

where Ψ is the Fourier transform operator, f is frequency, $\mu=1/2\pi\lambda$, j is the complex operator and $h_m(f,\mu)$ is the frequency domain associate Hermite polynomial. The term μ is the frequency scale factor and provides support in the frequency domain. Splitting the transform of (2.8) into its real and imaginary components gives

$$\Psi_R\left(h_m(t,\lambda)\right) = \sum_{k=0}^{M\geq 2k} (-1)^k h_{2k}(f,\mu) \tag{2.9}$$

$$\Psi_I\left(h_m(t,\lambda)\right) = -\sum_{k=0}^{M\geq 2k+1} (-1)^k h_{2k+1}(f,\mu) \tag{2.10}$$

Using (2.8), the Fourier transform of the approximation $\hat{y}(t)$ in (2.5-6) is calculated substituting f for t and μ for λ

$$\Psi\left(\hat{y}(t)\right)=\Psi\left(\sum_{m=0}^{M}(-j)^m a_m h_m(t,\lambda)\right)$$

$$\Psi\left(\hat{y}(t)\right)=\hat{Y}(f)=\sum_{m=0}^{M}(-j)^m a_m h_m(f,\mu) \qquad 0\le f\le f_w \qquad (2.11)$$

where f_w is the frequency window width or bandwidth at P frequency samples. Splitting (2.11) into its real and imaginary components [68]

$$\hat{Y}_R(f)=\sum_{k=0}^{M\ge 2k}(-1)^k a_{2k} h_{2k}(f,\mu) \qquad 0\le f\le f_w \qquad (2.12)$$

$$\hat{Y}_I(f)=-\sum_{k=0}^{M\ge 2k+1}(-1)^k a_{2k+1} h_{2k+1}(f,\mu) \qquad 0\le f\le f_w \qquad (2.13)$$

An important point worth noting is that (2.5-6) and (2.12-13) all share the same $\underline{a}$ model parameters and has been studied previously in the field of circuit analysis [73]. Equations (2.12) and (2.13) are given in an expanded matrix form in (2.14) and (2.15), respectively.

$$\underline{\hat{Y}}_R=\underline{h}_f\,\underline{a}$$

$$\underline{h}_f=\begin{bmatrix} h_0(f_1,\mu) & 0 & -h_2(f_1,\mu) & \cdots & h_M(f_1,\mu)\\ h_0(f_2,\mu) & 0 & -h_2(f_2,\mu) & \cdots & h_M(f_2,\mu)\\ \vdots & \vdots & \vdots & \vdots & \vdots\\ h_0(f_{P-1},\mu) & 0 & -h_2(f_{P-1},\mu) & \cdots & h_M(f_{P-1},\mu)\\ h_0(f_P,\mu) & 0 & -h_2(f_P,\mu) & \cdots & h_M(f_P,\mu)\end{bmatrix}_{P\times(M+1)}$$

$$\underline{\hat{Y}}_R=\begin{bmatrix}Y_R(f_1) & Y_R(f_2) & \cdots & Y_R(f_{P-1}) & Y_R(f_P)\end{bmatrix}^T \qquad P\times 1$$

$$\underline{a}=\begin{bmatrix}a_0 & a_1 & \cdots & a_{M-1} & a_M\end{bmatrix}^T \qquad (M+1)\times 1 \qquad (2.14)$$

where P is the number of frequency samples, $\underline{h}_f$ is the frequency domain associate Hermite matrix and M is the order.

$$\underline{\hat{Y}}_I = -\underline{h}_f \times \underline{a}$$

$$\underline{h}_f = \begin{bmatrix} 0 & -h_1(f_1,\mu) & \cdots & (-1)^{M/2} h_{M-2}(f_1,\mu) & 0 \\ 0 & -h_1(f_2,\mu) & \cdots & (-1)^{M/2} h_{M-2}(f_2,\mu) & 0 \\ \vdots & \vdots & \vdots & \vdots & \vdots \\ 0 & -h_1(f_{P-1},\mu) & \cdots & (-1)^{M/2} h_{M-2}(f_{P-1},\mu) & 0 \\ 0 & -h_1(f_P,\mu) & \cdots & (-1)^{M/2} h_{M-2}(f_P,\mu) & 0 \end{bmatrix}_{P\times(M+1)}$$

$$\underline{\hat{Y}}_I = \begin{bmatrix} Y_I(f_1) & Y_I(f_2) & \cdots & Y_I(f_{P-1}) & Y_I(f_P) \end{bmatrix}^T \qquad P\times 1$$

$$\underline{a} = \begin{bmatrix} a_0 & a_1 & \cdots & a_{M-1} & a_M \end{bmatrix}^T \qquad (M+1)\times 1 \qquad (2.15)$$

Fig. 2.3 shows a set of curves for the real and imaginary Fourier transforms of $a_m h_m(t,\lambda)$ represented by (2.14-15) with μ=1 and $\underline{a}$=1.

It should be noted that except for the change of sign on the Fourier representations and substitution of variables, curves in Figs. 2.2 and 2.3 could be substituted for one another [65, 67-70]. This is due to the isomorphism property between the time and frequency domains inherent to the AHE polynomials. As noted in Chapter 1, [65] observed the similarity of the curves in Figs. 2.2 and 2.3 to truncated sine and cosine functions making them appropriate for harmonic analysis.

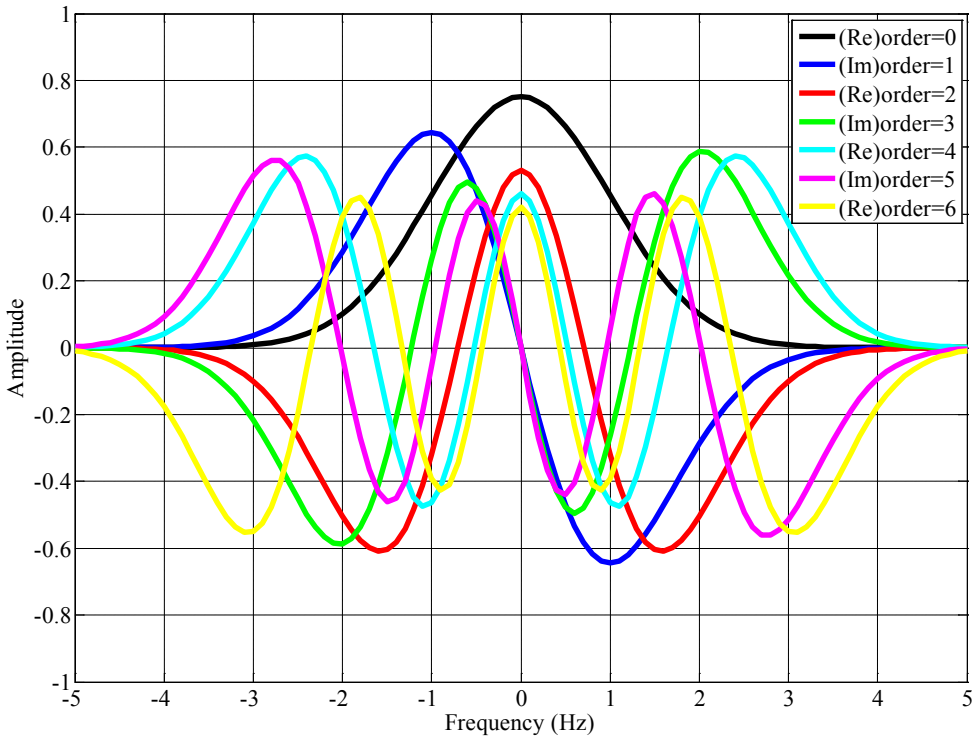

Fig. 2.3. Frequency domain AHE polynomials (2.14-15) with mu=1.

Isomorphism between $\hat{y}(t)$ and its Fourier transform also provides other useful properties that can be exploited for use with the AHE polynomials. Even and odd ordered polynomials in the time and frequency domains are also have even and odd symmetry, respectively, that can be seen in Figs. 2.2 and 2.3. The real portion of the Fourier transform of the approximated function $\hat{y}(t)$ is even while the imaginary portion has odd symmetry. Using actual power system measurements such as real power flow on a transmission line, the Fourier transform of the approximating function $\hat{y}(t)$ is a symmetric function [72]. Table 2.1 shows other properties of the AHE polynomials [67].

Table 2.1. Properties of the AHE polynomials [67].

Property	Description
Orthogonal	Both time and Fourier representation.
Expansion	Even=even ordered functions.
	Odd=odd ordered functions.
Fourier transform	Symmetric for a real signal.
Energy	The sum of squares of the model
	parameters (Parseval's Theorem).
Calculation	Order recursive $m \geq 2$ for both domains.
Time & frequency support	Support increases as the order M increases.

2.3 Time scale factor and order selection

Choice of the time scale factor λ affects the amount of support the AHE polynomials provide not only in the time domain but also in the frequency domain through the frequency scale factor μ. The AHE polynomials in (2.3-4) have finite time support due to the presence of $e^{-.5\left(t/\lambda\right)^2}$ for each term in the expansion up to 1+M elements. Conversely, the original Hermite polynomials in (2.1) do not have the $e^{-.5\left(t/\lambda\right)^2}$ term and, thus, have infinite time support. In addition, the original Hermite polynomials are not orthogonal to one another.

Selection of λ was initially proposed by mapping the range of available measurements to a scaled set of expansion terms [69-70]. Later, an iterative

calculation was employed by another set of researchers to determine not only λ but also the order M [68, 73]. As was mentioned before, the order of the approximation also affects the amount of support given in the time domain. In [74], the authors developed an empirical relationship (2.16) that defines the approximate bounds on the value of λ

$$\frac{t_w}{2\left(\sqrt{\pi M/1.7}+1.8\right)} < \lambda < \frac{\sqrt{\pi M/1.7}+1.8}{2\pi f_w} \tag{2.16}$$

where t_w is the expected time window, f_w is the expected bandwidth and M is the order of the approximation. An example calculation will show how the relationship in (2.16) is used. In estimating electromechanical modes in power system it is not uncommon to have large observation windows of 60 seconds or more and a bandwidth of 2 Hz giving a value of M=240 based on the work by [75]. With M=240, a scale factor range of $1.31<\lambda<1.82$ is obtained using (2.16). However as been noted before [69], a large value of M may cause the matrices in (2.5-6) and (2.14-2.15) to become ill-conditioned. Consequently, arbitrarily selecting an order and calculating a range of values of λ using (2.16) is probably not the most effective method of choosing both parameters. This is also true if the goal is to keep the system matrices well-conditioned so as to accurately estimate small signal modes in the presence of noise. As a result, a better way to calculate the order is needed that accounts for all these needs. Several methods have already been proposed and used by researchers in the field of spectral analysis.

Many methods for selecting order for spectral estimators involve some type of searches. In order to minimize the time necessary to perform the search,

knowing the desired criteria to end the search is critical. This is true for on-line as well as off-line small signal mode estimators. Fortunately, estimating model orders are only needed for parametric methods such as the ARYW technique, Prony's method and the AHE algorithm. Nonparametric methods like the HHT and O'Shea algorithms do not have this requirement. An incorrect order selection can have can negative impact the model and ultimately the estimators ability to identify the modes. If the chosen model order is too high the variance in the frequency domain increases with the potential of creating extraneous modes or line splitting. If the order is too low resolution is lost in the frequency domain and adjacent modes cannot be distinguished regardless of the size of the data record.

Some order selection techniques utilize an estimator's prediction error whether in the time or frequency domain. For example, the ARYW method using ACS estimates has a prediction error as shown below [84]

$$Error_{j+1} = Error_j\left(1-\left(a_{jj}\right)^2\right) \tag{2.17}$$

where a_{jj} are the model parameters. However, researchers have noted that the form of the error in (2.17) is still subjective since the function is monotonic and continues to decrease without reaching a minimum as the order approaches infinity. Also worth noting, the relationship in (2.17) also represents the energy in the predicted error and would also be applicable to the AHE algorithm due to the energy property noted in Table 2.1.

Several search methods to set criteria for selecting estimator orders have been developed. Some of the techniques or rules have been found to favor one model over another such as ARMA, AR, etc. Some methods work well for narrowband or lightly damped signals while other methods operate well for wideband or heavily damped signals. Many rules for choosing orders include a penalty factor as a result of representing too many terms in the model. Table 2.2 shows some of the more frequently used order selection criterion methods or rules. All the criterion rules in Table 2.2 can be used for selecting the order of an AR process. A model order m that is ultimately chosen is one that minimizes the criterion rule given the total number of samples N in the data window and the prediction error ε.

Table 2.2. Search order criterion rules.

Order selection criterion rules	Description
Akaike Final Prediction Error (FPE) Criterion	$FPE = \varepsilon\left(\frac{N+m+1}{N-m-1}\right)$
Akaike Information Criterion (AIC)	$AIC(m) = -2\ln(\varepsilon) + 2m$
Corrected Akaike Information Criterion (AIC_C)	$AIC_C(m) = -2\ln(\varepsilon) + \frac{2N}{N-m-1}N$
Bayesian information criterion (BIC), also known as the minimum description length (MDL) criterion	$BIC(m) = -2\ln(\varepsilon) + m\ln(N)$

Parzen's Criterion Autoregression Transfer (CAT) function	$CAT(m)=\left[\frac{1}{N}\sum_{j=1}^{m}\frac{N-j}{N\varepsilon_j}\right]-\frac{N-m}{N\varepsilon_m}$
Generalized information criterion (GIC)	$GIC(m)=-2\ln(\varepsilon)+(1+nu)m$ where nu = 2-6

The magnitude of the approximation order M in (2.5-6) and (2.14-15) not only determines the size of the AHE time and frequency domain matrices, but also the noise mitigation characteristic of the identification process. One choice for the order was suggested by the work of [75] and noted by [74] in which the minimum degree of a bandlimited and timelimited signal is defined as

$$M > 2t_w f_w \tag{2.18}$$

Although (2.18) provides a starting point for estimating the order of time and frequency approximations for the AHE algorithm based on window lengths, it can produce an excessively large order for the $\underline{h}_t$ and $\underline{h}_f$ matrices and thus forcing them to be less well-conditioned. It needs to be noted that (2.18) originates from the dimensionality theorem and only implies the size of the dimensional space that a system matrix may to span but not how well-conditioned the system matrix is constructed. For a 50 second time window and a 2 Hz frequency window, the estimate provided by (2.18) suggests that the order should be no smaller than 200.

Many researchers have suggested that a reduced rank matrix can provide an adequate approximation, under some basis, for an initially ill-conditioned matrix. Once determined, the effective rank of the original matrix would then be

used as the order of whatever model is being constructed. To determine the effective rank of the initial $\underline{h}_t$ matrix, the same researchers propose using only the largest singular values of the system matrix and discard the remaining singular values and their associated singular vectors.

Obtaining the singular values requires decomposing the matrix, which can be accomplished by several methods. One of the most popular direct decomposition methods is the use of SVD. After a SVD has been performed on the $\underline{h}_t$ matrix, the component matrices ($\underline{U}$, $\underline{\Sigma}$, $\underline{V}$) are produced. Equation (2.19) shows the component matrices of the $\underline{h}_t$ matrix,

$$\underline{U}\underline{\Sigma}\underline{V} = SVD(\underline{h}_t) \tag{2.19}$$

where $\underline{\Sigma}$ contains the singular values of $\underline{h}_t$ along its main diagonal, and $\underline{V}$ and $\underline{U}$ contain the eigenvectors of $\underline{h}_t^{\mathrm{T}}\underline{h}_t$ and $\underline{h}_t\underline{h}_t^{\mathrm{T}}$, respectively. By removing the weakest singular values from the $\underline{\Sigma}$ matrix, the model becomes less sensitive to noise in the input measurements and thus accomplishes one of the goals stated earlier. With the smallest singular values removed, the order of the approximation will change from M to K and the model parameters can be determined in a least squares sense

$$\underline{a} = \sum_{m=1}^{K} \frac{1}{\sigma_m} \underline{u}_m^T \underline{v}_m \underline{y} \tag{2.20}$$

where σ_m are the largest singular values of $\underline{h}_t$, $\underline{y}$ are the measurements, and $\underline{u}_m$ and $\underline{v}_m$ are the column vectors of $\underline{U}$ and $\underline{V}$, respectively.

To demonstrate an idea of how singular values can be used to select the rank and, thus the order of the matrix, Fig. 2.4 shows the singular values for a typical $\underline{h}_t$ matrix. In the figure, the singular value magnitudes are maximum at low orders of the $\underline{h}_t$ matrix. However, as the order transitions from 70 to 75 the magnitudes of the singular values drop dramatically. Researchers suggest that the effective rank of the matrix is defined by the decrease in singular value magnitudes in this area. As was mentioned before, researchers further suggest that a matrix with an order in this range is a suitable approximation to the original matrix [85]. Other methods have been proposed to identify the effective rank of a reduced order matrix using singular values and SVD.

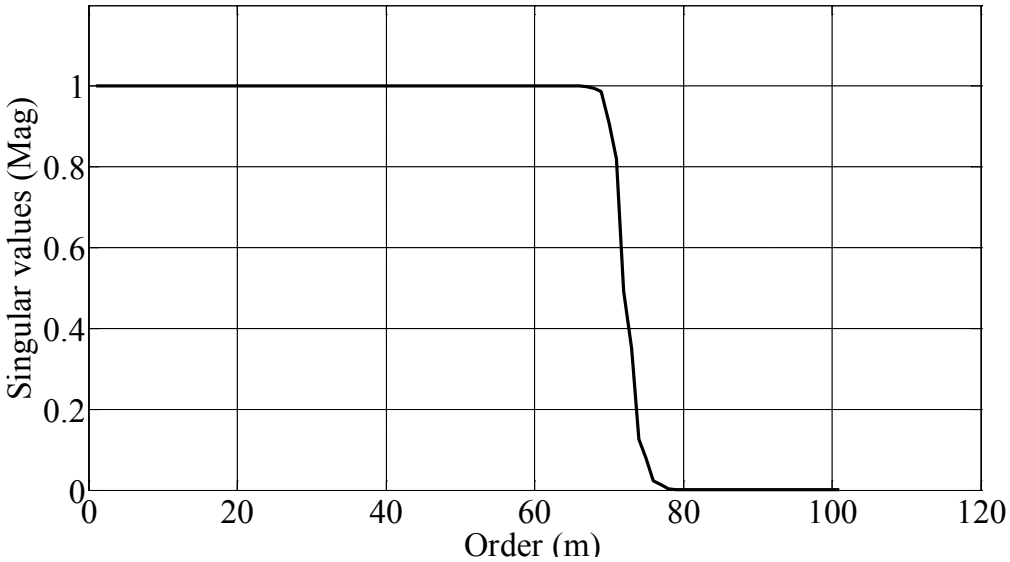

Fig. 2.4. Normalized singular values vs. order for an example $\underline{h}_t$ matrix.

One method for estimating the rank of a matrix has been proposed in [71] and later demonstrated in [82]. In these publications, the author calculates a ratio of l_2 norms as seen in (2.21)

$$v(r) = \frac{\left\| \underline{h}_t^{(r)} \right\|}{\left\| \underline{h}_t^{(m)} \right\|} = \left(\frac{\sigma_1^2 + \sigma_2^2 + \sigma_3^2 + \cdots + \sigma_r^2}{\sigma_1^2 + \sigma_2^2 + \sigma_3^2 + \cdots + \sigma_m^2} \right)^{1/2} \qquad 1 \le r \le m \qquad (2.21)$$

where r represents the largest singular value in the approximated matrix and m represents the order of the initial matrix. The largest value that the ratio $v(r)$ can acquire is 1 when $r=m$, or $\underline{h}_t^{(r)} = \underline{h}_t^{(m)}$. If the ratio is near 1 for low values of r relative to m, then the $\underline{h}_t$ matrix has a low rank or order, while for high values of r the $\underline{h}_t$ matrix has a high rank or order. In all cases, the norm ratio is bounded from 0 to 1. Fig. 2.5 shows a plot of $v(r)$ from (2.21) using the same matrix used in Fig. 2.4.

Fig. 2.5. Ratio of norm v(r) per order.

Another technique to identify the order of a reduced rank matrix while again using singular values was proposed by [83]. In the authors' technique, the condition number is calculated from the initial matrix using the relationship in (2.22)

$$k(\underline{h}_t) = \left\|\underline{h}_t\right\| \cdot \left\|\underline{h}_t^{-1}\right\| \tag{2.22}$$

where $k(\underline{h}_t)$ represents the condition number of the $\underline{h}_t$ matrix. As admitted by the authors in [83], the condition number in (2.22) can be difficult to calculate since it requires the computation of the inverse of the original matrix. If the original matrix was severely ill-conditioned or nearly singular, finding an inverse of the system matrix may be a challenge. An estimate for the condition number in (2.22) is given in (2.23) and requires only the SVD algorithm to be performed. The ratio of the largest and smallest singular values provides an approximation of the condition number for the original matrix.

$$k(\underline{h}_t) \cong \frac{\sigma_{\max}}{\sigma_{\min}} \tag{2.23}$$

As the condition number increases from 1, the effective rank is noted and becomes the estimate for the order of the original matrix.

An important difference between the condition number based method for estimating rank and the norm ratio method described earlier are the bounds for each method. For the condition number technique, the range is only bounded on one side and extends from 1 to infinity, with 1 indicating a well conditioned matrix. This approach provides a clearer assessment than the rank estimation found in the norm ratio technique (Fig. 2.5). Fig. 2.6 shows the effect on the condition number as the order increases for the same matrix used in Fig. 2.4.

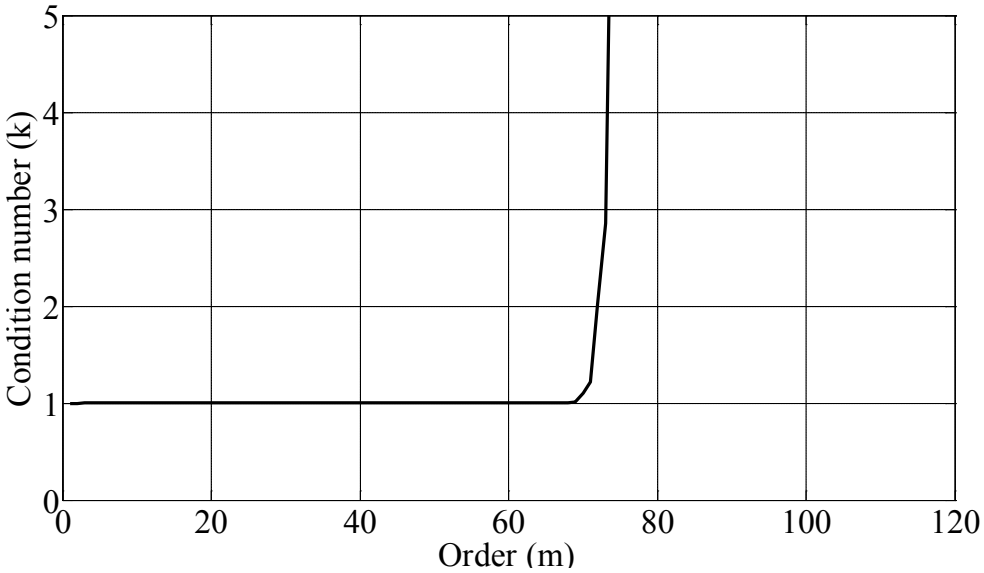

Fig. 2.6. Condition number (k) per order.

In [71], the author concedes that for the norm ratio based method choosing a value for r to position $v(r)$ close to one is somewhat subjective and is based on experience and experimentation. This can also said to be true for the condition number technique.

Section 2.2 and 2.3 state that a unique feature of the AHE functions is that the order of the approximation provides both frequency and time domain support. This can be verified by reviewing Figs. 2.2 and 2.3 such that a higher order provides greater window length or support. The risk for using a higher order for greater support is the possible generation of an ill-condition $\underline{h}_t$ matrix. On the other hand, if the AHE estimator is intended to be used in low SNR environments and this requires avoiding use of an ill-conditioned system matrix. As discussed previously, the three methods that estimate the rank of the reduced system matrix by selecting the span between the largest and smallest singular values will

produce a noise tolerant model. Unfortunately, all three singular value-based rank selection methods chose the order somewhat arbitrarily and, thus, require some previous experience by the user. In order to satisfy the requirements of selecting an order that gives adequate time and frequency support and creates a system matrix that is noise tolerant, a compromise needs to be reached in the estimation of the order.

If (2.16) is solved in terms of the order M assuming a constant time scale factor λ, the relationship in (2.24) is defined. Using the value for the order M, the time scale factor is calculated in (2.25). The procedure for calculating both the order and the time scale factor is outlined in Fig. 2.7.

$$M = \frac{1.7}{\pi}\left(\sqrt{\pi t_w f_w} - 1.8\right)^2 \tag{2.24}$$

$$\lambda = \frac{t_w}{2\left(\sqrt{\pi M / 1.7} + 1.8\right)} \tag{2.25}$$

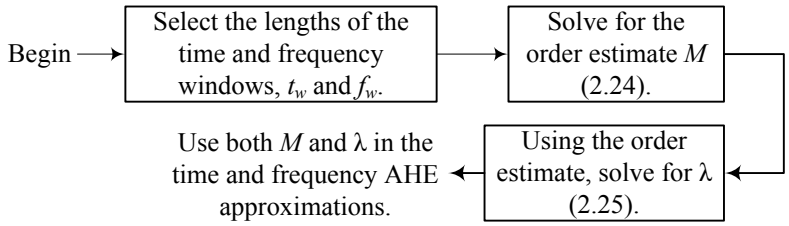

Fig. 2.7. Calculation of order and time scale factor.

According to [74], both (2.18) and (2.24) determine an order for the AHE polynomials that provide adequate support for approximating for time and frequency domains. However, an important objective of this thesis is to also develop a noise tolerant estimator. To find which order estimator is better for this

purpose, the l_2 norm condition number for $\underline{h_t}$ was calculated for increasing values of order using the methods of (2.18) and (2.24). Fig. 2.8 shows the percent difference between the condition numbers from the two methods. The figure shows that the method of (2.24) generates a lower condition number than the technique of (2.18).

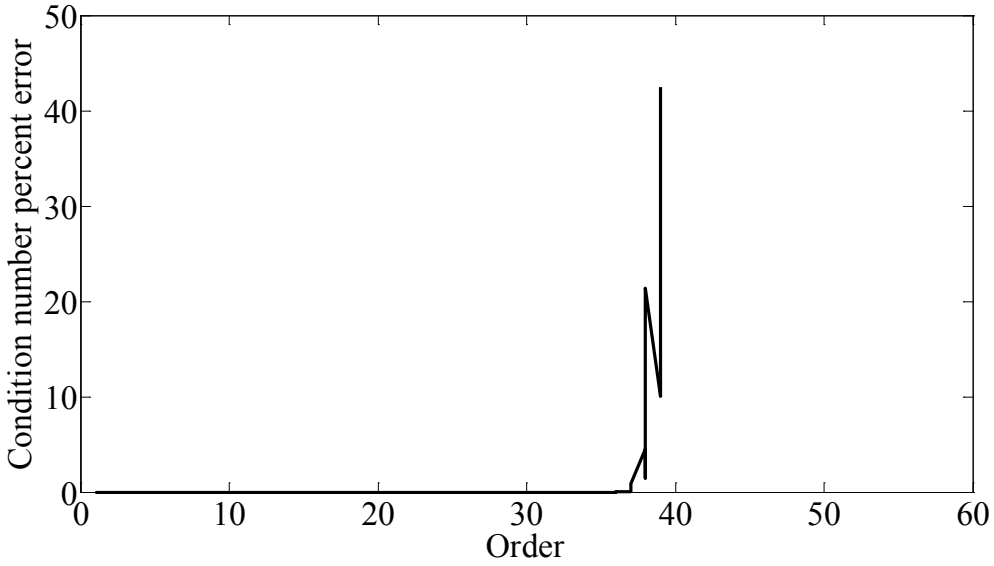

Fig. 2.8. Condition number percent error vs. order.

The method of (2.24) is the technique employed in the remainder of this thesis.

2.4 Mode identification and damping estimation

Once the model parameters $\underline{a}$ have been determined and the spectrum extrapolated, the estimated modes are identified by locating the peaks in the magnitude response using (2.26), where D is the maximum number of peaks in the spectrum. For the rest of this section, the reference to f_i is as an estimated modal frequency in the algorithm.

$$f_i = \arg\max\left(\left|\hat{\underline{Y}}(f)\right|\right) \qquad i = 1,2,3,\ldots D \qquad (2.26)$$

Next, the damping associated with the estimated frequencies is calculated using a modified sliding window technique. The method used here evolved from a technique by the authors of [76]. Using two time domain windows (Fig. 2.9), the researchers of [76] used the discrete Fourier transform definition to calculate the magnitudes of the peaks identified using (2.26) from two windows (Fig. 2.10). Using the relationship in (2.27), the damping factor of the mode was estimated

$$\alpha_i = \left(\frac{1}{T_G}\right)\ln\left(\frac{\left|F(2\pi f_i)\right|_{t_2}^{t_2+t_w}}{\left|F(2\pi f_i)\right|_{t_1}^{t_1+t_w}}\right) \qquad (2.27)$$

where t_1 and t_2 are the start times of the first and second windows respectively, T_G is the difference in the start times t_2–t_1, t_w is the window width and $|F(2\pi f_i)|$ is the magnitude of the spectrum at the frequency f_i.

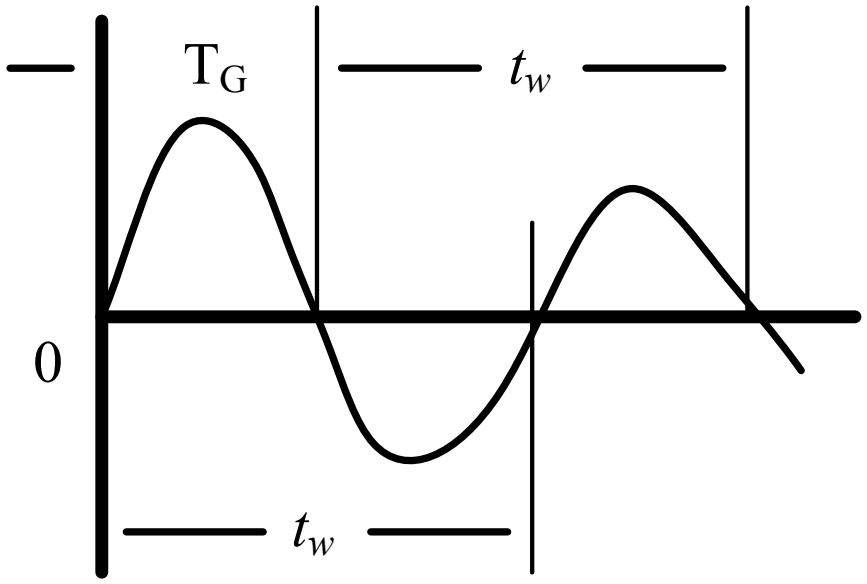

Fig. 2.9. Sliding time domain windows.

In the calculation of (2.26) and (2.27), the authors assumed the signal to be stationary in order to apply a linear approximation to solve for the damping factor. The values of $|F_A|$ and $|F_B|$ are the Fourier spectrum magnitudes representing their respective time domain windows.

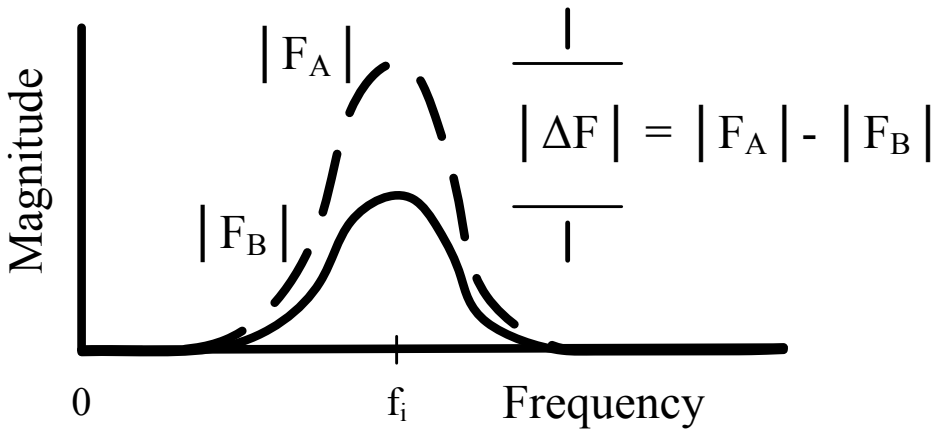

Fig. 2.10. Fourier spectrum of two time domain windows.

At a given frequency, the Fourier spectrum magnitude represents the square root of the signal's energy. As a result, if the magnitude of the peak decreases from the first to the second window the energy of the mode is decreasing and the mode is deemed to be positively damped. Stated another way, a decrease in the Fourier magnitude from the first to the second window represents a stable mode located in the left side of the pole-zero plane. If the peak increases from one window to the next, damping is judged to be negative and the mode exists in the right side of the pole-zero plane.

The authors in [76] noted that the size of t_w is restricted to be equal to or greater than integer multiples of the period of the mode f_i. Secondly, the

difference in the starting times of the two windows T_G also is required to be an integer multiple of the period of *f*. as well. These two assumptions are necessary to derive the relationship of (2.27) as used by the authors. However, these assumptions also impose restrictions on the size of the window along with the start times between the windows. In [77], this author proposes using a tapered window in lieu of a rectangular window used in [76]. The benefits of the tapered window are that it reduces leakage effects that are produced by the rectangular window and thus removes the restrictions on the start times imposed by [76]. However to accommodate noise in the signal, the procedure outlined in [77] requires an iterative solution.

The author in [77] updated his methodology [78-79] to include linear prediction using frequency samples instead of the time measurements themselves. Prior to this research, the author proposed essentially non-parametric methods using only two sliding windows. In his new version, the author of [78-79] uses a unique combination of non-parametric and parametric tools for electromechanical damping estimation. Using sliding tapered windows from his early research, a description of the algorithm is given below. If the complex signal within a noiseless measurement is described as

$$y(t) = Ae^{(j\omega_i + \alpha_i)t} \qquad t = 0, \ldots, t_w \qquad (2.28)$$

where A is the amplitude, ω_i is the angular frequency, and α_i is the damping factor. The first step in the process is to downshift to the baseband, or f_i, using (2.29).

$$y_d(t) = y(t)e^{-j2\pi f_i} \tag{2.29}$$

This procedure removes the oscillatory component of (2.28) and, assuming $2\pi f_i=\omega_i$, leaves an approximation of a damped exponential (2.30).

$$y_d(t) \cong Ae^{\alpha_i t} \tag{2.30}$$

In the case of a real signal

$$y(t) = Ae^{\alpha_i t}\cos(2\pi f_i t) \qquad t = 0,\ldots,t_w \tag{2.31}$$

$$\begin{aligned} y_d(t) &= y(t)\cos(2\pi f_i t) \\ &= Ae^{\alpha_i t}\left(\frac{1}{2}+\frac{1}{2}\cos(4\pi f_i t)\right) \qquad t = 0,\ldots,t_w \end{aligned} \tag{2.32}$$

The first term in the parenthesis of (2.32) indicates that evaluating the spectrum of $y_d(t)$ at f=0 will provide the damping information from the original time series in (2.31) without the oscillatory component, and the artifacts represented by the second term can be ignored. As an example of the downshifting effect and using α_i=-.005 s^{-1} and f_i=1.0 Hz in (2.31), the spectrums for $y(t)$ and $y_d(t)$ are estimated as shown in Fig. 2.11.

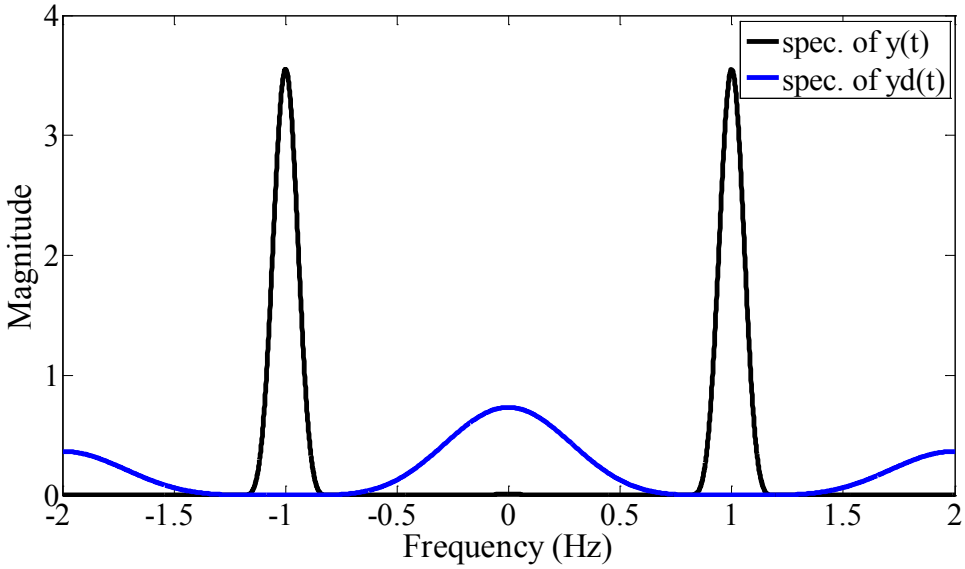

Fig. 2.11. Estimated spectrums for $y(t)$ and $y_d(t)$.

In this thesis, the AHE polynomials are used to approximate time measurements representing (2.31). Next, the spectrum is estimated and critical frequencies are identified. With the frequencies located, the AHE polynomials are now fitted to the downshifted measurements generated from (2.32) to generate a new set of model parameters using a sliding window. For each subwindow, its spectrum is estimated and the magnitude of $|\underline{\hat{Y}}_{f0}|$ at f=0 is recorded. A vector of frequency samples is created and used within a linear predictor algorithm. The type of linear predictor used in the AHE algorithm is a forward predictor, which is also an FIR filter (2.33).

$$\begin{bmatrix} \left|\hat{Y}_{f0}(l+1)\right| \\ \left|\hat{Y}_{f0}(l+2)\right| \\ \vdots \\ \left|\hat{Y}_{f0}(d)\right| \end{bmatrix} = \begin{bmatrix} \left|\hat{Y}_{f0}(l)\right| & \ldots & \left|\hat{Y}_{f0}(0)\right| \\ \left|\hat{Y}_{f0}(l+1)\right| & \ldots & \left|\hat{Y}_{f0}(1)\right| \\ \vdots & . & \vdots \\ \left|\hat{Y}_{f0}(d-1)\right| & \ldots & \left|\hat{Y}_{f0}(d-l-1)\right| \end{bmatrix} \begin{bmatrix} a_{f0} \\ a_{f1} \\ \vdots \\ a_{fl} \end{bmatrix} \tag{2.33}$$

where d is the shift index, l is the order of the predictor, $\underline{a_f}$ are the predictor model parameters and $|\underline{\hat{Y}_{f0}}|$ is the estimated spectrum of the downshifted measurements. As an alternative to (2.33), other linear predictors can be used for estimating the model parameters. A combination of forward or backward linear predictors can be substituted for the simple predictor in (2.33) [31]. Also, depending on whether the data is windowed, pre-windowed or non-windowed also affect the type of predictor that can be selected as well as its overall performance.

The damping factor is calculated by solving for the roots of the characteristic equation of the linear predictor and provides an estimate of the true damping factor in (2.28) or (2.31). A new estimate of the frequency is now computed (2.34)

$$f_{iu} = f_{id} + f_i \tag{2.34}$$

where f_{iu} is the "upshifted" frequency estimate from the linear predictor that replaces the original estimate f_i. A summary of the estimation process is given in Fig. 2.12. The process is repeated until all the relevant modes have been identified and their damping levels estimated.

2.5 Summary of the proposed AHE algorithm

An outline of the AHE algorithm is shown in Fig. 2.13. The order of the time and frequency domain approximations is set using the relationship in (2.24), and the value of λ is calculated using (2.25). Next, the $\underline{h_l}$ matrix is calculated. The coefficients in (2.5-6) are solved in a least square sense using the pseudo-inverse formula of (2.7) with the order M and time scale factor λ. With the $\underline{a}$

coefficients found, the approximation of the spectrum is calculated (2.14-15) and the significant frequency estimates are identified (2.26). For each significant mode, the original observation is downshifted with the baseband frequency estimate f_i (2.29) or (2.31) and the model coefficients are recalculated using the new time signal. The spectrum is estimated again and the magnitude of the downshifted frequency response $|\underline{\hat{Y}}_{f0}|$ at f=0 is recorded. This is repeated for a set of sliding windows of length n_d samples until a vector is generated. The vector is applied to a linear predictor (2.33) and the downshifted frequency f_{id} and damping factor estimates are calculated by solving for the roots of the characteristic equation of the linear predictor. The downshifted frequency estimate is added to the original estimate f_i to obtain a new estimate f_{iu} (2.34). This process is repeated for all the significant modes found from the original spectrum approximation.

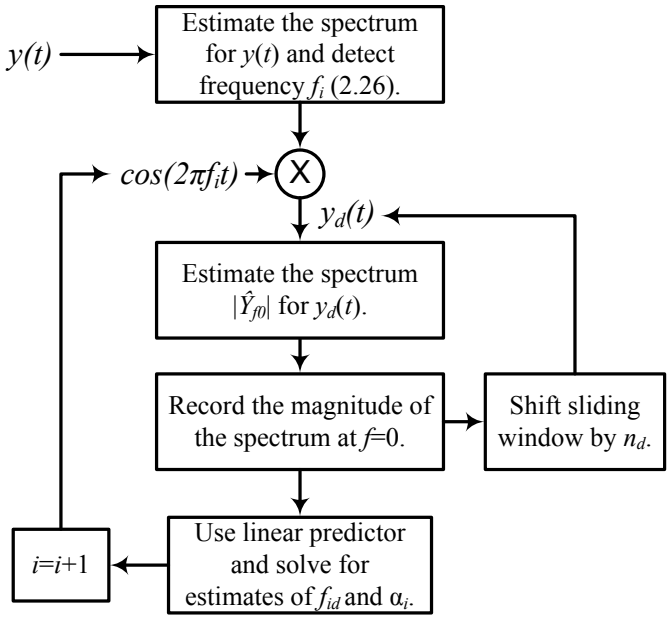

Fig. 2.12. Damping estimation process for a real measurement [78-79].

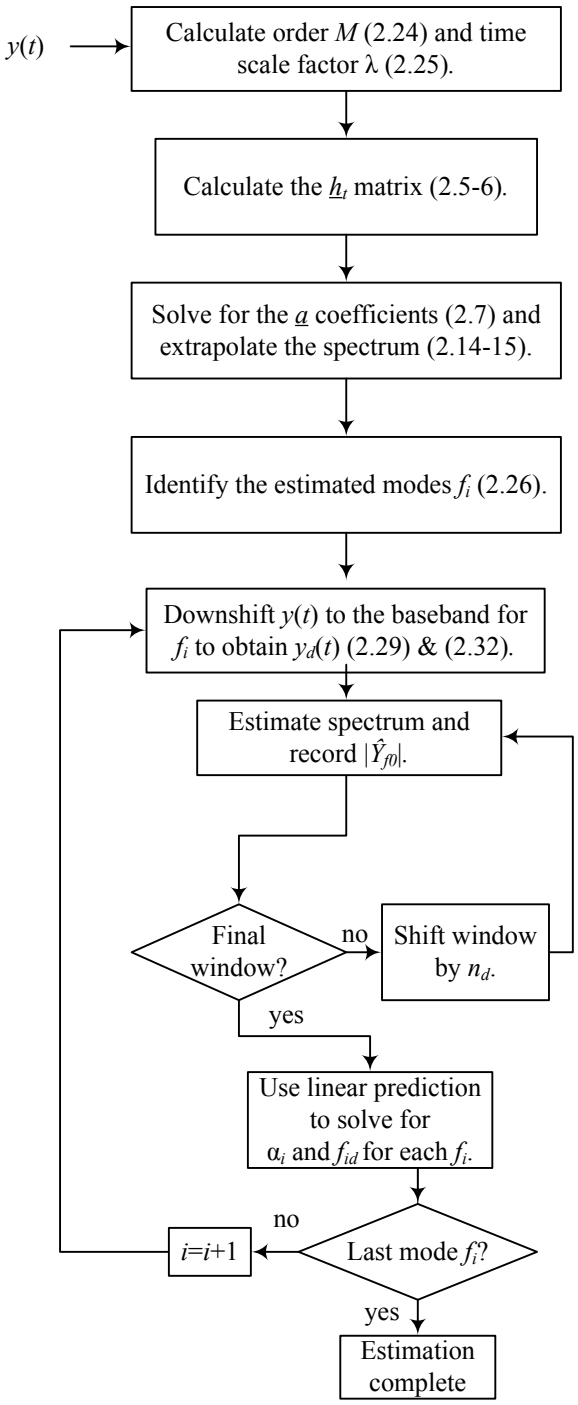

Fig. 2.13. AHE algorithm for estimating small signal modes.

2.6 Example calculation of the AHE algorithm

To demonstrate the proposed AHE algorithm as described in this chapter and shown in Fig. 2.13, an example estimation is performed. The simulated rotor angle of Fig. 1.1 is assessed and the input and output results are obtained. A graphical user interface (GUI) was written using MATLAB that incorporated the AHE algorithm along with other spectral estimators. The GUI allows the user to select the sampling frequency, the AHE polynomial order, the LP order and the selection of an optional tapered window among other items. The estimated spectrum can be displayed along with the output of the LP filter. Fig. 2.14 shows a view of the GUI written for this thesis.

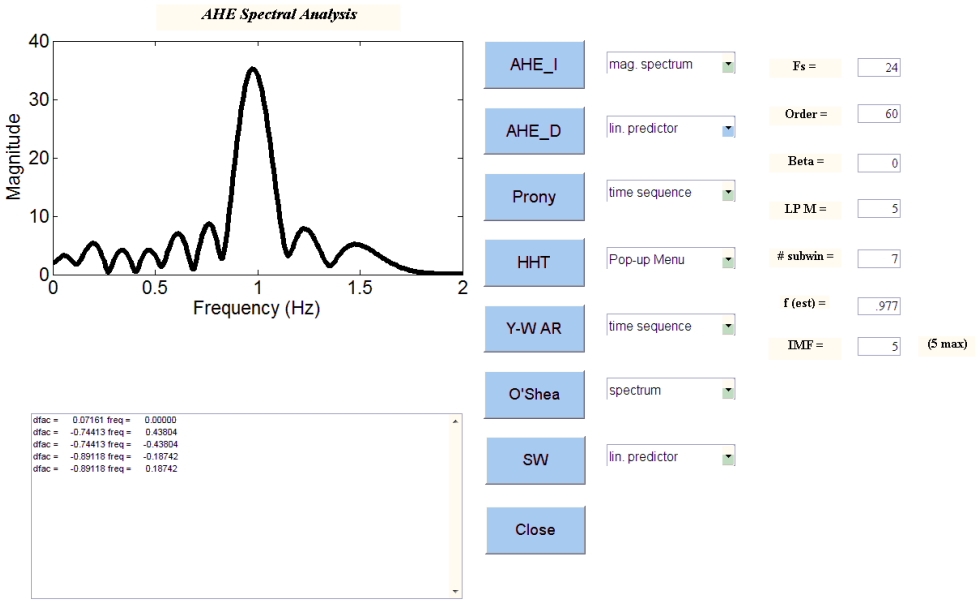

Fig. 2.14. Graphical User Interface with the AHE algorithm.

A simulated input measurement of a generator rotor angle was created using a commercial transient stability program and was sampled at 240 Hz and decimated to 24 Hz over a window of approximately 10 seconds. This simulated

measurement was applied to the algorithm in Fig. 2.13. Next, the order M was calculated to be 20 using (2.14) and the time scale factor λ was calculated to be 0.627 using (2.25). The matrix $\underline{h}_t$ was calculated and the model coefficients $\underline{a}$ were determined using (2.7). With the model coefficients known, the model estimate of the time domain output $\hat{y}(t)$ and the estimated spectrum $|\hat{Y}(f)|$ were calculated (2.14-15). With the spectrum estimated, the modes of the model can be identified using (2.26). Table A.1 in Appendix A contains the original simulated measurement, the model time domain estimate, the estimated spectrum and the model coefficients. The estimated spectrum $|\hat{Y}(f)|$ for identification of the mode can be seen in Fig. 2.14. A mode at approximately .98 Hz was identified from the estimated spectrum.

With the mode found, the original signal is downshifted to the baseband or estimated modal frequency and the model coefficients re-determined. The estimated spectrums for six windows were recalculated and the spectrum magnitude $|\underline{\hat{Y}}_{f0}|$ at f=0 was recorded. With the values of $|\underline{\hat{Y}}_{f0}|$ known, a fifth order forward linear predictor was used to estimate the damping. Results from the linear predictor show the .98 Hz mode has a negative damping ratio of approximately 1.17%. Table A.2 in Appendix A lists the values of the seven estimated spectrums along with the values of used in the LP filter to estimate damping.

Chapter 3

OTHER ESTIMATION METHODS

3.1 Introduction

In Chapter 1 many estimation methods were discussed in terms of their abilities to accurately predict the components of power system modes. In this chapter, four techniques are reviewed in detail that will be used in this thesis as a comparison to the AHE method. Two of these methods are parametric estimation techniques while one is a Fourier based non-parametric method and the last estimator is a combination of parametric and non-parametric methods. The reason these four estimators were chosen to have their capabilities compared with the AHE algorithm in this thesis is that all four algorithms have been successfully utilized in the estimation of small signal stability in power systems.

The first method to be review is the basic least squares Prony's method. Initially proposed by Baron de Prony in 1795 to study the relationship between pressure and volume in gases, this estimation technique has only been used in the last 25 years as a method to estimate power system modes for small signal events. The other parametric method is based on the Yule-Walker equations. For this thesis, the Yule-Walker method will employ ACS estimates compiled from measured values. The non-parametric method has been recently proposed for predicting the instantaneous frequency and damping components of power system modes and is referred to as the Hilbert-Huang Transform (HHT) estimation method. As the name implies, a HHT analysis uses the Hilbert transform as well

as empirical mode decomposition (EMD) to separate the different modes within the original measurements. For the last method, the estimator used here that has both parametric and non-parametric characteristics is an older sliding window method referred hereto as the O'Shea sliding window method. Although both the AHE algorithm and the O'Shea method rely on simple linear predictors for determining damping levels, they utilize different means for generating the spectrum approximations for identifying the frequency components of the modes and creating the downshifted spectrums used by the LP. All four of these methods were briefly discussed in Chapter 1, but will be discussed here in more detail.

3.2 Least squares Prony's method

As explained earlier, the basic least squares Prony's method used today is a parametric method that employs block processing of measurements into an exponential model. The steps to perform the least squares Prony's method were given in Fig. 1.3. Because it does utilize block processing, the method is generally not appropriate for non-stationary signals and steps need to be taken to isolate the measurements into a non-time varying form to use Prony's method. The order selection discussed in the literature is usually in the range of $N/3$ to $N/2$ [27-28], where N is the number of samples in the window.

The exponential model used in basic Prony's analysis is shown in (3.1) in the continuous time form

$$\hat{y}(t) = \sum_{k=1}^{M} B_k e^{s_k t} \qquad t = 0, \ldots, t_w \tag{3.1}$$

where s_k are the continuous time eigenvalues as defined in (1.4), M is the order, T_s is the sampling period and B_k are the complex residues. A more convenient form of (3.1) is the discrete time model shown in (3.2)

$$\hat{y}[j] = \sum_{k=1}^{M} B_k z_k^j \tag{3.2}$$

where z_k are the discrete time poles of the estimated response as defined as (3.3). Its important to note that the complex residues contain the information how the modal information is allocated along the state $y(t)$.

$$z_k = e^{s_k T_s} \tag{3.3}$$

To solve for the poles in (3.2) and thus completing steps one and two of Fig. 1.3, various methods can be employed. However, the simplest way to obtain the poles is to form a forward linear predictor using solely the measurements $y(t)$ as opposed to the linear predictor model in (2.33) that uses frequency samples. The closed form of the linear predictor is shown in (3.4) and the matrix form is shown in (3.5).

$$y(j) = \sum_{k=1}^{M} a_k y(j-k) \tag{3.4}$$

$$\begin{bmatrix} y(M+1) \\ y(M+2) \\ \vdots \\ y(N) \end{bmatrix} = \begin{bmatrix} y(M) & \ldots & y(0) \\ y(M+1) & \ldots & y(1) \\ \vdots & . & \vdots \\ y(N-1) & \ldots & y(N-M-1) \end{bmatrix} \begin{bmatrix} a_0 \\ a_1 \\ \vdots \\ a_M \end{bmatrix} \tag{3.5}$$

Its worth noting here that there is no requirement to use the simple linear predictor in (3.4-5) to find the poles of the measurement. In fact, more complex linear predictors can be used in place of (3.4-5), such as a backward predictor or a combination of forward and backward predictors as found in the covariance and modified covariance spectral estimators. As was mentioned before, actual measurements $y(t)$ can be replaced with ACS estimates. At this point, the characteristic equation of (3.4-5) is formed in the least squares Prony's method and the roots determined.

In the last two steps, the roots z_k are inserted into the exponential model of (3.2). The complex residues are solved by taking product of the inverse of a Van Der Monde matrix containing the poles and a vector containing the measurements. With the residues found, the model is complete. At this point, an estimate of the measurement, the variance, and the spectrum estimate can be obtained. In addition, the damping α_k and frequency f_k components of the mode as well as the phase θ_k of the individual modes can be predicted using the values in (3.6-8). The amplitude of the mode is equal to the absolute value of the complex residues, B_k.

$$\theta_k = \arctan\left(\frac{\mathrm{Im}(B_k)}{\mathrm{Re}(B_k)}\right) \tag{3.6}$$

$$\alpha_k = \frac{\ln(z_k)}{T_s} \tag{3.7}$$

$$f_k = \frac{1}{2\pi T_s}\arctan\left(\frac{\mathrm{Im}(z_k)}{\mathrm{Re}(z_k)}\right) \tag{3.8}$$

3.3 AR Yule-Walker (ARYW) estimation method

In Chapter 1 the Yule-Walker method was introduced in regards as another technique for estimating electromechanical or power system modes. In this section the equations are provided in detail for using this method for computation comparison. The ARYW estimation method assumes that an autoregressive process can be estimated by calculating the model parameters for an all pole estimator. These parameters are found by assembling an estimate of the ACS matrix and finding the product of its inverse and the ACS vector, as seen in matix form (3.9)

$$\underline{a} = -\underline{R}^{-}\underline{r} \tag{3.9}$$

where $\underline{R}$ is the ACS estimate matrix and $\underline{r}$ is the ACS estimate vector. Like Prony's method in section 3.2, the data manipulation for the ARYW normal equations includes block processing.

As shown in Fig. 1.4, the first step in the ARYW estimation method is to select a maximum lag or order *M* for the estimator. The methodology here is similar to the order selection method used for the Prony estimation method discussed in the previous section. In addition, the order selection rules such as AIC, BIC and FPE described in Table 2.2 can be used here as well. Next, the ACS estimates are generated using (3.10)

$$\breve{r}(m) = \frac{1}{N}\sum_{k=0}^{N-m-1} y(k+m)y^{+}(k) \qquad 0 \le m \le N-1 \tag{3.10}$$

where m is the lag index, N is the number of samples, + is the complex conjugate operator and $y(k)$ are the data measurements. Only the positive ACS estimates need to be determined since the property holding that real positive estimates with positive lags equal complex conjugate estimates for negative lags holds (3.11). Also, biased ACS estimates are used in lieu of unbiased estimates in order to force the ACS estimate matrix to be positive semi-definite and thus ensuring that a solution to (3.9) exists.

$$\breve{r}(m) = \breve{r}^{+}(-m) \tag{3.11}$$

With the ACS estimates calculated, the values are used to populate the ACS estimate matrix $\underline{R}$ and estimate vector $\underline{r}$ in the matrix form of (3.9) as well as (3.12). By inspection, the ACS estimate matrix is Toeplitz. Also because the positive lag elements equal the negative conjugate lag elements, the matrix is Hermitian or conjugate symmetric. The model parameters $\underline{a}$ are then solved either in a least squares sense or using fast algorithms such Levinson or Levinson-Durbin. This completes the model building process for the ARYW estimation method.

$$\begin{bmatrix} a_1 \\ a_2 \\ a_3 \\ \vdots \\ a_M \end{bmatrix} = -\begin{bmatrix} \breve{r}(0) & \breve{r}(-1) & \breve{r}(-2) & \cdots & \breve{r}(1-M) \\ \breve{r}(1) & \breve{r}(0) & \breve{r}(-1) & \cdots & \breve{r}(2-M) \\ \breve{r}(2) & \breve{r}(1) & \breve{r}(0) & \cdots & \breve{r}(3-M) \\ \vdots & \vdots & \vdots & \vdots & \vdots \\ \breve{r}(M-1) & \breve{r}(M-2) & \breve{r}(M-3) & \cdots & \breve{r}(0) \end{bmatrix}^{-1} \begin{bmatrix} \breve{r}(1) \\ \breve{r}(2) \\ \breve{r}(3) \\ \\ \breve{r}(M) \end{bmatrix} \tag{3.12}$$

3.4 Hilbert-Huang Transform estimation with Empirical Mode Decomposition

A method briefly described in Chapter 1 that is becoming increasingly popular in estimating small signal modes is based on the Hilbert transform and is collectively referred to as the HHT estimator. In addition, since this method calculates the instantaneous frequency and damping components of a small signal mode as a time domain function, it holds the promise of being used in an on-line prediction method. Unlike the Fourier transform that converts a time domain function into the frequency domain, the Hilbert transform of a time domain signal remains in the time domain

$$H\left[x(t)\right] = \frac{1}{\pi t} * x(t) \tag{3.13}$$

where * represents the linear convolution operator. Assume that $x(t)$ is an exponentially damped sinusoid given in (3.14).

$$x(t) = Ae^{\alpha_i t}\cos(\omega_i t + \delta) \tag{3.14}$$

The objective in using the HHT method is to first form the analytic function $X_A(t)$, in (3.15), as the complex sum of the original signal and the Hilbert transform of the original signal.

$$X_A(t) = x(t) + jH\left[x(t)\right] \tag{3.15}$$

To identify the damping associated with $x(t)$, the derivative of the function $\ln(X_A(t))$ (3.16) is calculated. To identify the frequency component of the mode, the derivative of the phase of the analytic function $X_A(t)$ (3.17) is computed.

$$\ln\left(\left|X_A(t)\right|\right) = \alpha_i t + \ln(A) \tag{3.16}$$

$$\angle X_A(t) = \omega_i t + \delta \tag{3.17}$$

The method as outlined so far will work for disturbances with a single mode. However, many actual power system disturbances contain more than one mode and these will need to be isolated. To accomplish isolating modes in order to use the HHT method, empirical mode decomposition (EMD) is executed to separate multiple signals into a single mode individual signal or intrinsic mode function (IMF). A limitation of using EMD as proposed is that it can only effectively separate signals that are more than an octave apart. Under this scenario instead of producing a single frequency component, the standard EMD algorithm produces a multimodal signal that cannot be easily processed by the HHT algorithm. The problem is compounded by the fact that if the prior or higher frequency IMF is not completely isolated, the other lower frequency IMF's will be contaminated. To overcome this constraint, masking signals are used as proposed by some researchers. A FFT based empirical masking method is one technique that has been proposed and demonstrated [86]. The following steps highlight the FFT based masking approach:

- Perform a FFT analysis to identify all the frequencies in the original signal.
- Build masking signals starting from the highest frequency component.

- Reconstruct IMF's using one or more masking signals depending on the frequency distance between the highest two frequencies and their magnitudes.
- For each successfully recreated IMF, execute the HHT algorithm to identify the damping and frequency components for that mode.

Other masking methods have also been proposed by researchers based on energy within the mode.

Once the individual components of the original signal have been removed, the combination of the original EMD and the HHT algorithms are used as before. Fig. 3.1 shows an overview of the HHT estimation method with EMD and masking.

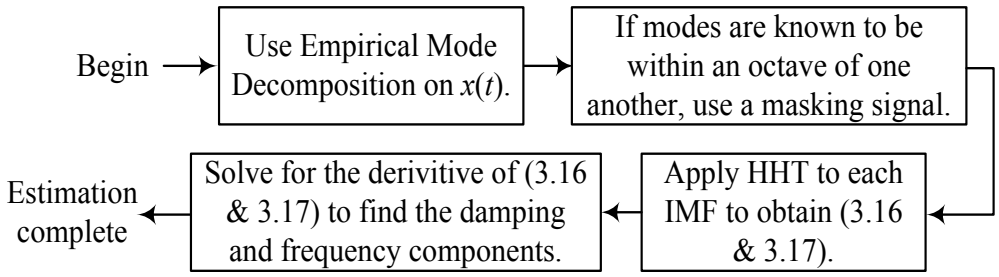

Fig. 3.1. Summary of the HHT algorithm.

3.5 O'Shea sliding window estimator

As explained in previous chapters, the O'Shea sliding window estimator was derived from another sliding window algorithm proposed by [76]. Unfortunately, the previous method imposed restrictions on the location and size of the subwindows in order to ease the calculation of the damping factor. The O'Shea estimator brought two innovations to the other method, with the most

important change being the use of a LP to estimate damping factors in lieu of single formula. Once the frequencies were identified using the FFT, the original signal was downshifted thus removing a particular oscillatory component of the signal and allowing the linear predictor to find the modes damping level. Fig. 3.2 shows the O'Shea sliding window estimator with linear prediction. Some of the relationships in the O'Shea method are used in the AHE algorithm.

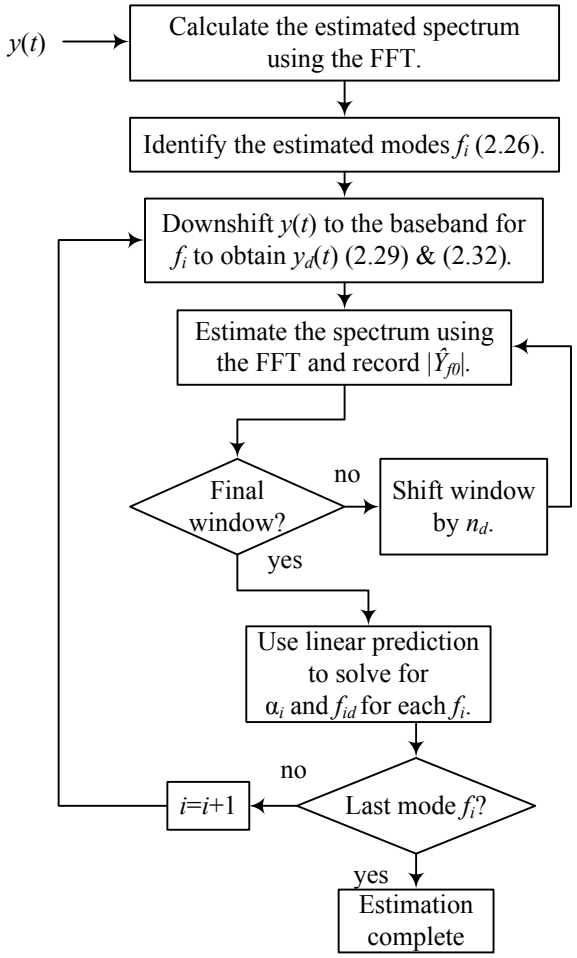

Fig. 3.2. O'Shea sliding window algorithm.

Chapter 4

AHE COMPARATIVE ASSESSMENT

4.1 Single and multi-mode comparison

To assess the ability of the AHE algorithm described in Chapter 2 a number of comparisons were performed using four other identification methods reviewed in Chapter 3. In this section, an assessment is made using simple noiseless single and multi-mode functions. A Prony analysis, an autoregressive technique using the Yule-Walker (ARYW) equations, the Hilbert based HHT algorithm using EMD, the O'Shea sliding window estimator as well as the AHE method were applied to two noiseless, stationary real functions

$$s(t) = e^{\alpha_1 t}\cos(2\pi f_1 t) \tag{4.1}$$

$$s(t) = e^{\alpha_1 t}\cos(2\pi f_1 t) + e^{\alpha_2 t}\cos(2\pi f_2 t) \tag{4.2}$$

where α is the damping factor, f is the frequency, and $s(t)$ is the artificial test function in the analysis.

Different frequencies and damping factors were used in the single-mode case (4.1) to measure the efficacy of each method. Table 4.1 shows the results of the five methods for the single mode case using a single 50 second window length.

Table 4.1. Comparison results for the single mode scenarios.

Test Signals		**AHE**		**Prony**		**ARYW**		**HHT**		**O'Shea**	
f	α	f	α	f	α	f	α	f	α	f	α
(Hz)	(s^{-1})	(Hz)	(s^{-1})	(Hz)	(s^{-1})	(Hz)	(s^{-1})	(Hz)	(s^{-1})	(Hz)	(s^{-1})
.200	-.005	.200	-.005	.200	-.005	.203	-.023	.200	-.005	.200	-.005
.200	-.100	.200	-.100	.200	-.100	.214	-.105	.200	-.100	.200	-.100
2.00	-.005	2.00	-.005	2.00	-.005	2.00	-.021	2.00	-.005	2.00	-.005
2.00	-.100	2.00	-.100	2.00	-.100	2.00	-.100	2.00	-.100	2.00	-.100
.200	+.005	.200	+.005	.200	+.005	.203	+.023	.200	+.005	.200	+.005
2.00	+.005	2.00	+.005	2.00	+.005	2.00	+.021	2.00	+.005	2.00	+.005

For the multi-mode case, differing combinations of frequencies and damping factors were used in (4.2) to generate the simulated test measurements. Table 4.2 shows the results of the five estimators for the noiseless, stationary multi-mode case using a 50 second window.

Table 4.2. Comparison results for the multi-mode scenarios.

Test Signals		**AHE**		**Prony**		**ARYW**		**HHT**		**O'Shea**	
f	α	f	α	f	α	f	α	f	α	f	α
(Hz)	(s^{-1})	(Hz)	(s^{-1})	(Hz)	(s^{-1})	(Hz)	(s^{-1})	(Hz)	(s^{-1})	(Hz)	(s^{-1})
.200 2.00	-.100 -.100	.200 2.00	-.100 -.100	.200 2.00	-.100 -.100	.215 2.00	-.113 -.095	.200 2.00	-.100 -.100	.200 2.00	-.101 -.100
.200 2.00	-.005 -.100	.200 2.00	-.005 -.100	.200 2.00	-.005 -.100	.203 2.00	-.026 -.086	.200 2.00	-.005 -.100	.200 2.00	-.005 -.100
.200 2.00	-.050 -.010	.200 2.00	-.050 -.010	.200 2.00	-.050 -.010	.208 2.00	-.059 -.021	.200 2.00	-.050 -.010	.200 2.00	-.050 -.010
.200 .300	-.005 -.500	- -	- -	.200 .300	-.005 -.500	- -	- -	- -	- -	- -	- -

.200 .300	-.005 -.005	.200 .301	- +.050	.200 .300	-.005 -.005	- -	- -	.199 .299	-.006 +.005	.200 .300	+.002 -.003
.200 .250	-.001 -.001	.200 .250	-.008 +.031	.200 .250	-.001 -.001	.230 -	-.048 -	.149 .229	+.058 -.117	.200 -	- -

A review of the single mode results show that all five methods reasonably agreed in terms of the identification frequency components of the modes. The only notable difference among the five estimators was the damping prediction of the ARYW method and the frequency estimates for low frequency values. One solution may be to reduce the lag of the estimator to improve the variance of the damping estimate without sacrificing resolution of the frequency estimate.

As was the case for the single-mode estimator results, the five methods predicted the frequency components reasonably successfully when two modes are provided with different frequencies and damping factors. Again, the only exception was for the ARYW estimate. This method had difficulty proving accurate frequency and damping estimates for low frequency modes. When the frequencies were within .100 Hz of each other, only the Prony assessment accurately estimated all the modal values. If the damping levels were minimal, the AHE technique could identify the modes but not their damping levels. Results from using the O'Shea algorithm nearly matched the results from the AHE method. For the HHT method, neither mode was estimate accurately when the frequencies were within an octave of one another. However, the limitation of the basic HHT algorithm to estimate accurate modes that are within an octave is well known and masking methods have been proposed to remedy this effect. Table 4.3 shows the last three modes in Table 4.2 with a proposed masking scheme applied.

As can be seen, the masking method did improve the frequency identification as compared to not using a mask. However, the damping component estimation was still problematic. One solution may be to use a better derivative estimator or another type of masking method.

Table 4.3. HHT masking results.

Test Signals		**Without masking**		**With masking**	
f	α	f	α	f	α
(Hz)	(s^{-1})	(Hz)	(s^{-1})	(Hz)	(s^{-1})
.200	-.005	-	-	.119	+.021
.300	-.500	-	-	.189	-.146
.200	-.005	.199	-.006	.191	-.014
.300	-.005	.299	+.005	.303	-.037
.200	-.001	.149	+.058	.194	+.138
.250	-.001	.229	-.117	.253	+.052

4.2 Additive noise comparison

White noise $q(t)$ was introduced into two multi-mode signals (4.3) and each of the five estimators used in the previous section was employed to assess each mode for increasing levels of noise. The values of the components of the modes used in (4.3) are given in Table 4.4.

$$s(t) = e^{\alpha_1 t}\cos(2\pi f_1 t) + e^{\alpha_2 t}\cos(2\pi f_2 t)$$
$$w(t) = s(t) + q(t) \qquad (4.3)$$

Table 4.4. Mode components for noise assessment.

Signal	Mode	Frequency	Damping	
#1	#1	.25 Hz	-.050 s^{-1}	3.18%

	#2	1.25 Hz	-.005 s^{-1}	.064%
#2	#1	.45 Hz	-.005 s^{-1}	.177%
	#2	.85 Hz	-.050 s^{-1}	.936%

The order of the AHE approximation for the noise assessment was chosen by selecting the largest order needed to supply the time and frequency support for the AHE functions and at the same time keeping the order as small as possible to allow the condition number of the $\underline{h}_t$ matrix to be very nearly equal to 1 for the noise mitigation requirement. Using (2.24-25), the order M and the time scale factor λ were calculated for a 50 second window to be 137 and 1.41, respectively. As shown in Fig. 2.8, the use of (2.24) provides a low condition number which is required for generation of a noise tolerant AHE estimator.

The mean square error (MSE) of the estimate of the damping factor and the frequency component was used as an error metric and the SNR in (4.4) was used as measure for the amount of white noise introduced into the artificial measurement.

$$SNR = 10\log_{10}\left(\frac{\sum\left(s(t)-mean(s)\right)^2 / N}{\mathrm{var}(q(t))}\right) \qquad (4.4)$$

Figs. 4.1 and 4.3 show the results from the five estimators for signal #1 after repeated trials at a different noise levels for the frequency components of the .25 Hz and 1.25 Hz modes, respectively. Similarly Figs. 4.2 and 4.4 show the

estimator results of the damping components of the .25 Hz and 1.25 Hz modes, respectively.

For signal #1, the AHE method performed better than the other estimators in predicting the frequency and damping components of the two modes as the noise levels increased. In the case of the .25 Hz mode, all five estimators predicted the correct frequency components to as low as a SNR of 15 dB. However below 15 dB, the AHE method performed significantly better that the other estimators. An observation made from the Figs. 4.1 and 4.2 is that as the SNR decreases from 15 to 2 dB the HHT, ARYW and O'Shea methods accuracy remains relatively constant. However, the accuracy of the Prony method continuously decreases as the noise level increases.

In the case of the moderately damped mode for signal #1, the AHE estimator performed better than the other four predictors from a SNR of 15 to 2 dB for both mode components. As was noted before, an examination of the Figs. 4.3 and 4.4 shows that the accuracy of Prony estimation continuously decreased as the noise level increased where as the accuracy of the other estimators remained relatively flat in this noise range.

For signal #2, the AHE method again performed better than the other four estimation methods for both the frequency and damping components between an SNR of 15 and 2 dB. Fig. 4.5 shows the frequency component results for the .45 Hz mode and Fig. 4.6 shows the damping component of the mode while Figs. 4.7 and 4.8 show the frequency and damping performance of the .85 Hz mode. As

before, the Prony analysis performance continuously worsened as the noise level increased. However, the performance of the other estimators remained relatively flat in this noise range.

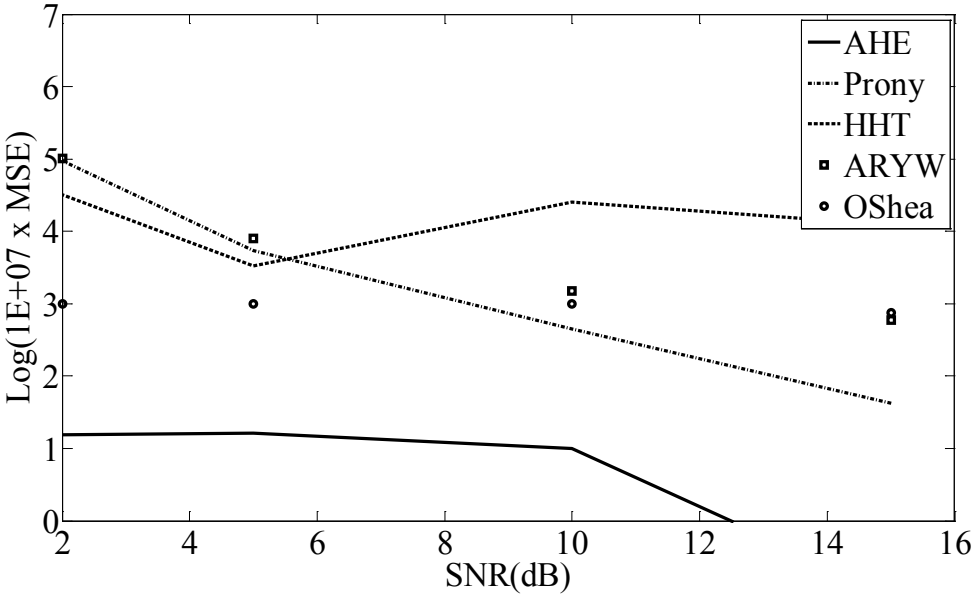

Fig. 4.1. Noise results for the frequency component of the .25 Hz mode.

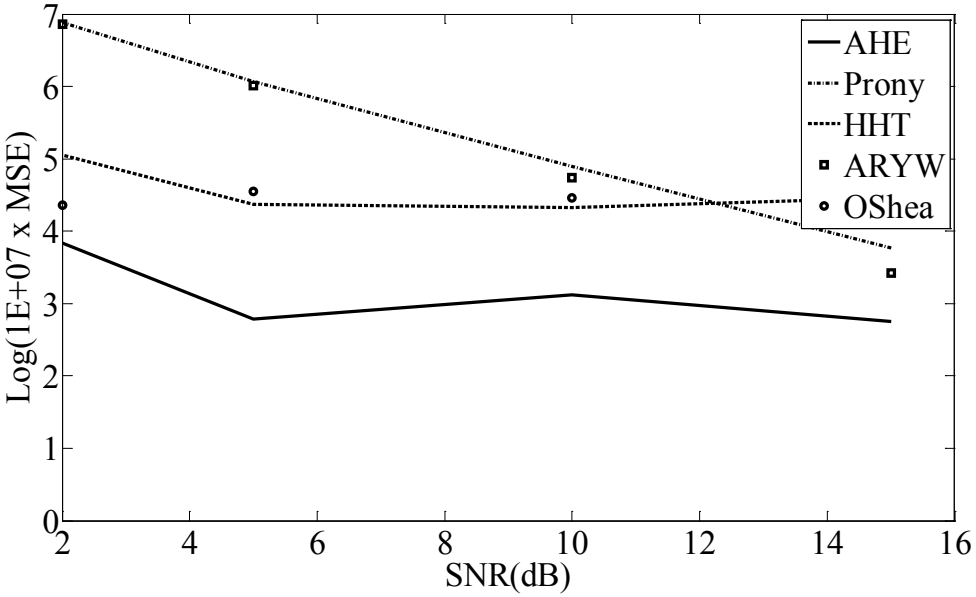

Fig. 4.2. Noise results for the damping component of the .25 Hz mode.

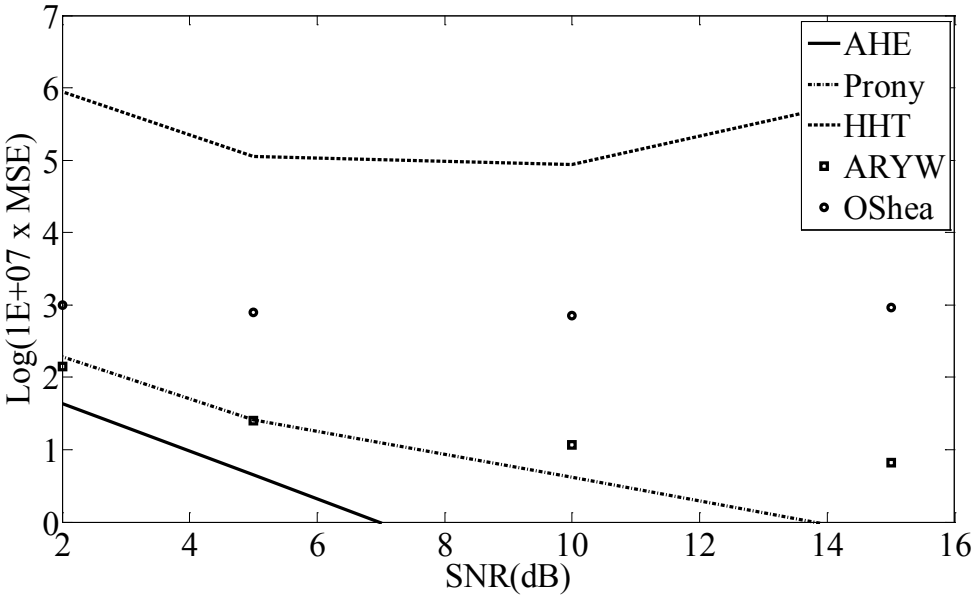

Fig. 4.3. Noise results for the frequency component of the 1.25 Hz mode.

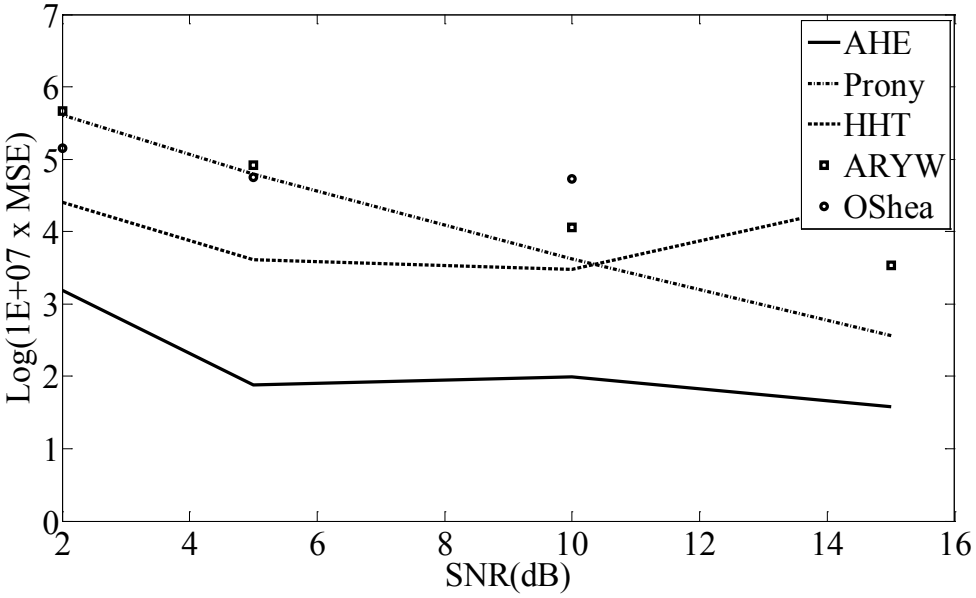

Fig. 4.4. Noise results for the damping component of the 1.25 Hz mode.

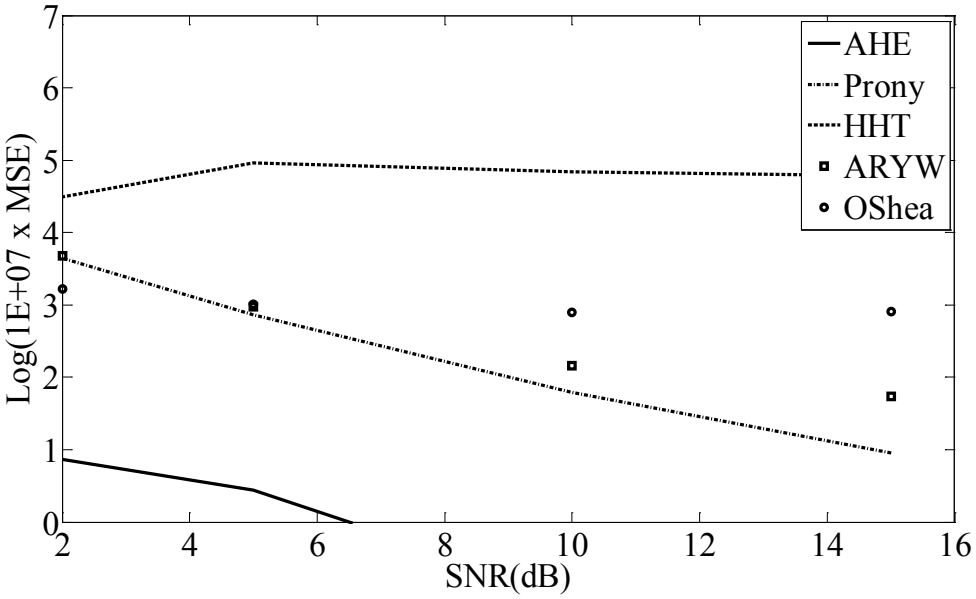

Fig. 4.5. Noise results for the frequency component of the .45 Hz mode.

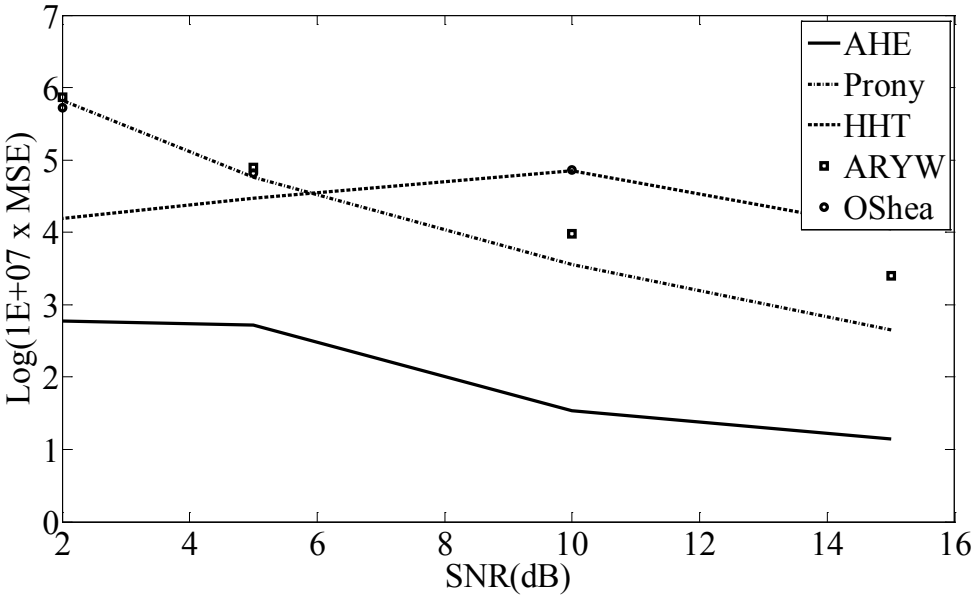

Fig. 4.6. Noise results for the damping component of the .45 Hz mode.

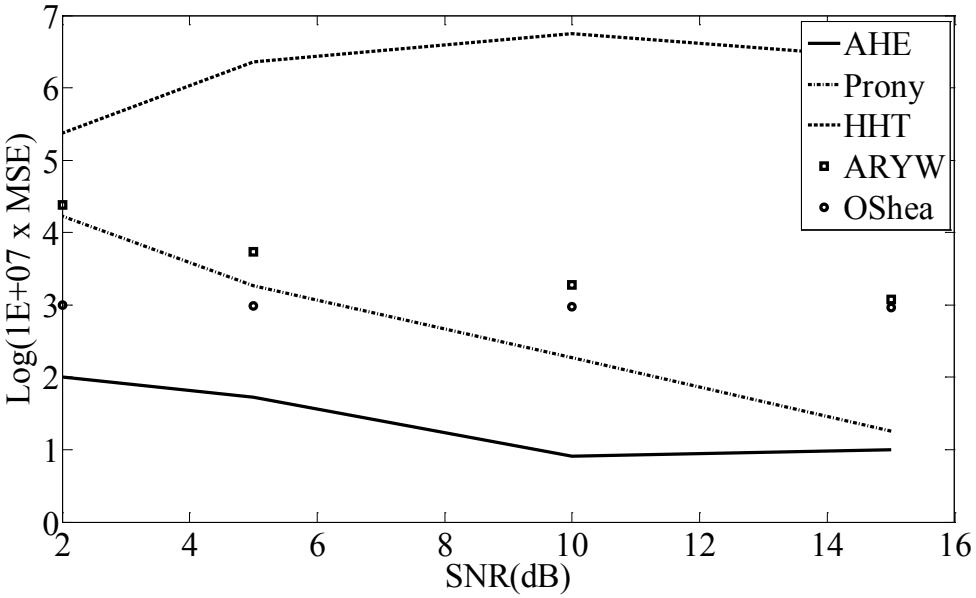

Fig. 4.7. Noise results for the frequency component of the .85 Hz mode.

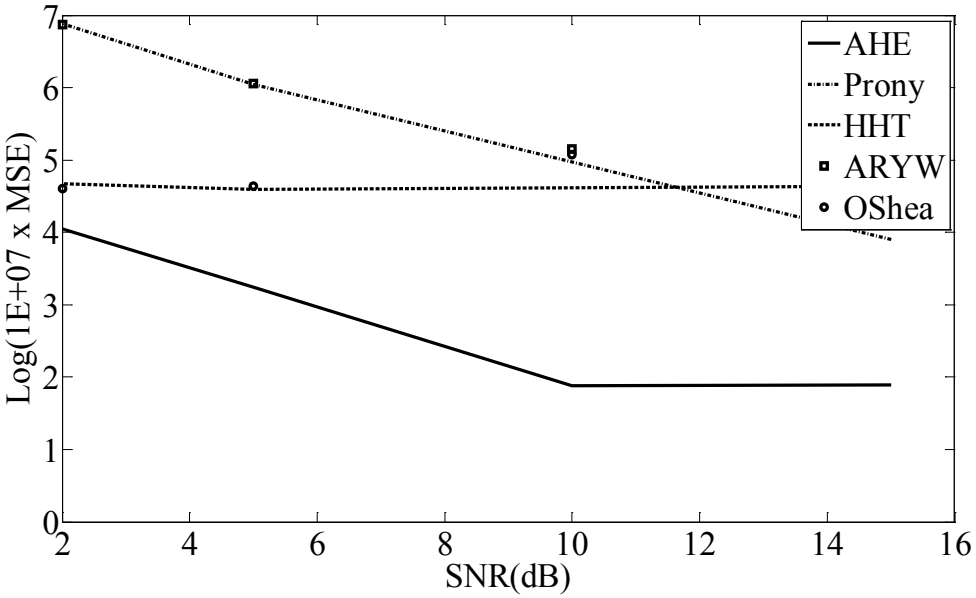

Fig. 4.8. Noise results for the damping component of the .85 Hz mode.

4.3 Window length comparison

Using the artificial signal in (4.3) but with f_1=.20 Hz, α_1=-.05s^{-1}, f_2=1.20 Hz and α_2=-.005s^{-1} and without the noise component $q(t)$, the length of the observation window was reduced from 180 seconds to assess the accuracy of the five methods relative to one another. Unlike, however, the previous analysis the percent error was calculated in lieu of the MSE for both the frequency and damping components of the mode as the window was reduced.

Figs. 4.9 and 4.11 show the frequency components for the .20 Hz and 1.20 Hz modes, respectively. The damping component effects as the observation window is reduced are shown in Figs. 4.10 and 4.12 for the .20 Hz and 1.20 Hz modes, respectively.

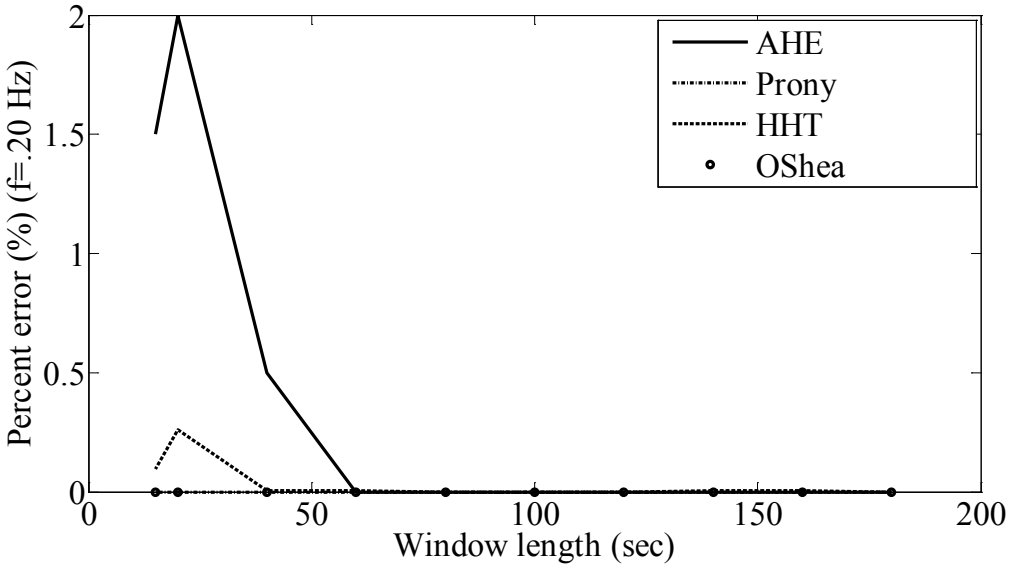

Fig. 4.9. Reduced window length results for .20 Hz frequency component.

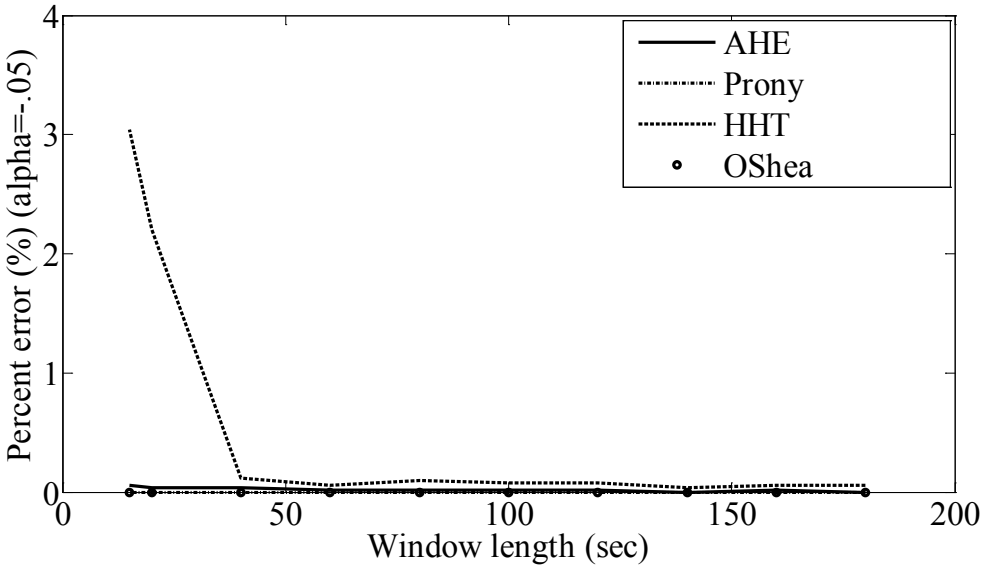

Fig. 4.10. Reduced window length results for damping component of .20 Hz mode.

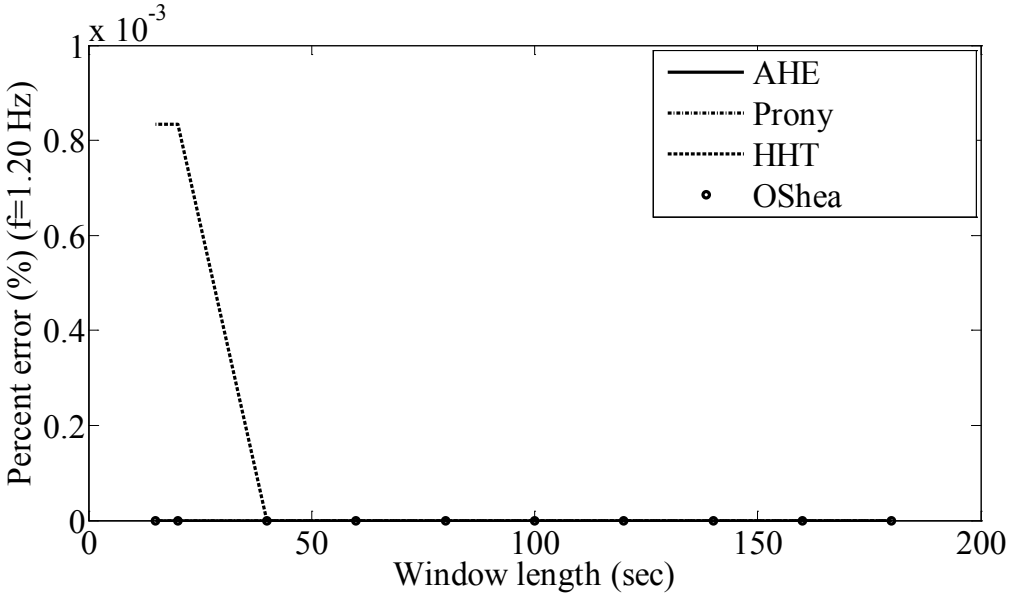

Fig. 4.11. Reduced window length results for frequency component of 1.20 Hz mode.

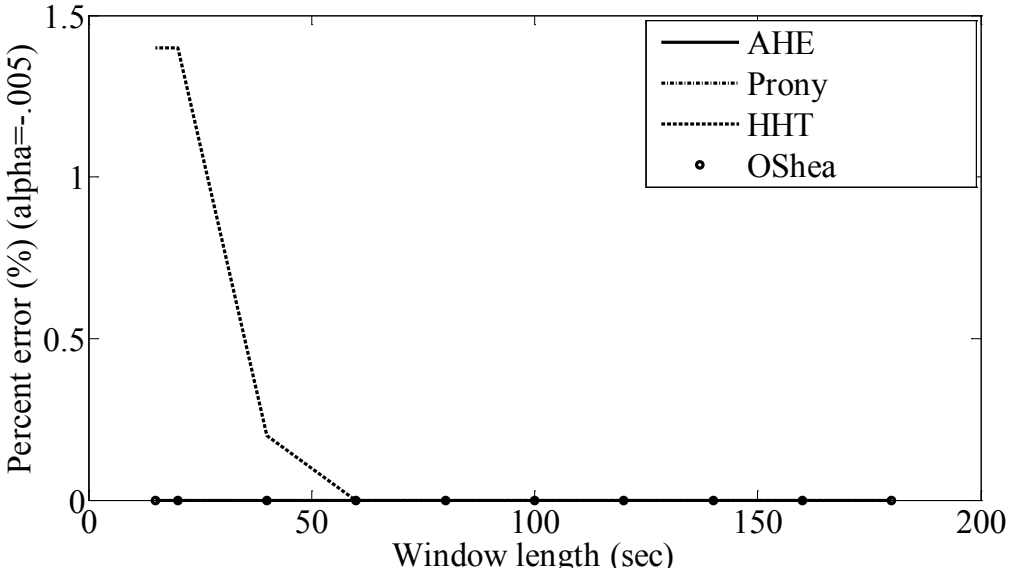

Fig. 4.12. Reduced window length results for damping component of 1.20 Hz mode.

For both modes, the ARYW algorithm was markedly inferior to the other four estimators and consequently it was not plotted with the other results. The remaining four estimators accurately predicted the frequency components of the modes, with the notable exception of the low frequency mode. The AHE method was slightly less accurate as the other methods when the window length approached the .20 Hz frequency's fundamental period. For the frequency component of the 1.20 Hz mode, all estimators performed nearly equally well.

For the damping components of each mode, the AHE algorithm predicted as accurately as the other estimators to a window length of 15 seconds. The only method that showed any noticeable deviation was the HHT algorithm. At relative small window lengths, the HHT had difficultly predicting the damping level. The error is likely due to the selection of the slope of natural log of the analytic

function (3.15) that is relatively constant. Choosing the location of the slope of this function is somewhat subjective and thus can be improved through careful attention.

4.4 Sampling rate comparison

A comparison was made using the synthetic signal studied in section 4.3 along with the five estimators. In these tests, the sampling rate was varied to highlight any differences in prediction capability among the estimators. As was found in the previous section, the Yule-Walker algorithm's performance was substantially weaker than the other four estimators and its results were not recorded here. In general, the various sampling rate frequencies were kept relatively low due to the fact that most power system recording devices sample at low rates such as 30 Hz for a typical phasor measurement unit (PMU).

Figs. 4.13 and 4.15 show the results of reducing the sampling rate for the frequency components for the .20 Hz and 1.20 Hz modes, respectively. Next the performance of each estimator's ability to predict the damping components for the .20 Hz and 1.20 Hz modes are given in Figs. 4.14 and 4.16, respectively. Like the window length analysis, the error metric used was the absolute percent error in lieu of the MSE. Again, the MSE was not used in this comparison since there were not multiple trials so no random variable was introduced. The window size used for this assessment was 50 seconds, which was the same record length used in the assessments for the additive noise and single and multi-mode assessments.

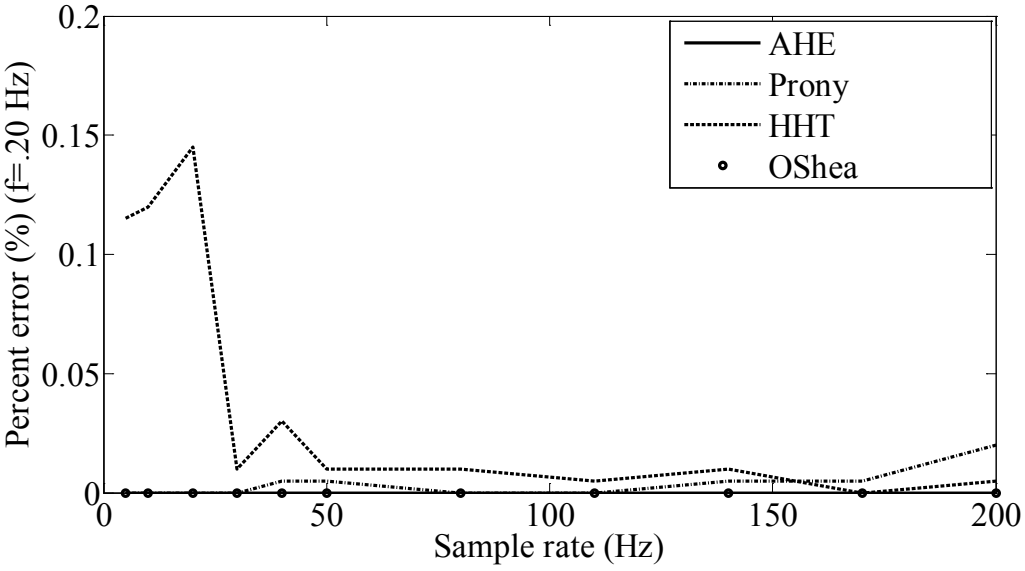

Fig. 4.13. Sampling rate results for frequency component of .20 Hz mode.

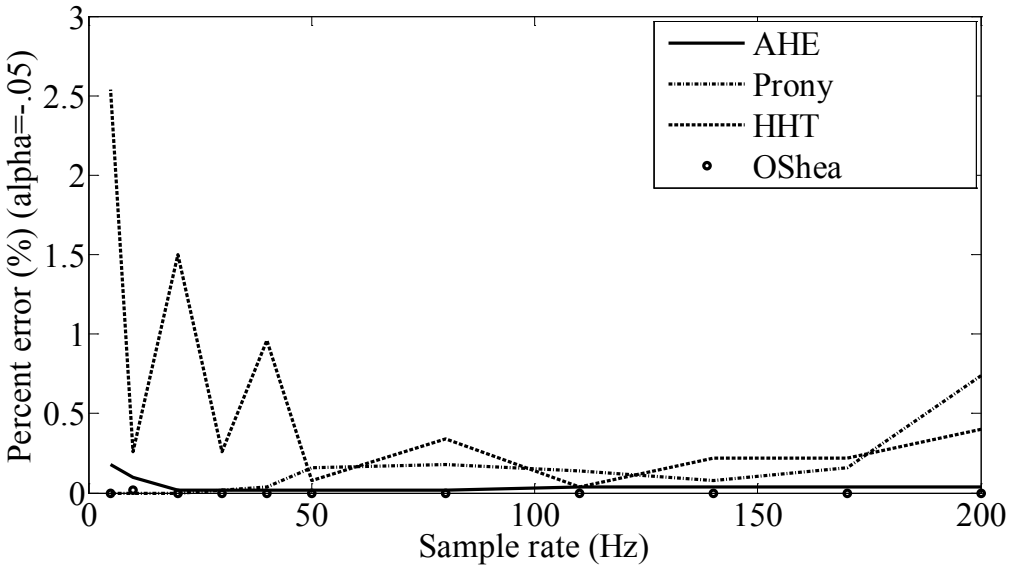

Fig. 4.14. Sampling rate results for damping component of .20 Hz mode.

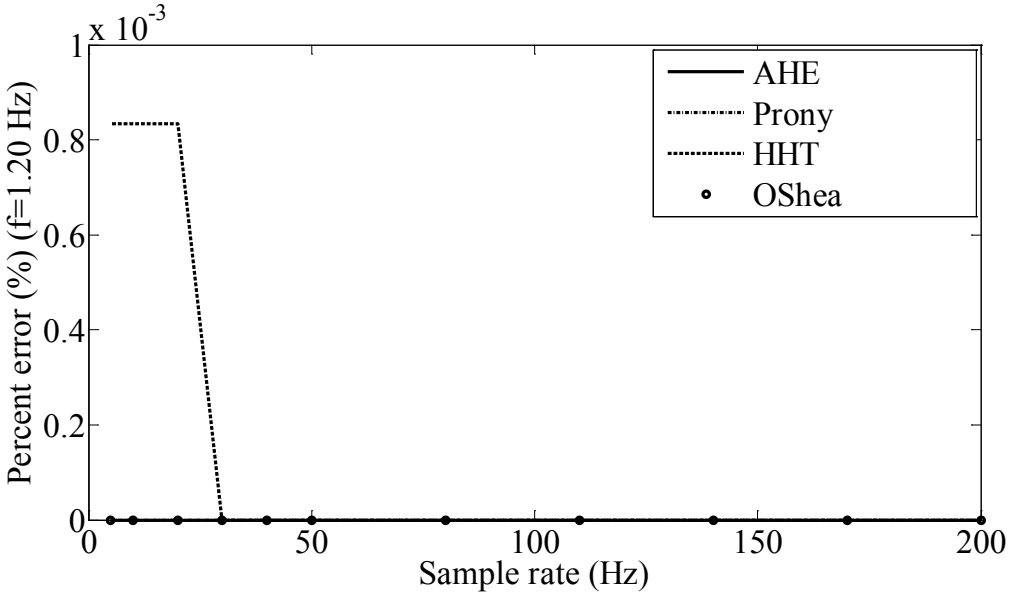

Fig. 4.15. Sampling rate results for frequency component of 1.20 Hz mode.

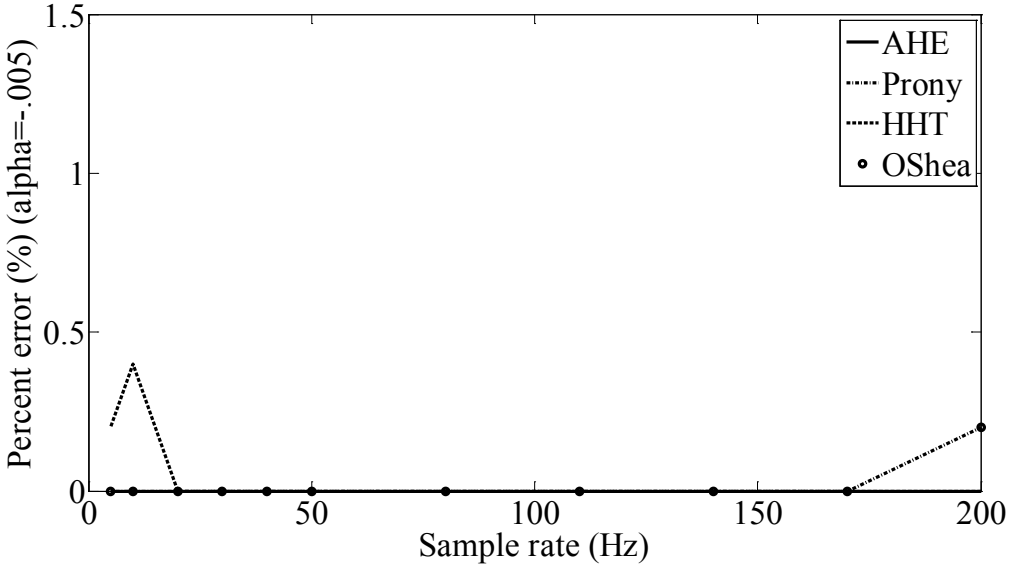

Fig 4.16. Sampling rate results for damping component of 1.20 Hz mode.

A review of Figs. 4.13 and 4.15 show that the AHE and O'Shea algorithms perform better than the HHT and Prony methods while estimating the frequency component for both modes down to a sample rate of 5 Hz, particularly for the .2 Hz mode. This result is important particularly for the low frequency mode of .2 Hz where low interarea oscillations occur and may suggest a lower sampling rate could be applied. Also, Fig. 4.13 shows the AHE algorithm is nearly as accurate at low sample rates than at high rates indicates that there is probably no benefit for sampling at higher rates for this algorithm. The consequence of this observation is that the estimation can be achieved with less data for the same amount of time.

As was the case with the frequency component, the AHE and O'Shea algorithms estimated the damping components of both modes more accurately down to a sample rate of 5 Hz. However, all the methods performed relatively well in the prediction of damping levels with no noticeable difference between the high and low frequency modes. The HHT algorithm appeared to perform least accurately than the other methods particularly for the low frequency mode but the results overall are still acceptable.

4.5 Non-stationary assessment

Because a non-stationary assessment of the various estimators is difficult to perform, a non-computational review of the methods is discussed here. Most parametric and non-parametric estimators, including Prony's method, are generally acknowledged not to be appropriate for non-stationary measurements.

This is particularly so for estimating damping levels. This is true as well for the for the AHE algorithm as a simple example will show. Using the modes from the previous section, a multi-mode artificial signal is generated over a 50 second window but with only the .20 Hz mode existing in the first 25 seconds of the measurement and only the 1.20 Hz mode in latter 25 seconds. Such an abrupt change would not be expected in a physical measurement but it does represent a true non-stationary measurement. Fig. 4.17 shows the generated artificial time measurement.

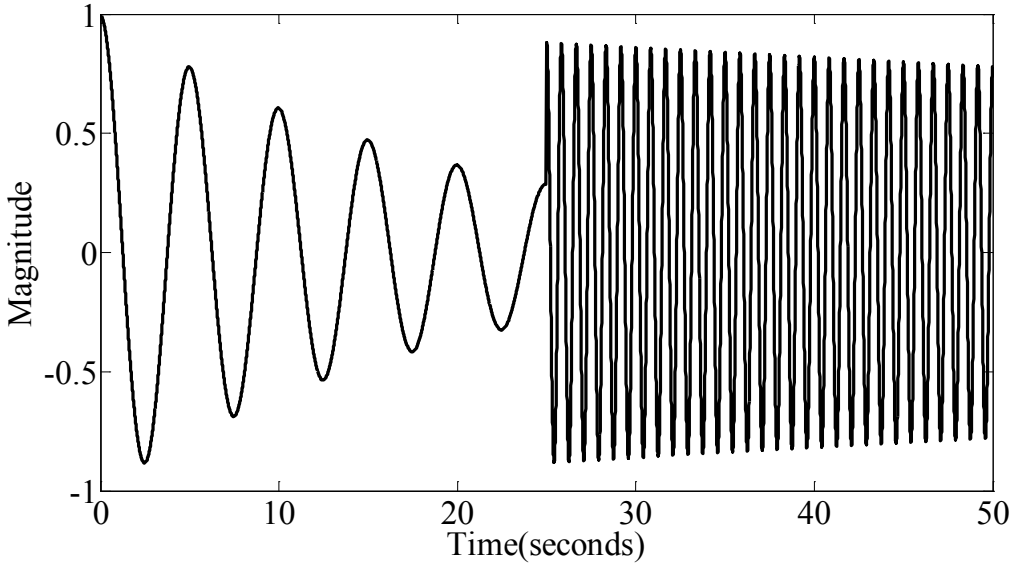

Fig. 4.17. Non-stationary test signal.

Table 4.5 shows just the Prony and AHE estimator results for the abrupt change measurement and for a multi-mode signal containing both modes over the entire 50 second window. As can be seen both predictors were able to identify the oscillatory components of the modes. On the other hand, the damping results are not as accurate as accurate as in the case where both modes exist throughout the

entire window. For the AHE, the damping estimate for the 1.20 Hz mode is extremely inaccurate due to the fact that the sliding window mechanism that estimates damping occurs in the initial portion of the window. In this case, the number of subwindows used by the linear predictor is 18 and each subwindow is shifted by 5 samples. With the subwindows 10 seconds wide and the sampling rate set at 12 Hz, the effective span of the FIR filter is 17.5 seconds and thus the estimator never sees the second signal since it exists in the latter half of the measurement.

Table 4.5. Non-stationary results.

Window Sizes	**Test Signals**		**Prony**		**AHE**	
	f	α	f	α	f	α
	(Hz)	(s^{-1})	(Hz)	(s^{-1})	(Hz)	(s^{-1})
25 sec+	.200	-.050	.202	-.070	.201	-.050
25 sec	1.20	-.005	1.20	-.006	1.20	-.053
50 sec	.200	-.050	.200	-.050	.200	-.050
	1.20	-.005	1.20	-.005	1.20	-.005

In the simple example, the AHE algorithm fails to identify the non-stationary measurement. However, the users could adjust the amount of shift between subwindows or the size of the subwindows even though this requires prior knowledge of the measurement. Researchers have proposed a method to calculate the instantaneous frequency and damping estimates of known non-stationary measurements using the HHT algorithm employed in previous sections of this chapter [86]. Although the method is still being refined, the authors have successfully demonstrated its ability to find the mean of the frequency and

damping estimates for individual windows of a disturbance event. Fig. 4.18 shows the estimation results for the same signal as seen in Fig. 4.17 and reported in Table 4.4. In the figure, the derivative of the instantaneous phase of the analytic function in (3.15) is calculated using (4.5) and (4.6). Note that the frequency component of 0.20 Hz is clearly seen in the window from 0 to 25 seconds. The mean is recorded over a stable range of the signal and found to be 0.194 Hz. For the 1.20 Hz mode, the mean of this signal was recorded to be 1.200 Hz over the stable range of the response.

$$X_A(t) = x(t) + jH[x(t)] \tag{3.15}$$

$$\varphi_i(t) = \arctan\left(\frac{\mathrm{Im}(X_A(t))}{\mathrm{Re}(X_A(t))}\right) \tag{4.5}$$

$$f(t) = \frac{1}{2\pi}\frac{d\varphi_i(t)}{dt} \tag{4.6}$$

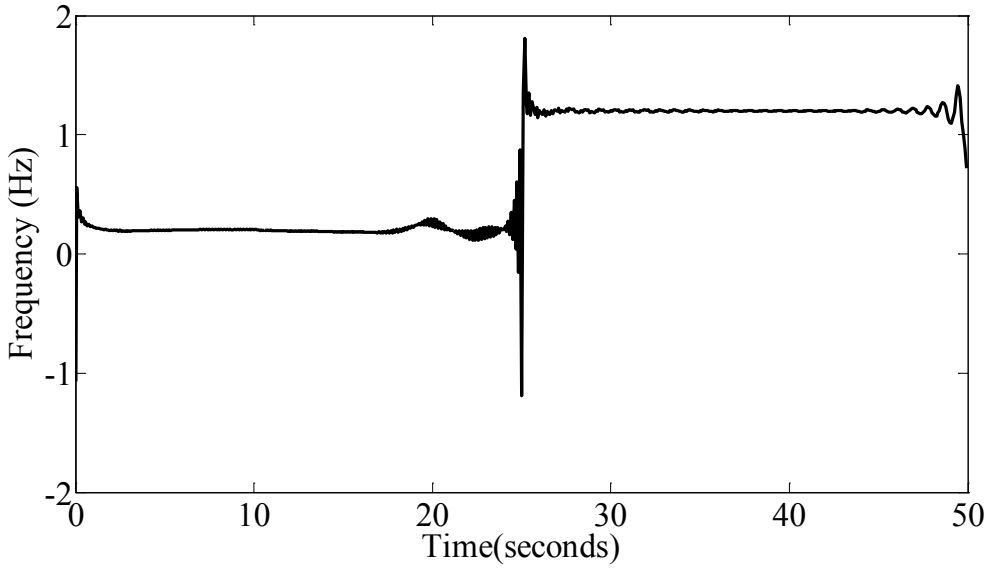

Fig. 4.18. HHT frequency decomposition of signal in Fig. 4.17.

For the HHT assessment of the damping level of the modes in Fig. 4.17, the instantaneous damping factors for the .20 and 1.20 Hz modes were found to be -.050 and -.005. To calculate the instantaneous damping factor, the derivative of the natural log of the analytic function of (3.15) or $\ln(|X_A(t)|)$ was computed. Although the scale is difficult to read, Fig. 4.19 shows the instantaneous damping level of the signal in Fig. 4.17. However, the mean of the two windows does verify the damping levels have been successfully isolated.

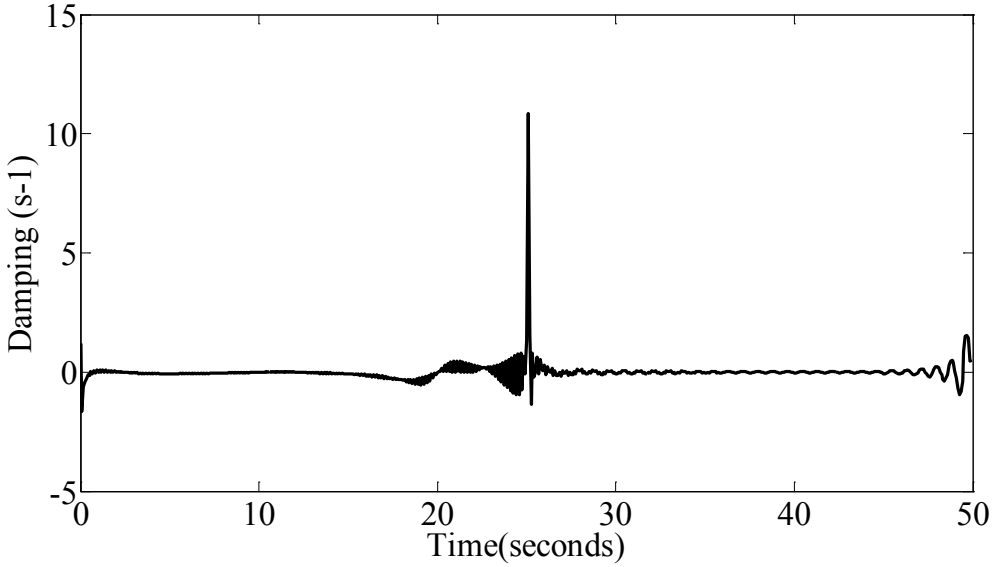

Fig. 4.19. HHT damping decomposition of signal in Fig. 4.17.

4.6 Field measurement assessment

A search was performed for actual field testing by a utility and measurements were obtained of a brake insertion test on a transmission network in northwest area of the United States. Using the five methods employed in this chapter, one of the field test measurements was analyzed and the results compared with those reported by the initial researchers. Fig. 4.20 shows the field measurement of real power flow on a 500 kV transmission line over a 15 second

window following a brake insertion. Table 4.6 shows the results of the assessment of the signal in Fig. 4.20 including those reported by the initial researchers. Only two modes with a damping ratio of less than 10%, .246 Hz and .363 Hz, were found by the researchers from this test and these are the modes assessed by the AHE algorithm and the other four estimators.

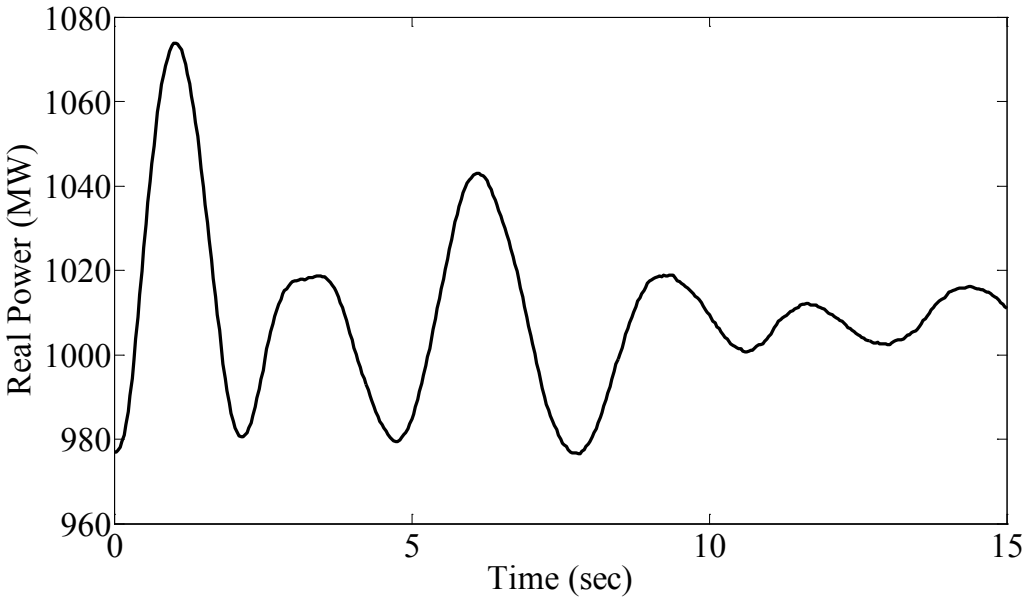

Fig. 4.20. Field measurement of a brake insertion.

Table 4.6. Field test comparison.

Initial field assessment		**AHE**		**Prony**		**ARYW**		**HHT**		**O'Shea**	
f	α	*f*	α	*f*	α	*f*	α	*f*	α	*f*	α
(Hz)	(s^{-1})	(Hz)	(s^{-1})	(Hz)	(s^{-1})	(Hz)	(s^{-1})	(Hz)	(s^{-1})	(Hz)	(s^{-1})
.246	-.151	.231	-.186	.238	-.191	.187	-.483	.144	-.062	.200	.489
.363	-.213	.363	-.193	.360	-.165	.387	-.228	.264	-.098	.333	.454

As can be seen in the table, the AHE algorithm performed well in relation to the findings from the initial researchers for the two dominant modes in the field measurement. Also, the AHE algorithm exceeded the predictions from the other algorithms with the exception of one frequency estimate from the Prony analysis.

4.7 Comparative assessment summary

In this chapter a group of established spectral estimators performances were compared to the performance of the AHE algorithm under five different scenarios. The four estimators included an analysis using Prony's method, an autoregressive model using the Yule-Walker equations with ACS estimates, the Hilbert-Huang Transform algorithm with Empirical Mode Decomposition and the O'Shea sliding window technique. In all scenarios, artificial signals were created for processing by each estimator.

The first assessment evaluated the all five algorithms ability to distinguish single and multi-mode signals with varying assumptions over a 50 second time window. For the single mode case, each method accurately identified the frequency and damping components of complex modes over a frequency range of .2 to 2 Hz and with growing and decaying oscillations. The notable exception was the slightly inferior performance of the autoregressive Yule-Walker method. In the multi-modal case with two modes, the estimators were able to identify both frequency components and damping levels when the frequencies were well separated. However, only Prony's method was able to distinguish both frequency and damping levels when the frequencies were within .05 to .1 Hz of each other

regardless of damping levels. The AHE algorithm was able to distinguish frequency components with these closely adjacent modes where the other estimators, other than Prony's method, had difficulty.

For the second assessment, white noise was added to two multi-modal artificial signals each with one lightly damped mode and one moderate damped mode (Table 4.4). The window length was again kept at 50 seconds and a number of trials were completed at specified SNR levels. As the SNR was reduced, the MSE was recorded for each estimator and the results were recorded. Results showed that the AHE algorithm performed more accurately than the other estimators at SNR levels below 15 dB. However, the AHE algorithm was able to accurately estimate all four modal components to a SNR of 2 dB as compare to the other four methods.

For the window length assessment, the ARYW method was not considered due to its overall inferior performance. The other four estimators were actually able to predict the frequency components fairly accurately to windows as small as 15 seconds. The AHE algorithm had difficulty isolating the .20 Hz mode since the window was approaching the fundamental period of the oscillatory component. When the 1.20 Hz mode was evaluated, the AHE algorithm was as accurate as the other estimators in its prediction. For the damping component analysis, the AHE was as accurate as the other methods. The only exception was the HHT algorithm which appeared to have a problem extrapolating the phase of the analytic function for small window sizes.

For the sampling rate comparison, the AHE algorithm was generally more accurate than the other estimators for both high (200 Hz) to low (5 Hz) sampling frequencies. Other than accuracy considerations, the results also suggest no benefit is obtained from the additional data resulting from higher sampling rates if the AHE algorithm is used. Alternately, the results suggest use of the lower sampling rates would translate into lower computational speeds.

Finally, the issue of non-stationary signals and their predictive abilities is discussed. Other than the HHT algorithm, all the other estimators are parametric in nature and are generally believed not to be capable of providing meaningful results. A simple example is performed using the Prony and the AHE methods. Although able to identify the frequencies correctly, both methods could not isolate the damping levels accurately. Research has shown that the only estimator of the five used in this chapter capable of predicting modes in non-stationary signals successfully is the HHT technique. This technique was applied to the signal in Fig. 4.17 and successfully identified both the frequency and damping components of the modes in the artificial signal. Table 4.7 shows a synopsis of how the AHE algorithm performed for the various artificial measurement scenarios.

Table 4.7. AHE comparison results.

Scenario	AHE performance
Single/multi-mode prediction	Equal to or better than other estimators except for minor cases.
Noise tolerance	Performs better than other estimators down to SNR

	levels of 2 dB.
Reduced window length	Accuracy tied to the period of the lowest modal frequency.
Sample rate	Equal to or better than other estimators.
Non-stationary signal	Not suitable for non-stationary analysis.

Chapter 5

COMPARATIVE ASSESSMENT-SIMULATED MEASUREMENTS

5.1 Introduction

The intent of the previous chapter was to compare the performance of various measurement based estimators against the AHE algorithm using artificial measurements. To complement the results of Chapter 4, the performances of the five estimation methods were assessed using simulated measurements generated from time domain simulations. A WECC powerflow case and the GE powerflow and transient stability program PSLF were used to provide the time domain simulation values. To provide reference frequency and damping levels, a model based method was used to estimate the dominant modes within the WECC case. The model based method used here was the eigenvalue analysis routine described previously in Chapter 1. For the eigenvalue analysis, the PowerTech small signal analysis module SSAT in their DSATools software package was used with inputs from the WECC powerflow case and its accompanied dynamic representation. PowerTech's PSAT powerflow module was also used in eigenvalue analysis.

In order to excite the dominant angle and speed modes in the transient stability simulation an input was applied to the identified generator's control models. For these simulated measurements, the input was an approximated impulse applied to either the reference voltage of an excitation model or the reference load setting in a governor model. Fig. 5.1 shows the process used to generate the dominant modes in the eigenvalue analysis and the excitation of the modes in time-domain simulations. An example of the approximated impulse

applied to the models within the transient stability program can be seen in Fig. 5.2.

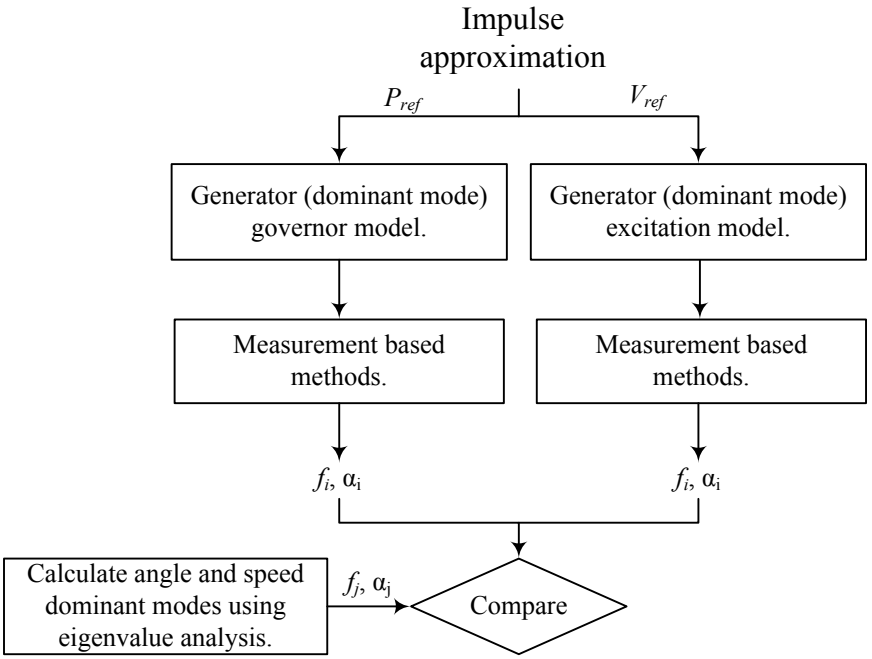

Fig. 5.1. Evaluation of simulated modes using the AHE and other estimation methods.

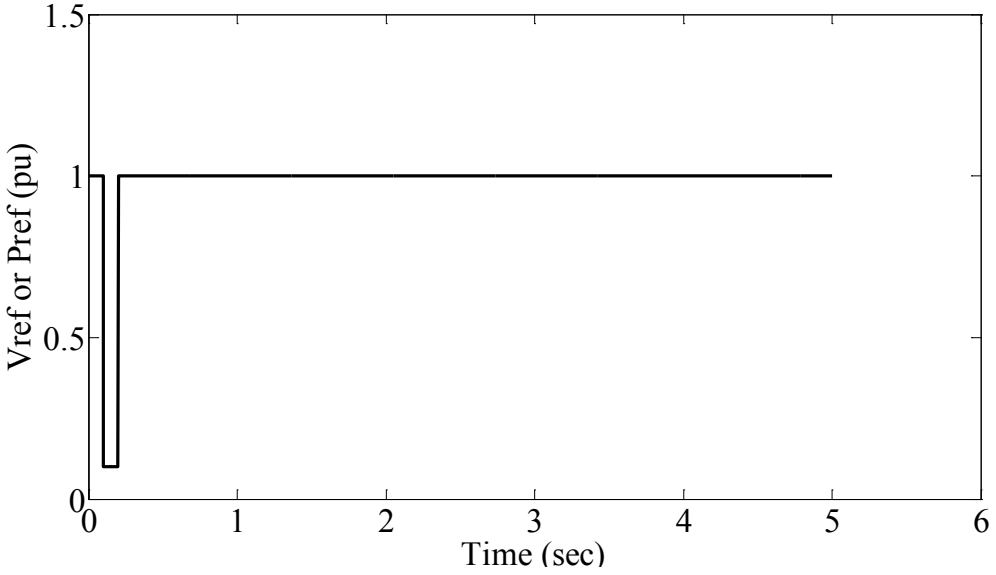

Fig. 5.2 Approximated impulse input.

With the time domain response resulting from the approximated impulse, the dominant frequencies and their associated damping levels were predicted using the five estimators. The results from the AHE algorithm and the other spectral estimators were then compared to the frequencies and damping levels predicted by the eigenvalue analysis.

5.2 Simulation results

As described before, a full-loop WECC powerflow case was selected with over 15000 buses and nearly 3000 generators and was assessed using the SSAT software package. The resulting set of lightly damped modes provided a benchmark for the other measurement-based estimators. Next, the impulse approximation was applied either to the machines voltage reference in its exciter model or the load reference in its governor model, depending on the eigenvalue state, using the GE transient stability program. This process is highlighted in Fig. 5.2. A control depiction of the application of impulse approximations of Fig. 5.2 in the transient stability simulations is given in Fig. 5.3 for both excitation system and governor models.

With the time-domain results obtained from the PSLF software package, the AHE algorithm, Prony's method, the Yule-Walker autregression algorithm, the O'Shea sliding window method and the Hilbert-Huang Transform estimator were then used to identify the dominant frequency and its associated damping level. As examples of the application of the approximated impulse to model reference signals, Figs. 5.4 and 5.5 show positively damped and negatively

damped speed responses from separate simulations, respectively. Eigenvalue analysis identified the mode in Fig. 5.4 with a frequency of 1.039 Hz and a damping ratio of 3.01%. For the speed deviation mode shown in Fig. 5.5, the SSAT software package determined the dominant mode to be 0.691 Hz with a damping level of -4.70%.

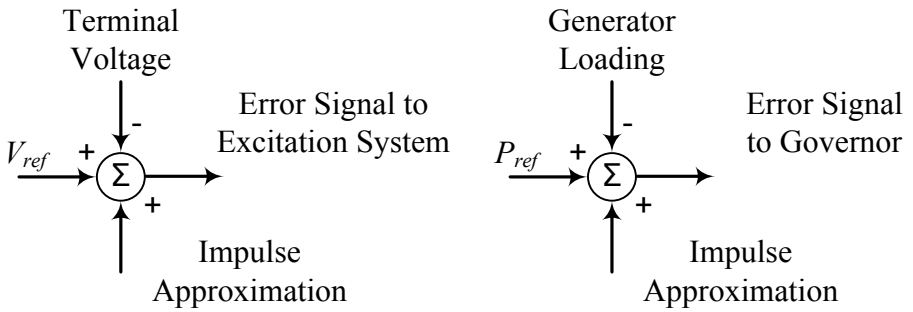

Fig. 5.3. Impulse approximation application.

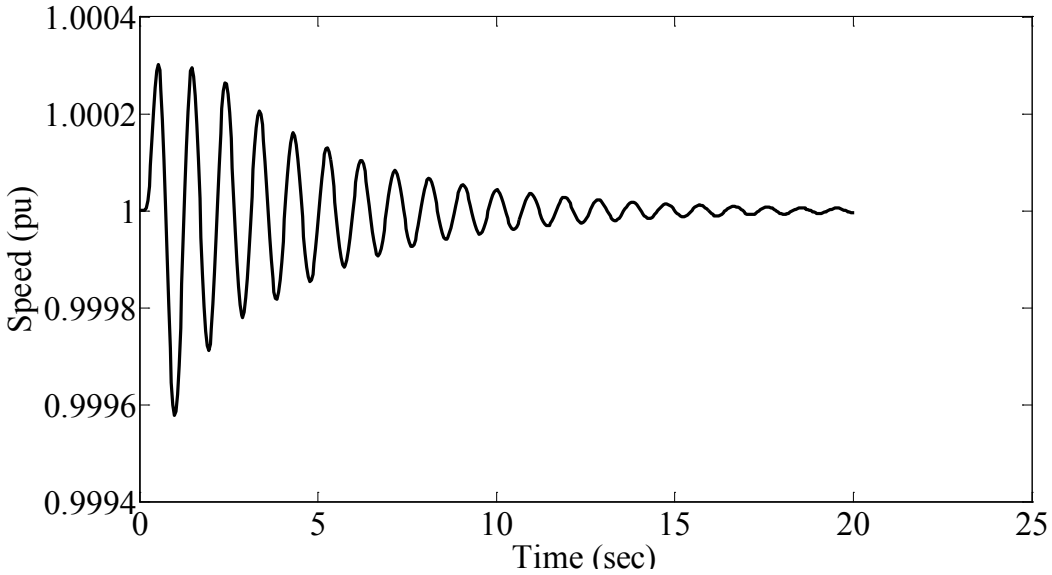

Fig. 5.4. Positively damped speed response from an impulse to an excitation system.

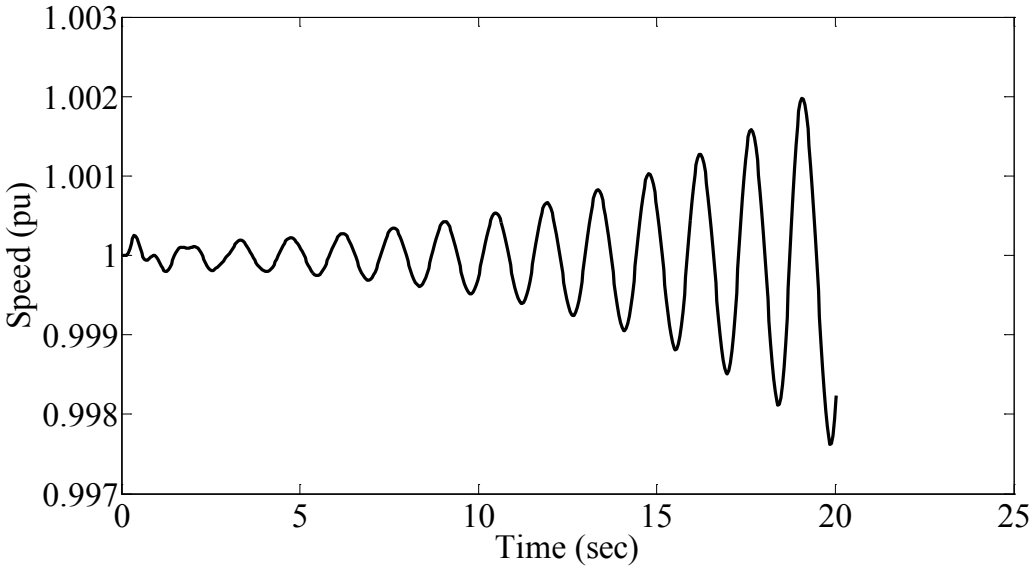

Fig. 5.5. Negatively damped speed response from an impulse to an excitation system.

Of all the dominant modes identified, 78 of the most lightly damped modes were selected using eigenvalue analysis to be subsequently evaluated by the five estimators. In this particular computation of the eigenvalues using SSAT, the modes are primarily local modes in the range of .6 to 2 Hz. Consequently, the modes reflect the weakness of the adjacent electrical network and the characteristics of the immediate generator.

The MSE was calculated for the frequency and damping ratio estimates from each method per mode relative to the frequency and damping level estimate obtained from the eigenvalue analysis. Specifically, the SSAT results provided the baseline or benchmark frequency and damping values for the MSE calculation. Although providing a benchmark for the other estimators, the eigenvalue analysis results should also be viewed as estimates as well since the

true damping levels and frequencies are essentially unknown. Within the results, the mean of the squared errors were computed over the 78 modes previously mentioned. Table 5.1 shows the summary of the results of the assessment.

Table 5.1. Results from simulated measurements.

Method	MSE	
	Frequency	Damping
AHE	0.0053	0.0002
Prony	0.0049	0.0005
HHT	0.0109	0.0020
ARYW	0.0070	0.0008
O'Shea	0.0092	0.0007

5.3 Simulated measurements assessment summary

A review of the results in Table 5.1 shows that using the modes generated by the SSAT eigenvalue analysis package as benchmarks and the PSLF time domain results as simulated measurements the five measurement based estimators predicted both components of the mode reasonably accurately. A further review shows the AHE algorithm did estimate the damping levels more accurately than the other four prediction methods. Least squares Prony's method predicted the frequency component of the modes more accurately than the other algorithms. However, the AHE algorithm was second only to the Prony analysis for accurate frequency identification. In addition, the AHE algorithm outperformed the other

sliding window algorithm in both modal categories and consequently the AHE technique appears to be an improvement to the O'Shea spectral estimator.

Chapter 6

DAMPING MITIGATION APPLICATIONS

6.1 Introduction

One of the primary uses of both the model and measurement based small signal estimators is the design of damping mitigation schemes. Of these schemes, the most widely used mitigation device is the power system stabilizer (PSS). The PSS has historically been a piece of physical equipment installed in the excitation system of synchronous generators to add positive damping to rotor oscillations typically caused by small signal phenomenon. Recent applications, however, have seen the implementation of the PSS moved from a hardware scheme to a purely software routine within the controls of an excitation system voltage regulator.

The rotor deviations that the PSS is meant to dampen are generally the result of changes in the electrical power that is seen at the terminals of the machine. This relationship is defined in (6.1)

$$\frac{2Hd\Delta w}{dt} = \Delta P_M - \Delta P_E$$
$$\Delta w = \frac{1}{2H}\int (\Delta P_M - \Delta P_E)dt \qquad (6.1)$$

where H represents the collective inertia of the rotating components of the generator, ΔP_M is the change in mechanical power, ΔP_E is the change in electrical power and Δw is the effective speed deviation. If the right hand side of (6.1) is positive the machine's rotor accelerates and if the relationship is negative the rotor decelerates. The intent of the PSS is not only to dampen rotor or speed

oscillations that can negatively affect the generator or cause the machine to inadvertently trip but to also prevent the generator from contributing to disturbances beyond the generator or the plant that are regional in nature. Regional oscillations are either local or interarea as defined in Chapter 1.

To dampen the rotor deviations, the PSS must generate electrical torque in phase with rotor deviations [3]. As was mentioned before, the typical location for a PSS to provide a supplementary signal is within the voltage regulator of a synchronous generators excitation system. Fortunately, the excitation system is an appropriate location to generate electrical torque, if only briefly, without the need to manipulate the generators prime mover. This is accomplished by modulating the field voltage of generator or, equivalently, the output voltage of the exciter or its field circuit. As the relationship in (6.2) shows [87], an increase in the field voltage of a generator will increase the electrical power of the machine

$$P_E = \frac{|E_f||V_t|}{X_s}\sin(\varphi) \qquad (6.2)$$

where E_f is the field voltage of the machine, V_t is the terminal voltage of the generator, φ is the angle between the internal and terminal voltages of the generator and X_s is the synchronous reactance. The relationship in (6.2) represents an ideal unsaturated, round-rotor synchronous generator under balanced conditions at constant speed without armature resistance. Fig. 6.1 [1] shows a simple representation of a PSS providing a supplementary signal to the voltage regulator in a typical excitation system control scheme. Its worth noting that the choice of input signals available to most PSS are not solely limited to

shaft speed deviation. Other inputs can include frequency and electrical power deviations depending on the manufacturers and customers preferences. In addition, most PSS that are installed today employ dual input signals as compare to older PSS that use single input signals to generate a supplementary signal in phase with the electrical torque of the machine.

In this chapter, several examples are provided showing the application of PSS to improve damping to generators without PSS that have lightly damped modes. The improvement of damping before and after the addition of the PSS will be evaluated using the AHE algorithm and Prony's method. The pre-PSS and post-PSS damping levels will also be verified using eigenvalue analysis. Three examples of generators without PSS will be taken from those studied in Chapter 4 with one example of three generators at a plant with their PSS schemes retuned. Consequently, this chapter demonstrates another potential use for the AHE algorithm besides the identification process performed in the previous chapter.

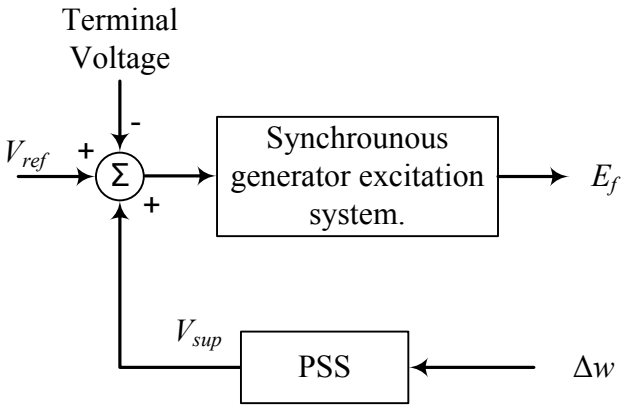

Fig. 6.1. Typical PSS application within an exciter [1].

6.2 PSS function and settings

The PSS typically employs phase lead compensation to the input signal for its control scheme. Other settings of the PSS for the four examples assessed in this chapter were kept the same with the exception being the gain of the controller. Some of the other elements included in the PSS controller that were not adjusted included the transducer time constant, the washout time constant and output limiters. Design of the PSS in terms of filtering either for noise or torsional effects, low power operation and disabling do to extreme events were not modeled here. Fig. 6.2 shows the simplified, continuous time control diagram of the PSS used in the examples in this chapter

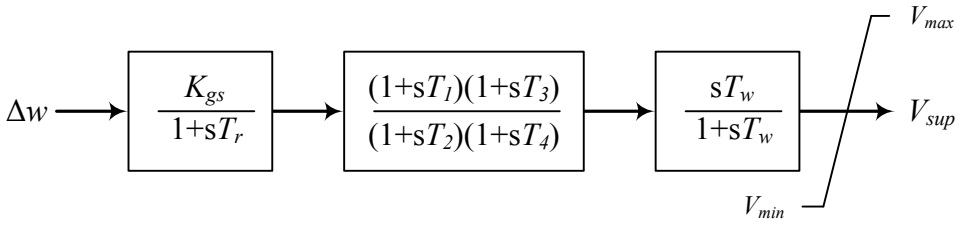

Fig. 6.2. Simplified control scheme for a speed deviation stabilizer.

where K_{gs} is the stabilizer gain, $1/T_1$ and $1/T_3$ are the zero locations, $1/T_2$ and $1/T_4$ are the pole locations, T_r is the transducer time constant, Δw is the change of speed input, T_w is the washout time constant, V_{max} and V_{min} provide the output limits, and V_{sup} is the output of the PSS.

The transducer time constant in the PSS represents the delay associated with the speed or frequency sensor and is usually not considered in choosing the overall compensation of the PSS. Also not part of the compensation scheme of

the PSS, the washout time constant T_w is selectable usually with a range of 10 to 20 seconds. Because the PSS is only meant to provide an output during small signal events, under normal conditions the PSS should provide no modulation to the field voltage of a generator. The purpose of the washout time constant is to remove any bias from the output of the PSS that may exist under steady state conditions.

As explained previously, the compensation provided by the PSS is phase lead in nature. Essentially, the PSS is a derivative approximation over the frequency range of interest. As a result, any spurious noise within the PSS prior to the compensation stages could be greatly amplified in the output V_{sup} which will be applied to the field winding of the synchronous generator. To mitigate any extreme outputs due to noise seen by the PSS, designers have installed adjustable output limits V_{max} and V_{min}. With the limits in place, a certain amount of protection from spurious signals within or before the PSS is be obtained.

The phase lead compensation of the PSS is accomplished using two stages representing the second functional block in Fig. 6.2. In each of the four examples, the amount of compensation is kept the same with only the location of the poles and zeros being modified according to the frequency f_i detected by the estimators in the pre-compensated scenario. Per stage, the amount of compensation was kept at approximately 48˚. The oscillatory frequency identified by the estimators and the amount of compensation per stage establishes the pole and zero locations. If a single stage can be represented as (6.3), the relationship in (6.4) can be used to

find the time constant associated with the pole location and subsequently the time constant representing the inverse of the zero location.

$$G(s) = \frac{(1 + sTq)}{(1 + sT)} \tag{6.3}$$

$$T = \frac{1}{2\pi f_i \sqrt{q}} \tag{6.4}$$

The value of q was set at 7, giving 48° of phase lead compensation per stage as defined by the relationship in (6.5).

$$\theta = \sin^{-1}\left(\frac{(q-1)}{(q+1)}\right) \tag{6.5}$$

6.3 PSS application example #1

The first example of simulated shaft speed oscillations from a synchronous generator is shown in Fig. 6.3. In this simulation, the generator initially does not have a PSS modeled. A 100 millisecond impulse to V_{ref} of the excitation system is used to generate a time domain response. Using the time response, the AHE algorithm identified the lightly damped mode at approximately .76 Hz with a damping ratio of 1.90%. An assessment using Prony's method revealed a mode at the same frequency as found by the AHE algorithm and a damping ratio of 1.56%. Eigenvalue analysis indicated the uncompensated mode to be .75 Hz with a damping ratio of 2.38%.

With the data collected using the AHE estimator, a shaft speed deviation PSS model was applied to the synchronous generator. Using (6.5), the value of q was set equal to 7 giving a phase lead compensation per stage of nearly 48°. And

the gain K_{gs} was fixed at 2.5 pu. The values of T_1 and T_3 were calculated to be .549 seconds while T_2 and T_4 were determined to be .078 seconds. Subsequently, the approximated impulse was applied to the exciter model to obtain the time domain response. Both the AHE algorithm and Prony's method revealed the dominant oscillatory mode to be .77 Hz. Prony's method showed that the damping level improved to 3.71% while the AHE method found the damping improved to 3.92%. Eigenvalue analysis verified that the damping increased but to 4.87% at .75 Hz. Fig. 6.3 shows the speed deviation response with the PSS modeled. As can be seen, damping to the generators speed deviations has improved through use of the tuned PSS.

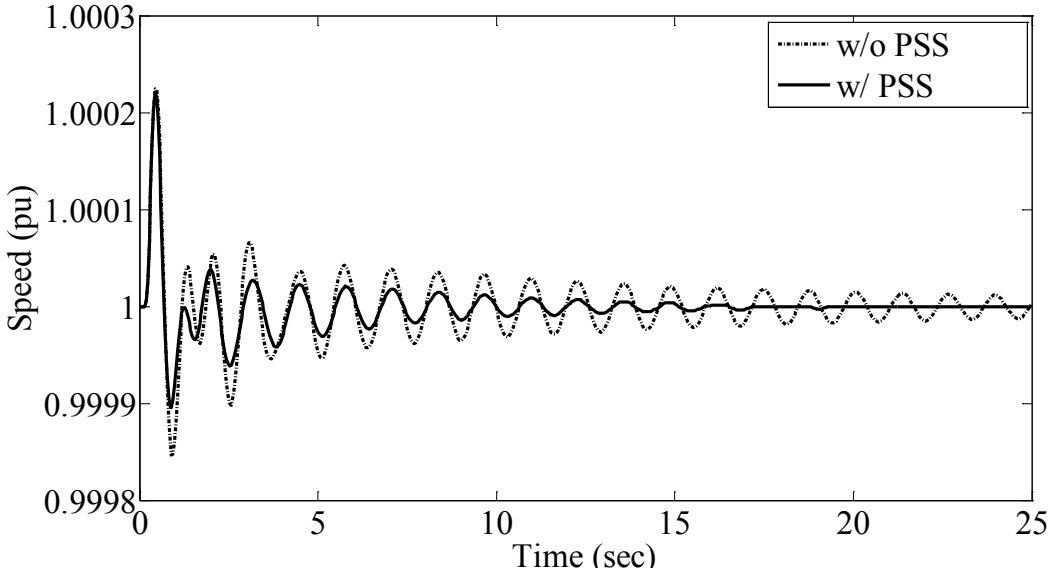

Fig. 6.3. PSS application example #1.

6.4 PSS application example #2

Fig. 6.4 shows a speed deviation response from a simulated impulse applied to another models excitation regulator. The model initially does not have

a PSS and both the AHE algorithm and Prony assessment estimated the dominant oscillatory frequency to be .96 Hz. However, the AHE method predicted the damping level to be 6.51% while the Prony estimator determined the damping level to be 6.44%. Eigenvalue analysis reported the dominant mode to have a damping ratio of 6.24% at a frequency of .95 Hz. Typically, a damping level in excess of 5% is deemed to be sufficiently damped. In this case a higher damping level was assumed to be desired.

With this information, a PSS model was applied to the generator and the phase lead compensation was set once again to be approximately 48˚ per stage. In this case, the gain of the PSS was set to 5 pu. Using (6.4), the values of T_1 and T_3 were computed to be .438 seconds while T_2 and T_4 were calculated to be .063 seconds. Again, the simulated impulse to the excitation system was performed and the time domain response was retrieved. Both Prony's method and the AHE technique found the dominant mode was moved to .95 Hz at a damping ratio of 9.90%. A slightly higher damping ratio of 10.21% was reported by eigenvalue analysis but at the same oscillatory frequency of .95 Hz. The speed deviation of the generator with the PSS modeled is shown in Fig. 6.4. As can be seen in the figure, damping has significantly improved as a result of the tuned controller.

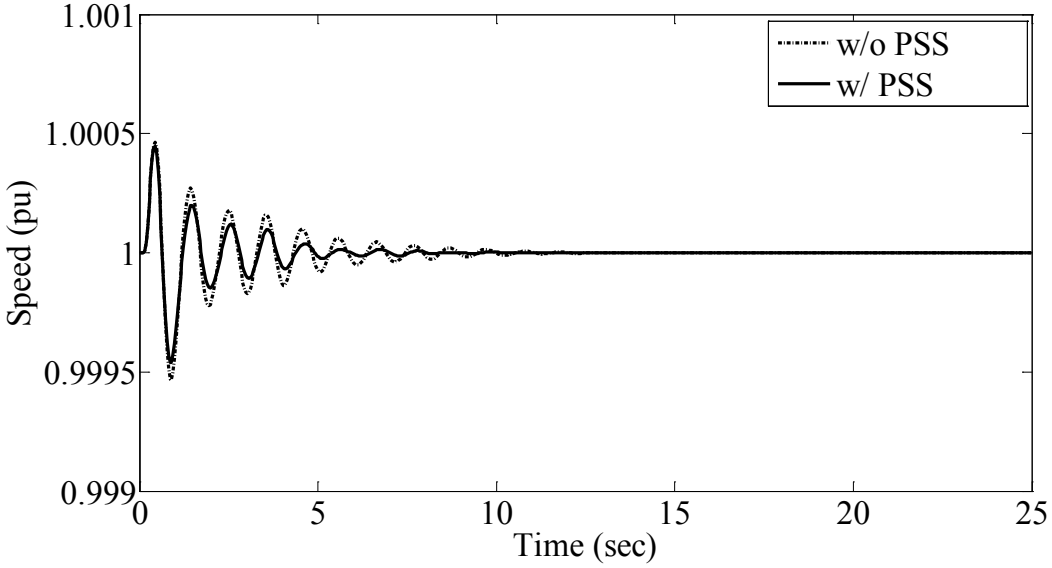

Fig. 6.4. PSS application example #2.

6.5 PSS application example #3

Fig. 6.5 shows a speed deviation response from a simulated impulse applied to another synchronous generators excitation regulator. This is the same simulated response as seen in Fig. 5.4 of the previous chapter. The model initially does not have a PSS and both the AHE algorithm and a Prony assessment estimated the dominant oscillatory frequency to be 1.052 Hz. Eigenvalue analysis identified the dominant frequency to be 1.039 Hz. The AHE technique found damping was 3.35% at 1.052 Hz, while Prony's method found the damping to be slightly greater at 3.53%. As stated earlier, the eigenvalue analysis found the damping at 1.039 Hz to be 3.01%.

Using the data collected, the settings were calculated for a PSS model using a gain K_{gs} of .50 pu and a 48˚ per stage of phase lead compensation. Next, values of T_1 and T_3 were calculated to be .400 seconds and T_2 and T_4 were found

to be .057 seconds. The impulse was applied to the model again and the time response recorded. In this case the AHE algorithm found the dominant mode increased to 1.081 Hz with a damping ratio of 5.56%. Prony's method found the frequency component of the mode was 1.083 Hz at a damping level of 5.79%. An eigenvalue assessment showed the frequency of the mode was 1.063 Hz and damping improved to 5.42%. The plot of the speed deviation of the synchronous generator with the tuned PSS model included is shown in Fig. 6.5. As was the case with the other examples, the damping at the frequency of interest has improved through use of the tuned PSS.

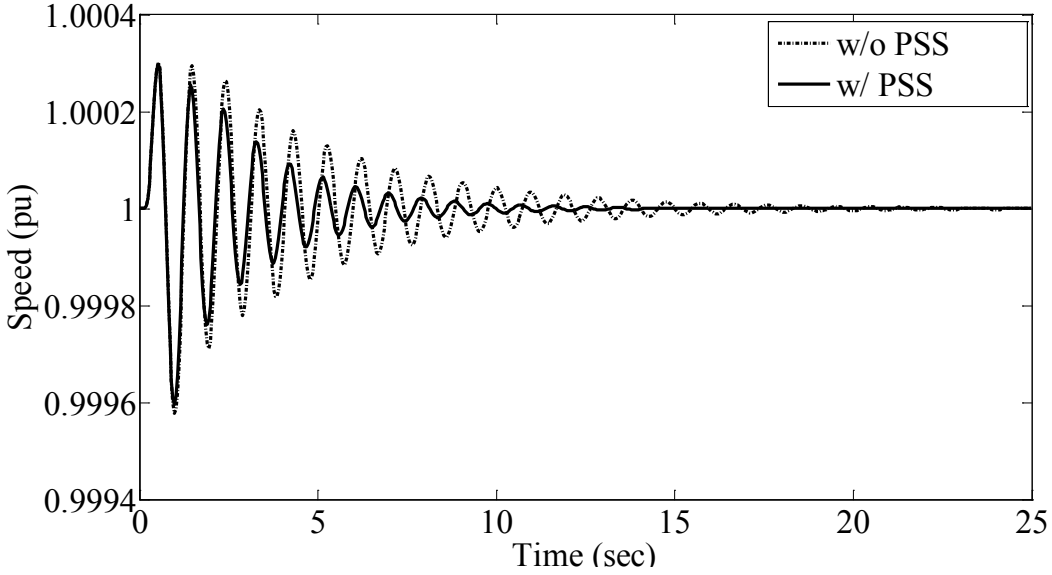

Fig. 6.5. PSS application example #3.

6.6 PSS application example #4

In the last example, a PSS model is re-tuned to the dominant frequency of the synchronous generator whose speed deviation is shown in Fig. 5.5 of the previous chapter. From a review of the plot, the generator has a growing

oscillation that the current PSS is unable to restrain effectively with the current settings. Eigenvalue analysis has revealed that the dominant mode is at .691 Hz with a damping ratio of -4.70%. The AHE algorithm and Prony's method found the dominant mode to be at .699 Hz and .697 Hz, respectively. Damping level for their associated frequencies was found to be -4.09% and -3.47% for the AHE and Prony's methods, respectively. The speed deviation response of the generator without the originally tuned PSS is shown again in Fig. 6.6 as a comparison.

The original speed input PSS model was retuned using the frequency estimated from the AHE algorithm. Keeping the same amount of phase lead compensation as was used in the previous examples, (6.4) was used to select the new controller time constants. A value of .609 seconds was calculated for the T_1 and T_3 time constants and a value of .087 seconds was determined for the T_2 and T_4 time constants. A PSS gain K_{gs} of 3.0 pu was chosen as well. An impulse was reapplied to the excitation system model of the synchronous generator and the time response was captured. Eigenvalue analysis showed the retuned PSS to have a dominant mode at .603 Hz and a damping ratio of 3.99%. The AHE algorithm found the dominant mode of the impulse response to be .594 Hz with a damping level of 5.11%. Prony's method found nearly the same frequency of the dominant mode at .595 Hz but the damping ratio was slightly higher at 6.38%. Fig. 6.6 shows the speed deviation of the generator with the retuned PSS represented. From the figure it is apparent that the generator response is now stable and well damped as a result of retuning the PSS.

6.7 PSS application summary

The AHE algorithm has been used in this chapter as a potential design tool for tuning or retuning PSS to dampen small signal events that occur in modeling power systems for purposes involving damping assessment. Actual PSS tuning activities are performed in the field in order to capture dynamics that are not present or accurately modeled in large base cases. The method described here is not meant to represent an optimal tuning procedure but simply to demonstrate the applicability of the AHE algorithm. Results of the pre- and post-design efforts were compared to results from both Prony and eigenvalue estimators. Both Prony's method and eigenvalue analysis have both been used successfully in the past in the design of damping devices in power systems. In addition, the AHE algorithm could be employed as a verification tool after a damping device has been installed or tuned in the field. Traditionally, tuning is performed primarily in the field using different methods. Verification of the damping devices performance is typically completed using simulations within a commercial transient stability program or a custom time domain simulation program. These results are then re-verified through simple field tests such as tripping of a local transmission element, switching between manual and automatic voltage regulators or switching a reactive element such as a capacitor or reactor.

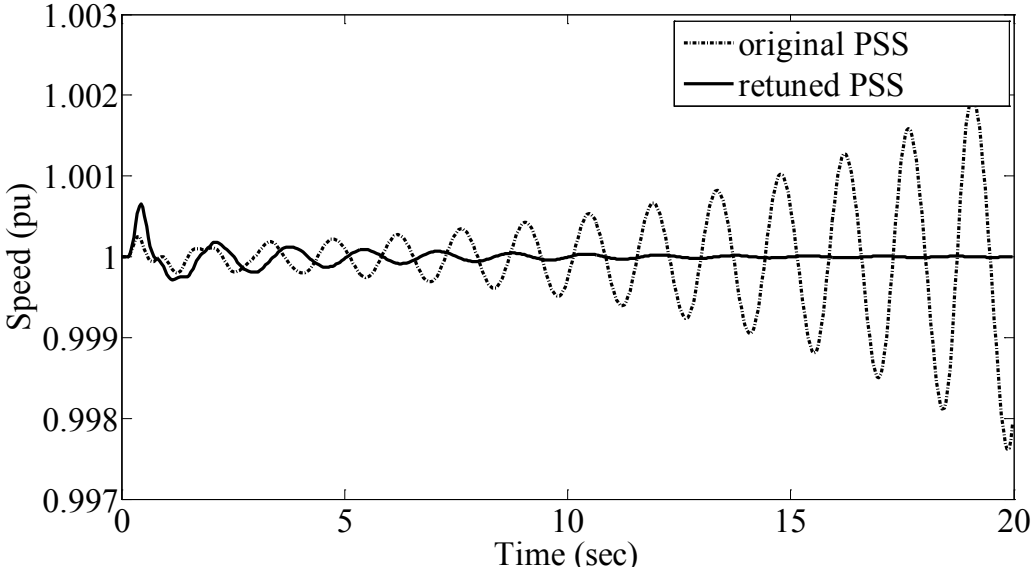

Fig. 6.6. PSS application example #4.

The purpose of this chapter was to demonstrate that the AHE algorithm could perform the design or verification task as well as other popular estimators such as Prony's method and eigenvalue analysis. Results from the four simple PSS design examples support this conclusion. Table 6.1 shows the results of the pre- and post-design estimates from the three prediction methods for the four examples assessed. Table 6.2 shows the final compensation settings for the four PSS examples used in this chapter. It should be noted that all other PSS settings were kept the same for the four examples.

Table 6.1. Damping application results.

		Before		After	
Example	Method	f_i	ζ_i	f_i	ζ_i
#1	AHE	.760 Hz	1.90%	.770 Hz	3.92%
	Prony's	.760 Hz	1.56%	.770 Hz	3.71%

	eigenvalue	.750 Hz	2.38%	.750 Hz	4.87%
#2	AHE	.960 Hz	6.51%	.950 Hz	9.90%
	Prony's	.960 Hz	6.44%	.950 Hz	9.90%
	eigenvalue	.950 Hz	6.24%	.950 Hz	10.21%
#3	AHE	1.052 Hz	3.35%	1.081 Hz	5.56%
	Prony's	1.052 Hz	3.53%	1.083 Hz	5.79%
	eigenvalue	1.039 Hz	3.01%	1.063 Hz	5.42%
#4	AHE	.699 Hz	-4.09%	.594 Hz	5.11%
	Prony's	.697 Hz	-3.47%	.595 Hz	6.38%
	eigenvalue	.691 Hz	-4.70%	.603 Hz	3.99%

Table 6.2. Example PSS settings.

Example	K_{gs}	T_1	T_2	T_3	T_4
#1	2.5 pu	.549 sec	.078 sec	.549 sec	.078 sec
#2	5.0 pu	.438 sec	.063 sec	.438 sec	.063 sec
#3	.50 pu	.400 sec	.057 sec	.400 sec	.057 sec
#4	3.0 pu	.609 sec	.087 sec	.609 sec	.087 sec

Chapter 7

CONCLUSIONS AND FUTURE WORK

7.1 Conclusions

As shown in this thesis, there are many off-line tools for engineers to use in assessing electromechanical modes in power systems. Some algorithms are applicable for only simulated measurements where no noise interference exists. One such case is use of estimators on simulated signals generated from a transient stability program. Because of the advent of devices like the PMU and other long-term recording equipment, many tools and techniques are now being employed to assess small signal stability phenomenon directly from measurements taken from the field. Uses of these measurements vary from tuning damping equipment to performing post-mortem analysis of power system disturbances. Whatever the intent of the assessment, field measurements are susceptible to noise interference. Consequently, the tools to perform off-line estimation of electromechanical modes in power systems must be capable of providing accurate predictions in the presence of noise. The finding of this thesis is that the orthogonal polynomial based AHE algorithm is a new method for estimating electromechanical modes and is an improvement over other popular small signal estimators when signals are corrupted with noise.

A comparison was performed in Chapter 4 between the AHE algorithm and four other estimators in terms of their performance under various aspects of artificially generated measurements. The other methods included a least squares Prony analysis, a Yule-Walker autoregressive estimator, the O'Shea sliding

window method employing the FFT algorithm, and the Hilbert-Huang Transform method. References to each of these other four methods are provided in Chapter 2 and a description of their function is given in Chapter 3.

In Chapter 4, the AHE algorithm capability was compared to the other four estimators using different combinations of single mode and multi-mode signals from .2 to 2 Hz over a fixed window. A review of the results shows that the accuracy of the AHE method met or exceeded the performance of the other estimators in identifying the different frequencies and damping levels. The exception was when the modes were sufficiently close in frequency with widely different damping levels.

In the additive white noise tests, a artificial measurement of 50 seconds was assessed. The added noise in this case was white or Gaussian, maintaining a constant variance across a spectrum from .2 to 2 Hz. For each SNR level, the MSE over different trials was recorded for each of the five estimators. Results of the analyses showed that the accuracy of the AHE algorithm modal estimation exceeded that of the other methods below a SNR of 15 dB to as low as 2 dB.

For the tests of reduced window length, a multi-mode signal was used except without the additive white noise. The observation window length was reduced and the absolute percent error was recorded for decreasing lengths for each frequency and damping component. Results from the analysis reveal that the AHE algorithm was as accurate as the other estimators for each modal component. For the sampling rate test, both sliding window algorithms

performed better than the other estimators as the sampling rate decreased as low as 5 Hz. This result was true for both frequency and damping component predictions. In addition, the AHE algorithm was found to be nearly as accurate at low sample rates than at high rates suggesting that there is little benefit for sampling at higher rates for this algorithm. The consequence of this observation is that the estimation can be achieved in a shorter amount of time with less data.

In Chapter 5, a commercial transient stability program was used to generate simulated power system measurements that were assessed using the five spectral estimators. The measurements were made by applying an impulse to the excitation system of a number of generators. Eigenvalue analysis provided a benchmark for the other estimators performance. The AHE algorithm performed better than the other four estimators in predicting damping levels. For the frequency component of the modes, the AHE algorithm was only slightly less accurate than the least squares Prony analysis. These results suggest that during actual recorded small signal disturbances the AHE algorithm will provide accurate results as compared to other established estimators.

Results from Chapter 6 suggest that the AHE algorithm can also be used in designing or verifying small-signal damping devices, such as the PSS. The AHE technique was able to accurately identify the oscillatory and damping components in the pre-mitigation scenario. These results provided the data to design the controller. After each PSS was tuned or retuned, the results were again assessed using the AHE algorithm to verify damping improvement. Results from

both Chapters 5 and 6 also suggest that the algorithm would be useful in post-mortem analysis that is often performed following a major power system disturbance.

Table 7.1 summarizes the primary benefits of the AHE algorithm reported and examined in this thesis. As was mentioned before, a GUI or graphical user interface was written in MATLAB that incorporated the AHE algorithm, the least squares Prony's method, the Yule-Walker autoregressive method, the Hilbert-Huang Transform algorithm and the O'Shea sliding window method. The GUI was used interactively for most of the research performed throughout this thesis. Results from the analyses were presented both graphically and through lists using the GUI. The code the AHE algorithm is provided in Appendix B. Also, the codes for the Prony analysis and the Yule-Walker algorithm are provided in Appendix C and D, respectively. The initial code for the HHT algorithm can be accessed at [88] and was modified for use in this thesis.

Table 7.1. Demonstrated benefits of the AHE algorithm.

Contribution	Synthetic Measurements	Simulated Measurements
Noise tolerant estimation.	X	
Estimation of simulated power system signals.		X
Damping mitigation device design and verification.		X

7.2 Future work

Utilities are often required to verify generator testing results before the data is accepted for modeling in large study cases. The verification process is not standardized and usually involves performing simulated large-signal transient stability disturbances. Although the results of this type of assessment are valuable, a small-signal stability analysis would provide further insight into the accuracy of the data. Currently, the small-signal tools that are available are part of suites of software modules. Incorporating the AHE algorithm directly into either the Siemens PTI or the GE PSLF power flow and dynamic packages would allow quick assessment of data accuracy without the need for a suite of modules. The assessment would be close to a linear simulation unlike simulations from large signal or transient stability results.

Calculating a small signal stability index for operators usage similar to other alarms they are encounter on a daily basis has been proposed by a number of researchers. The indices or alarms can simply prompt an operator that a condition exists or that the operator should take action. A controlled action could take the form of a remedial action or a protective scheme. An index could be associated with the most lightly damped mode or it can be linked to a frequency range of a known interarea or local modes. In either case, the AHE algorithm could be applied in the development of such an index even if the assessment is completed off-line.

Most of the actual power system disturbance events are non-stationary to some degree, which result in both the frequency and damping levels varying in time. Except for the HHT method, all the methods used in this thesis employ schemes applicable to stationary disturbances. Implementing a scheme using the AHE algorithm that could be used on-line provides an opportunity to assess the non-stationary characteristics of identified modes. The ability within the algorithm to generate frequency samples originates from overlapping windows. Use of small windows to track varying mode components has already been performed. A modification of components of the functional portions of the AHE algorithm and not necessarily the interpolative or extrapolative elements may be possible. Table 7.2 lists the possible future applications of the AHE algorithm through additional research.

Table 7.2. Potential future applications for the AHE algorithm.

Future work	Planning	Operations
Incorporate the algorithm directly into a commercial power flow package.	X	X
Stability index or alarm generation.		X
Non-stationary mode analysis.	X	X

REFERENCES

[1] P. Anderson and A. Fouad, *Power System Control and Stability*, Ames, Iowa: Iowa State University Press, 1977.

[2] P. Kundur, J. Paserba, V. Ajjarapu, G. Andersson, A. Bose, C. Canizares, N. Hatziargyriou, D. Hill, A. Stankovic, C. Taylor, T. Van Cutsem and V. Vittal, "Definition and classification of power system stability IEEE/CIGRE joint task force on stability terms and definitions," *IEEE Trans. Power Syst.,* vol. 19, no. 3, pp. 1387-401, Aug. 2004.

[3] P. Kundur, *Power System Stability and Control*, New York, New York: McGraw-Hill for EPRI, 1993.

[4] "Arizona Renewable Energy Assessment Final Report, Prepared for Arizona Public Service, Salt River Project and Tucson Electric Power" Black & Veatch, Sep. 2007.

[5] 2009 Interconnection Facilities. [Online]. Available: http://www.oatioasis.com/azps.

[6] "20% Wind Energy by 2030," United States Department of Energy, May 2008.

[7] E. Larsen and W. Price, "MANSTAB/POSSIM Power System Dynamic Analysis Programs – A New Approach Combining Nonlinear Simulation and Linearized State-space/Frequency Domain Capabilities," *IEEE PICA Conference Proceedings*, pp. 350-359, May 1977.

[8] D. Wong, G. Rogers, B. Porretta and P. Kundur, "Eigenvalue Analysis of Very Large Power Systems," *IEEE Trans. Power Syst.,* vol. 3, no. 2, pp. 472-80, May 1988.

[9] R.Byerly, R. Bennon, and D. Sherman, "Eigenvalue Analysis of Synchronizing Power Flow Oscillations in Large Electric Power Systems," *IEEE Trans. Power Apparatus and Syst.,* vol. 101, no. 1, pp. 235-243, Jan. 1982.

[10] N. Martins, "Efficient Eigenvalue and Frequency Response Methods Applied to Power System Small-Signal Stability Studies," *IEEE Trans. Power Syst.,* vol. 1, no. 1, pp. 217-24, Feb. 1986.

[11] P. Kundur, G. Rogers, D. Wong, L. Wang and M. Lauby, "A Comprehensive Computer Program Package for Small Signal Stability Analysis of Power Systems," *IEEE Trans. Power Syst.,* vol. 5, no. 4, pp. 1076-83, Nov. 1990.

[12] K. Anaparthi. B. Pal and H. El-Zobaidi, "Coprime factorization approach in designing mult-input stabilizer for damping electromechanical oscillations in

power systems," *IEE Proc.-Gen.-Trans. Distr.,* vol. 152, no. 3, pp. 301-08, May 2005.

[13] M. Joorabian, N. Ramandi and M. Ebadi, "Optimal Location of Static VAR Compensator (SVC) Based on Small Signal Stability of Power System," *IEEE 2nd Int. Power and Energy Conf.*, pp. 1333-38, Dec. 2008.

[14] A. Hemeida and G. El-Saady, "Damping Power Systems Oscillations Using FACTS Combinations," *UPEC 39th Inc. Conf.,* vol. 1, pp. 333-37, Sept. 2004.

[15] G.R.B. Prony, "Essai experimental et analytique, etc.," *Paris, J. de L'Ecole Polytechnique*, vol. 1, cahier 2, pp. 24-76, 1795.

[16] F. Hildebrand, *Introduction to Numerical Analysis*, New York, New York: McGraw-Hill, 1956.

[17] R. Kumaresan and D. Tufts, "Improved Spectral Resolution III: Efficient Realization," *Proc. of the IEEE,* vol. 68, no. 10, pp. 1354-55, 1980.

[18] S. Kay and S. Marple, "Spectrum Analysis-A Modern Perspective," *Proc. of the IEEE,* vol. 69, no. 11, pp. 1380-1419, Nov. 1981.

[19] J. Hauer, "Identification of power system models for Large Scale Damping Control," *Proc. of the 28th IEEE Conf. on Decision and Control,* vol. 2, pp. 1841-46, Dec. 1989.

[20] J. Hauer, C. Demeure and L. Scharf, "Initial Results in Prony Analysis of Power System Response Signals," *IEEE Trans. Power Syst.,* vol. 5, no. 1, pp. 80-89, Feb. 1990.

[21] J. Hauer and D. Trudnowski, "Using the Coherency Function in Measurement Based Small-Signal Analysis of Large Power Systems," *IEEE 2000 PES Summer Meeting,* vol. 2, pp. 809-11, July 2000.

[22] D. Trudnowski, J. Smith, T. Short and D. Pierre, "An Application of Prony Methods in PSS Design for Multimachine Systems," *IEEE Trans. Power Syst.,* vol. 6, no. 1, pp. 118-26, Feb. 1991.

[23] R. You and M. Nehrir, "A Systematic Approach to Controller design for SVC to Enhance Damping of Power System Oscillations," *IEEE 2004 Power Systems Conf. and Expo,* vol. 2, pp. 1134-39, Oct. 2004.

[24] C. Grund, S. Balser, G. Sweezy, S. Nilsson, and J. Hauer, "Dynamic System Monitoring (DSM) for HVDC Modulation Control," *IEEE Trans. Power Del.,* vol. 8, no. 3, pp. 853-60, July 1993.

[25] J. Hauer, "Application of Prony Analysis to the Determination of Modal Content and Equivalent Models for Measured Power System Response," *IEEE Trans. Power Syst.,* vol. 6, no. 3, pp. 1062-68, Aug. 1991.

[26] N. Zhou, J. Pierre and J. Hauer, "Initial Results in Power System Identification From Injected Probing Signals Using a Subspace Method," *IEEE Trans. Power Syst.,* vol. 21, no. 3, pp. 1296-02, Aug. 2006.

[27] T. Ulrych and R. Clayton, "Time Series Modeling and Maximum Entropy," *Phys. Earth Planetary Interiors.,* vol. 12, 1976.

[28] S. Marple, "A New Autoregressive Spectrum Analysis Algorithm," *IEEE Trans. Acoustics, Speech and Sig. Proc.*, vol. 28, no. 4, pp. 441-454, Aug. 1980.

[29] D. Trudnowski, J. Johnson and J. Hauer, "Making Prony Analysis More Accurate using Multiple Signals," *IEEE Trans. Power Syst.,* vol. 14, no. 1, pp. 226-31, Feb. 1999.

[30] J. Sanchez-Gasca and J. Chow, "Performance Comparison of Three Identification Methods for the Analysis of Electromechanical Oscillations," *IEEE Trans. Power Syst.,* vol. 14, no. 3, pp. 995-02, Aug. 1999.

[31] S. Marple, *Digital Spectral Analysis with Applications*, Englewood Cliffs, New Jersey: Prentice-Hall, 1987.

[32] B. Bujanowski, J. Pierre, S. Hietpas, T. Sharpe and D. Pierre, "A Comparison of Several System Identification Methods with Application to Power Systems," *Proc. 36th Midwest Symp. On Circuits and Systems,* vol. 1, pp. 64-67, Aug. 1993.

[33] H. Ni, G. Heydt and R. Farmer, "Autonomous Damping Controller Design for Power System Oscillations," *IEEE 2000 Power Eng. Society Meeting,* vol. 2, pp. 1133-38, July 2000.

[34] R. Wies, J. Pierre and D. Trudnowski, "Use of ARMA Block Processing for Estimating Stationary Low-Frequency Electromechanical Modes of Power Systems," *IEEE Trans. Power Syst.,* vol. 18, no.1, pp. 167-73, Feb. 2003.

[35] D. Jones, "Estimation of Power System Parameters," *IEEE Trans. Power Syst.,* vol. 19, no. 4, pp. 1980-89, Nov. 2004.

[36] R. Wies, A. Balasubramanian and J. Pierre, "Combining Least Mean Squares Adaptive Filter and Auto-regressive Block Processing Techniques for Estimating the Low-Frequency Electromechanical Modes in Power Systems," *IEEE 2006 Power Eng. Society Meeting*, pp. 1-8, 2006.

[37] J. Hernandez, E. Barocio and A. R. Messina, "Nonlinear Modal Identification of Power System Response Signals Using Higher Order Statistics," *IEEE 2007 Power Eng. Society Meeting,* pp. 1-8, 2007.

[38] H. Koseki and K. Yoshimura, "Estimation of Electromechanical Modes of Power System Using ARMA Model Based on Cross Spectrum," 2nd *IEEE Int. Conf. on Power and Energy,* pp. 508-13, Dec. 2008.

[39] Y. Hsu, C. Chen and C. Su, "Analysis of Electromechanical Modes Using an Artificial Neural Network," *IEE Proc.-Gen. Trans. Distr.,* vol. 141, no. 3, pp. 198-04, May 1994.

[40] I. Kamwa, R. Grondin, V. Sood, C. Gagnon, V. Nguyen and J. Mereb, "Recurrent Neural Networks for Phasor Detection and Adaptive Identification in Power System Control and Protection," *IEEE Trans. Inst. and Meas.,* vol. 45, no. 2, pp. 657-64, April 1996.

[41] Y. Zhang, G. Chen , O. Malik, and G. Hope, "An Artificial Neural Network Based Adaptive Power System Stabilizer," *IEEE Trans. Energy Conv.,* vol. 8, no.1, pp. 71-7, March 1993.

[42] Y. Zhang, O. Malik, G. Hope and G. Chen, "Application of an Inverse Input/Output Mapped ANN as a Power System Stabilizer," *IEEE Trans. Energy Conv.,* vol. 9, no. 3, pp. 433-41, Sept. 1994.

[43] Y. Zhang, O. Malik, and G. Chen, "Artificial Neural Network Power System Stabilizers in Multi-Machine Power System Environment," *IEEE Trans. Energy Conv.,* vol. 10, no. 1, pp. 147-55, March 1995.

[44] P. Shamsollahi and O. Malik, "An Adaptive Power System Stabilizer Using On-line Trained Neural Networks," *IEEE Trans. Energy Conv.,* vol. 12, no. 4, pp. 382-87, Dec. 1997.

[45] P. Shamsollahi and O. Malik, "Application of Neural Adaptive Power System Stabilizer in a Multi-Machine Power System," *IEEE Trans. Energy Conv.,* vol. 14, no. 3, pp. 731-36, Sept. 1999.

[46] P. Shamsollahi and O. Malik, "Real-Time Implementation and Experimental Studies of a Neural Adaptive Power System Stabilizer," *IEEE Trans. Energy Conv.,* vol. 14, no. 3, pp. 737-42, Sept. 1999.

[47] Y. Hua and T. Sarkar, "Matrix Pencil Method and its Performance," *ICASSP Int. Conf. Acoustics, Speech and Sig. Proc.,* vol. 4, pp. 2476-79, April 1988.

[48] Y. Hua and T. Sarkar, "Matrix Pencil Method for Estimating Parameters of Exponentially Damped/Undamped Sinusoids in Noise," *IEEE Trans. Acoustics, Speech and Sig. Proc.,* vol. 38, no. 5, pp. 814-24, May 1990.

[49] T. Sarkar and O. Pereira, "Using the Matrix Pencil Method to Estimate the Parameters of a sum of Complex Sinusoids," *IEEE Antennas and Propagation Magazine,* vol. 37, no. 1, pp. 48-55, Feb. 1995.

[50] M. Crow and A. Singh, "The Matrix Pencil for Power System Modal Extraction," *IEEE Trans. Power Syst.,* vol. 20, no. 1, pp. 501-02, Feb. 2005.

[51] J. Quintero, G. Liu and V. Venkatasubramanian, "An Oscillation Monitoring System for Real-time Detection of Small-Signal instability in Large electric Power Systems," *2007 IEEE PES Gen. Mtg.*, pp. 1-8, June 2007.

[52] J. Quintero, G. Liu and V. Venkatasubramanian, "Oscillation Monitoring System Based on Wide Area Synchrophasors in Power Systems," *2007 iREP Symp.,* pp. 1-13, Aug. 2007.

[53] J. Barquin, L. Rouco, and H. Vargas, "Generalized Selective Modal Analysis," *2007 2002 PES Winter Mtg.,* vol. 2, pp. 1194-99, Jan. 2002.

[54] Z. Du, W. Liu and W. Fang, "Calculation of Electromechanical Oscillation Modes in Large power Systems using Jacobi-Davidson Method," *IEE Proc.-Gener. Transm. Distrib.,* vol. 152, no. 6, pp. 913-918, Nov. 2005.

[55] H. Ghasemi, C. Canizares and A. Moshref, "Oscillatory Stability Limit Prediction using Stochastic Subspace Identification," *IEEE Trans. Power Syst.,* vol. 21, no. 2, pp. 736-45, May 2006.

[56] H. Ghasemi and C. Canizares, "Confidence Intervals Estimation in the Identification of Electromechanical Modes from Ambient Noise," *IEEE Trans. Power Syst.,* vol. 23, no. 2, pp. 641-48, May 2008.

[57] S. Haykin, *Adaptive Filter Theory*, 2nd ed., Englewood Cliffs, New Jersey: Prentice-Hall, 1991.

[58] N.Zhou, J. Pierre, D. Trudnowski and R. Guttromson, "Robust RLS Methods for Online Estimation of Power System Electromechanical Modes," *IEEE Trans. Power Syst.,* vol. 22, no. 3, pp. 1240-49, Aug. 2007.

[59] N.Zhou, D. Trudnowski, J. Pierre and W. Mittelstadt, "Electromechanical Mode Online Estimation Using Robust RLS Methods," *IEEE Trans. Power Syst.,* vol. 23, no. 4, pp. 1670-80, Nov. 2008.

[60] T.Browne, V. Vittal, G. Heydt and A. Messina, "A Comparative Assessment of Two Techniques for Modal Identification from Power System Measurements," *IEEE Trans. Power Syst.,* vol. 23, no. 3, pp. 1408-15, Aug. 2008.

[61] H. Ghasemi and C. Canizares, "On-line damping torque estimation and oscillatory stability margin prediction," *IEEE Trans. Power Syst.,* vol. 22, no. 2, pp. 667-74, May 2007.

[62] F. Demello and C. Concordia, "Concepts of Synchronous Machine Stability as Affected by Excitation Control," *IEEE Trans. Power App Syst.,* vol.pas 88, no. 4, pp. 316-29, April 1969.

[63] B. Nomikos and C. Vournas, "Investigation of Induction Machine Contribution to Power System Oscillations," *IEEE Trans. Power App Syst.,* vol. 20, no. 2, pp. 916-25, May 2005.

[64] D. Trudnowski, "Estimating Electromechanical Mode Shape From Synchrophasor Measurements," *IEEE Trans. Power Syst.,* vol. 23, no. 3, pp. 1188-95, Aug. 2008.

[65] J. Martens, "The Hermite Transform-Theory," *IEEE Trans. Acoustics, Speech and Sig. Proc.,* vol. 38, no. 9, pp. 1595-06, Sept. 1990.

[66] B. Kokanos and G. Karady, "Associate Hermite Expansion Small Signal Mode Estimation," *IEEE Trans. Power Syst.,* vol. 25, no. 2, pp. 999-1006, May 2010.

[67] L. Lo Conte, R. Merletti, and G. Sandri, "Hermite Expansions of Compact Support Waveforms: Applications to Myoelectric Signals," *IEEE Trans. Biomed. Engr.,* vol. 41, no.12, pp. 1147-59, Dec. 1994.

[68] J. Hu, C. Chan, and T. Sarkar, "Optimal Simultaneous Interpolation/Extrapolation Algorithm of Electromagnetic Responses in Time and Frequency Domains," *IEEE Trans. Micro. Theory and Tech.,* vol. 49, no.10, pp. 1725-32, Oct. 2001.

[69] M. Rao, T. Sarkar, T. Anjali and R. Adve, "Simultaneous Extrapolation in Time and Frequency Domains using Hermite Expansions," *IEEE Trans. Ant. and Prop.,* vol. 47, no.6, pp. 1108-15, June 1999.

[70] M. Rao, T. Sarkar, R. Adve, T. Anjali and J. Callegon, "Extrapolation of Electromagnetic Responses from Conducting Objects in Time and Frequency Domains," *IEEE Trans. Micro. Theory and Tech.,* vol. 47, no.10, pp. 1964-74, Oct. 1999.

[71] J. Cadzow, "Spectral Estimation: An Overdetermined Rational Model Equation Approach," *Proc. of the IEEE,* vol. 70, no.9, pp. 907-39, Sept. 1982.

[72] S. Mitra, *Digital Signal Processing: A Computer Based Approach*, 3rd ed. New York, New York: McGraw Hill, 2006.

[73] K. Harb, "Accurate Macromodeling of High-Speed Interconnects Characterized by Time-Domain Measurements," M.A.Sc. Dissertation, Dept. Elect., Carleton University, Ottawa, Canada, 2003.

[74] M. Yuan, A. De, T. Sarkar, J. Koh, and B. Jung, "Conditions for Generation of Stable and Accurate Hybrid TD-FD MoM Solutions," *IEEE Trans. Micro. Theory and Tech.,* vol. 54, no.6, pp. 2552-63, June 2006.

[75] D. Slepian, "On Bandwidth," *Proc. of the IEEE,* vol. 64, no.3, pp. 292-00, March 1976.

[76] K. Poon and K. Lee, "Analysis of Transient Stability Swings in Large Interconnected Power Systems by Fourier Transformation," *IEEE Trans. Power Systems,* vol. 3, no.4, pp. 1573-81, Nov. 1988.

[77] P. O'Shea, "The Use of Sliding Spectral Windows for Parameter Estimation in Power System Disturbance Monitoring," *IEEE Trans. Power Systems,* vol. 15, no.4, pp. 1261-67, Nov. 2000.

[78] P. O'Shea, "An Algorithm for Power System Disturbance Monitoring," *Proc*. *ICASSP 2000,* vol. 6, pp. 3570-73, June 2000.

[79] P. O'Shea, "A High-Resolution Spectral Analysis Algorithm for Power-System Disturbance Monitoring," *IEEE Trans. Power Systems,* vol. 17, no.3, pp. 676-80, Aug. 2002.

[80] M. Pai, D. Sen Gupta and K. Padiyar, *Small Signal Analysis of Power Systems*, Harrow, Middlesex U.K. Alpha Science Int. Ltd, 2004.

[81] M. Ghavami, L. Michael and R. Kohno, *Ultra Wideband Signals and Systems in Communication Engineering*, West Sussex U.K. John Wiley & Sons, Ltd, 2004.

[82] J. Cadzow, B. Baseghi and T. Hsu, "Singular-value decomposition approach to time series modeling," *IEE PROC.,* vol. 130, no.3, pp. 202-10, April 1983.

[83] G. Golub and C. Van Loan, *Matrix Computations*, Baltimore, Maryland: The John Hopkins University Press, 1983.

[84] M. Hayes, *Statistical Digital Signal Processing and Modeling*, Hoboken, New Jersey: John Wiley & Sons, Inc., 1996.

[85] G. Golub and W. Kahan, "Calculating the Singular Values and Pseudo-inverse of a Matrix," *Journal SIAM,* vol. 2, no.2, pp. 205-24, 1965.

[86] D. Laila, A. Messina, and B. Pal, "A Refined Hilbert-Huang Transform With Applications to Interarea Oscillation Monitoring," *IEEE Trans. Power Systems,* vol. 24, no.2, pp. 610-20, May 2009.

[87] A. Fitzgerald, C. Kingsley, Jr., A. Kusko, *Electric Machinery,* 3rd Ed., New York, New York McGraw-Hill, 1971.

[88] [Online]. Available: http://perso.ens-lyon.fr/patrick.flandrin/emd.html.

APPENDIX C

PRONY'S METHOD SUBROUTINE

```
function [dfac,freq,ampl,phase,H,theta,y_hat] =
Prony(y,v,order,fs)
%clear all

dt = 1/fs;
y = detrend(y,'constant');
N = length(y);

%snr = 10*log10(sum(y.^2) ./ sum(nse.^2))
for j=1:length(y) - order % row index
    for k=1:order  % column index
        Ylp(j,k) = y(order + j - k);  % N-M x M matrix.
    end
end

for i=1:length(y) - order
    ym(i) = y(order + i);
end

an = [];
lp = [];
an = pinv(Ylp)*ym';
lp = [1 -an'];
rLP = roots(lp);  % calculate the roots of the lp.


dfac = log(abs(rLP))/dt;
a = imag(rLP);
b = real(rLP);
freq = atan(a./b)/(2*pi*dt);

zz = [];
for k =1:length(y)
    for i=1:order
        zz(k,i) = rLP(i)^(k-1);
    end
end

yMM = y(1:length(y));

B = [];
B = pinv(zz)*yMM; % Calculate the residues.

z_z = zz(2,:);    % Calculate the Prony spectrum.
theta = [(2*pi/N).*[0:(N/2)-2]];
for jk=1:length(theta)
    H(jk) = 0;
    for k=1:length(B)
        H(jk) = B(k)/(1 - z_z(k)*exp(2i*pi*theta(jk)*dt)) +
H(jk);
```

```
    end
end

ampl = sqrt(real(B).^2 + imag(B).^2);
phase = atan(imag(B)./real(B))*(180/pi);
ampl = ampl/max(ampl);
[ampl,AI] = sort(ampl,'descend');
dfac = dfac(AI);
freq = freq(AI);
phase = phase(AI);

y_hat = zz*B;
pexp(1:length(y)) = 0;
for j=1:length(y)
    for i=1:order
        pexp(j) = pexp(j) + B(i)*(rLP(i)^(j-1));
    end
end

ki = order;
for k=1:ki
    f(k) = (k-1)*(4/ki);
    z = exp(2i*pi*f(k)*dt);
    for j=1:order
        xZ(k,j) = B(j)/(1 - rLP(j)*(z^-1));
    end
end
for k=1:ki
    xZZ(k) = 0;
    for j=1:order
    xZZ(k) = xZZ(k)+ xZ(k,j);
    end
end
xZZ = 20*log10(xZZ);
y_PR = xZZ;

y_hat = real(pexp);
SNR = 10*log10((y'*y)/((y-y_hat')'*(y-y_hat')));

end
```

APPENDIX B

ASSOCIATE HERMITE EXPANSION SUBROUTINE

```
function [y_AH,xtt1,y_AHf1,y_AHph,ff,sing,aaa,nexp] =
AHE(xtt,v,fs,Beta)

N = length(xtt); % Define the window size.

dt = 1/fs;
t0 = (N/2) * dt;
ff = 0:.001:2;

Xf_0 = [];Ylp = [];ym = [];

pk_1 = 0;frq1 = 0;
v1 = v(1:N);
f_w = 2;
t_w = max(v1);

xtt1 = xtt(1:N)';
xtt1 = detrend(xtt1,'constant');
xtt1 = xtt1.*kaiser(N,Beta)';
nt = length(v1);           % nt is the observation time window
size.
nf = length(ff);

nexp = (1.7/pi)*(sqrt(pi*t_w*f_w) - 1.8)^2;nexp = ceil(nexp);
%nexp = ceil(2 * f_w * t_w);
lamdat = t_w/(2*(sqrt(pi*nexp/1.7) + 1.8));
%nxp = nexp;

lamdaf = 1/(2*pi*lamdat);
ht_mas = [];
for k = 1:nt  % Calculation of the time domain hermite matrix per
row.
    t(k)=(v1(k)-t0)/lamdat;
    ht_mas(k,1)=exp(-.5*(t(k)^2))/((pi^.25)*sqrt(lamdat));
    ht_mas(k,2)=sqrt(2)*t(k)*exp(-
.5*(t(k)^2))/((pi^.25)*sqrt(lamdat));
    for m=3:nexp+1,
        ht_mas(k,m)=((sqrt(2)*t(k)*ht_mas(k,(m-1)))-(sqrt(m-
2)*ht_mas(k,(m-2))))/sqrt(m-1);
    end
end

aaa = pinv(ht_mas)*xtt1'; % for singular value process
[U,S,V] = svd(ht_mas);
sing = diag(S);

for k = 1:nf        % Build the frequency domain master matrix.
    f(k) = ff(k)/lamdaf;
    hf_mas(k,1) = exp(-.5*(f(k)^2))/((pi^.25)*sqrt(lamdaf));
    hf_mas(k,2) = sqrt(2)*f(k)*exp(-
.5*(f(k)^2))/((pi^.25)*sqrt(lamdaf));
    for m=3:nexp+1,
```

```
        hf_mas(k,m) = ((sqrt(2)*f(k)*hf_mas(k,(m-1)))-(sqrt(m-
2)*hf_mas(k,(m-2))))/sqrt(m-1);
    end
end

Hfr = zeros(nf,nexp+1);                     % Build real
component of master frequency matrix.
Hfr(:,1:2:nexp+1) = hf_mas(:,1:2:nexp+1);
z = 0;
for k = 3:2:nexp+1
    Hfr(:,k) = Hfr(:,k).*(-1)^(k-z);
    z = z + 1;
end

Hfi = zeros(nf,nexp+1);                     % Build imag
component of master frequency matrix.
Hfi(:,2:2:nexp+1) = hf_mas(:,2:2:nexp+1);
z = 1;
for k = 4:2:nexp+1
    Hfi(:,k) = Hfi(:,k).*(-1)^(k-z);
    z = z + 1;
end
Hfi = -Hfi;

Hfrr = zeros(nf,nexp+1);
Hfii = zeros(nf,nexp+1);
for k = 1:nf
    Hfrr(k,:) = Hfr(k,:)*cos(2*pi*t0*ff(k)) +
Hfi(k,:)*sin(2*pi*t0*ff(k));
    Hfii(k,:) = -Hfr(k,:)*sin(2*pi*t0*ff(k)) +
Hfi(k,:)*cos(2*pi*t0*ff(k));
end
Hr = Hfrr;
Hi = Hfii;

for k=1:nt, % Calculation of the approximating function over the
observation window.
    t(k)=(v1(k)-t0)/lamdat;
    ht(k,1)=exp(-.5*(t(k)^2))/((pi^.25)*sqrt(lamdat));
    ht(k,2)=sqrt(2)*t(k)*exp(-
.5*(t(k)^2))/((pi^.25)*sqrt(lamdat));
    for m=3:nexp+1,
      ht(k,m)=((sqrt(2)*t(k)*ht(k,(m-1)))-(sqrt(m-2)*ht(k,(m-
2))))/sqrt(m-1);
    end
    y_AH(k)=0;
    for n=1:nexp+1,
      y_AH(k) = y_AH(k)+(aaa(n)*ht(k,n));
    end
end

for k=1:nf %Calculate the approx spectrum for freq ident
    y_AHfr(k) = 0;
```

```
    y_AHfi(k) = 0;
    for n=1:nexp+1,
        y_AHfr(k) = y_AHfr(k) + aaa(n)*Hr(k,n);
        y_AHfi(k) = y_AHfi(k) + aaa(n)*Hi(k,n);
    end
    y_AHf1(k) = (y_AHfr(k)^2 + y_AHfi(k)^2)^.5;
    y_AHph(k) = (180/pi)*angle(complex(y_AHfr(k),y_AHfi(k)));
end

y_AHph = unwrap(y_AHph);
end
```

APPENDIX A

EXAMPLE AHE CALCULATION DATA

Table A.1. Input and output data from an example AHE calculation.

time	$y(t)$	$\hat{y}(t)$	$\lvert\hat{Y}(f)\rvert$	$\underline{a}$
0	80.6527	79.311304	1.975111	0.744922
0.0417	81.1617	79.310074	2.089462	-0.380106
0.0833	82.2834	79.308407	2.374095	0.816212
0.1250	83.1279	79.306160	2.715052	-1.656779
0.1667	83.4560	79.303155	3.016348	-0.097947
0.2083	83.2546	79.299163	3.214241	2.765953
0.2500	82.5580	79.293895	3.270887	0.435847
0.2917	81.4361	79.286995	3.169431	-7.999669
0.3333	79.9889	79.278019	2.913277	-1.556073
0.3750	78.3400	79.266428	2.530467	11.363199
0.4167	76.6260	79.251567	2.088887	3.326055
0.4583	74.9846	79.232655	1.734169	-5.397153
0.5000	73.5433	79.208766	1.702625	-1.046159
0.5417	72.4105	79.178818	2.095016	-7.144679
0.5833	71.6702	79.141566	2.741710	-2.063448
0.6250	71.3747	79.095590	3.460345	6.347110
0.6667	71.5428	79.039303	4.140169	1.278241
0.7083	72.1590	78.970961	4.711060	7.974523
0.7500	73.1750	78.888677	5.124359	1.414623
0.7917	74.5150	78.790473	5.346395	-2.057287
0.8333	76.0821	78.674327	5.356684	-1.789636
0.8750	77.7671	78.538239	5.147506	
0.9167	79.4577	78.380354	4.723655	
0.9583	81.0456	78.199070	4.101934	
1.0000	82.4327	77.993184	3.310284	
1.0417	83.5342	77.762095	2.386781	
1.0833	84.2829	77.505996	1.380474	
1.1250	84.6302	77.226081	0.398106	
1.1667	84.5490	76.924822	0.793041	
1.2083	84.0355	76.606196	1.749509	
1.2500	83.1102	76.275895	2.612165	
1.2917	81.8194	75.941575	3.322978	
1.3333	80.2334	75.612988	3.844201	
1.3750	78.4464	75.302030	4.149484	
1.4167	76.5708	75.022757	4.224042	
1.4583	74.7314	74.791184	4.065197	
1.5000	73.0577	74.624921	3.682496	
1.5417	71.6738	74.542667	3.097239	
1.5833	70.6890	74.563415	2.341431	
1.6250	70.1873	74.705460	1.456180	
1.6667	70.2200	74.985181	0.489719	
1.7083	70.8007	75.415602	0.506157	
1.7500	71.9042	76.004875	1.475471	
1.7917	73.4687	76.754587	2.365505	
1.8333	75.4013	77.658198	3.126310	

1.8750	77.5856	78.699730	3.714449	
1.9167	79.8904	79.852603	4.095301	
1.9583	82.1787	81.079183	4.245149	
2.0000	84.3169	82.331089	4.153012	
2.0417	86.1822	83.550092	3.822556	
2.0833	87.6686	84.670276	3.275283	
2.1250	88.6916	85.621231	2.559967	
2.1667	89.1909	86.332023	1.792583	
2.2083	89.1329	86.736313	1.330161	
2.2500	88.5132	86.777998	1.730946	
2.2917	87.3574	86.417035	2.683375	
2.3333	85.7222	85.635156	3.757969	
2.3750	83.6956	84.440600	4.789809	
2.4167	81.3947	82.871642	5.691910	
2.4583	78.9617	80.997977	6.402483	
2.5000	76.5543	78.919451	6.874415	
2.5417	74.3361	76.762392	7.073522	
2.5833	72.4633	74.672609	6.978809	
2.6250	71.0705	72.805607	6.582996	
2.6667	70.2581	71.315050	5.892816	
2.7083	70.0837	70.339329	4.928929	
2.7500	70.5565	69.988039	3.725656	
2.7917	71.6386	70.329687	2.332050	
2.8333	73.2483	71.381572	0.839287	
2.8750	75.2694	73.103753	0.937689	
2.9167	77.5619	75.397575	2.526985	
2.9583	79.9735	78.109913	4.091941	
3.0000	82.3506	81.043341	5.531261	
3.0417	84.5480	83.970829	6.772928	
3.0833	86.4352	86.655103	7.753099	
3.1250	87.9035	88.870352	8.416544	
3.1667	88.8694	90.423569	8.718556	
3.2083	89.2776	91.174425	8.627033	
3.2500	89.1026	91.050472	8.124837	
3.2917	88.3502	90.055927	7.213488	
3.3333	87.0589	88.273103	5.922306	
3.3750	85.3009	85.855401	4.342817	
3.4167	83.1811	83.013208	2.814681	
3.4583	80.8336	79.993302	2.667394	
3.5000	78.4161	77.054180	4.589995	
3.5417	76.0994	74.440974	7.323209	
3.5833	74.0536	72.361528	10.361584	
3.6250	72.4337	70.967259	13.533695	
3.6667	71.3652	70.341259	16.733981	
3.7083	70.9321	70.493986	19.875435	
3.7500	71.1691	71.367571	22.879893	
3.7917	72.0595	72.847393	25.676333	
3.8333	73.5371	74.779051	28.201278	

3.8750	75.4939	76.988411	30.399744	
3.9167	77.7903	79.301053	32.226204	
3.9583	80.2675	81.559282	33.645377	
4.0000	82.7598	83.634185	34.632742	
4.0417	85.1064	85.430994	35.174762	
4.0833	87.1603	86.888721	35.268786	
4.1250	88.7959	87.974455	34.922675	
4.1667	89.9133	88.674122	34.154144	
4.2083	90.4421	88.982811	32.989887	
4.2500	90.3425	88.896683	31.464498	
4.2917	89.6071	88.408681	29.619265	
4.3333	88.2629	87.509374	27.500870	
4.3750	86.3715	86.192751	25.160059	
4.4167	84.0307	84.466224	22.650362	
4.4583	81.3729	82.362319	20.026932	
4.5000	78.5604	79.949240	17.345655	
4.5417	75.7769	77.338055	14.662764	
4.5833	73.2138	74.683129	12.035480	
4.6250	71.0553	72.174664	9.525046	
4.6667	69.4612	70.023916	7.205954	
4.7083	68.5509	68.441223	5.193161	
4.7500	68.3925	67.610328	3.715360	
4.7917	68.9970	67.662846	3.168164	
4.8333	70.3177	68.656173	3.626742	
4.8750	72.2565	70.559424	4.550557	
4.9167	74.6745	73.249505	5.521290	
4.9583	77.4044	76.519079	6.372755	
5.0000	80.2650	80.096126	7.044845	
5.0417	83.0741	83.671755	7.517829	
5.0833	85.6598	86.934062	7.789991	
5.1250	87.8689	89.602765	7.869193	
5.1667	89.5739	91.459116	7.769103	
5.2083	90.6769	92.368497	7.507176	
5.2500	91.1116	92.291626	7.103398	
5.2917	90.8460	91.283443	6.579436	
5.3333	89.8844	89.480761	5.958052	
5.3750	88.2688	87.080399	5.262817	
5.4167	86.0814	84.312356	4.518251	
5.4583	83.4443	81.411488	3.750826	
5.5000	80.5167	78.592077	2.992034	
5.5417	77.4884	76.029534	2.286983	
5.5833	74.5672	73.849950	1.717033	
5.6250	71.9637	72.128727	1.430963	
5.6667	69.8702	70.897462	1.545095	
5.7083	68.4445	70.155680	1.940625	
5.7500	67.7926	69.884903	2.438462	
5.7917	67.9603	70.061594	2.945348	
5.8333	68.9296	70.665820	3.421189	

5.8750	70.6221	71.684205	3.847759	
5.9167	72.9082	73.106375	4.216422	
5.9583	75.6202	74.916131	4.523464	
6.0000	78.5672	77.079655	4.768087	
6.0417	81.5513	79.533101	4.951419	
6.0833	84.3808	82.173586	5.075939	
6.1250	86.8811	84.856101	5.145105	
6.1667	88.9030	87.397458	5.163067	
6.2083	90.3269	89.588984	5.134457	
6.2500	91.0671	91.216323	5.064202	
6.2917	91.0720	92.083655	4.957376	
6.3333	90.3268	92.039999	4.819072	
6.3750	88.8557	91.002908	4.654298	
6.4167	86.7245	88.976233	4.467884	
6.4583	84.0418	86.058943	4.264420	
6.5000	80.9599	82.442628	4.048197	
6.5417	77.6699	78.398480	3.823167	
6.5833	74.3916	74.253555	3.592920	
6.6250	71.3581	70.359335	3.360667	
6.6667	68.7954	67.057276	3.129234	
6.7083	66.9008	64.643591	2.901069	
6.7500	65.8225	63.338580	2.678248	
6.7917	65.6446	63.264302	2.462494	
6.8333	66.3798	64.431980	2.255201	
6.8750	67.9704	66.741591	2.057452	
6.9167	70.2954	69.992537	1.870050	
6.9583	73.1846	73.904468	1.693546	
7.0000	76.4351	78.145895	1.528265	
7.0417	79.8295	82.365948	1.374337	
7.0833	83.1520	86.227503	1.231722	
7.1250	86.2012	89.437392	1.100240	
7.1667	88.8004	91.769961	0.979591	
7.2083	90.8043	93.083695	0.869383	
7.2500	92.1022	93.328539	0.769149	
7.2917	92.6196	92.544040	0.678369	
7.3333	92.3196	90.849802	0.596483	
7.3750	91.2047	88.429066	0.522911	
7.4167	89.3191	85.508465	0.457060	
7.4583	86.7522	82.335518	0.398339	
7.5000	83.6406	79.156268	0.346165	
7.5417	80.1676	76.196012	0.299971	
7.5833	76.5577	73.643224	0.259214	
7.6250	73.0621	71.638435	0.223374	
7.6667	69.9391	70.268919	0.191962	
7.7083	67.4287	69.567849	0.164521	
7.7500	65.7289	69.518212	0.140625	
7.7917	64.9747	70.060341	0.119880	
7.8333	65.2248	71.101646	0.101928	

7.8750	66.4573	72.527802	0.086438	
7.9167	68.5754	74.213767	0.073113	
7.9583	71.4187	76.034156	0.061684	
8.0000	74.7811	77.872168	0.051910	
8.0417	78.4297	79.626086	0.043575	
8.0833	82.1245	81.213940	0.036487	
8.1250	85.6353	82.575945	0.030476	
8.1667	88.7555	83.674600	0.025393	
8.2083	91.3095	84.493490	0.021106	
8.2500	93.1574	85.034729	0.017500	
8.2917	94.1983	85.315431	0.014476	
8.3333	94.3696	85.363988	0.011945	
8.3750	93.6481	85.216200		
8.4167	92.0531	84.911676		
8.4583	89.6492	84.490737		
8.5000	86.5515	83.991845		
8.5417	82.9283	83.449794		
8.5833	78.9983	82.894453		
8.6250	75.0220	82.350082		
8.6667	71.2826	81.835265		
8.7083	68.0606	81.363118		
8.7500	65.6060	80.941787		
8.7917	64.1114	80.575226		
8.8333	63.6915	80.263957		
8.8750	64.3721	80.005853		
8.9167	66.0917	79.796957		
8.9583	68.7104	79.632121		
9.0000	72.0270	79.505583		
9.0417	75.7996	79.411437		
9.0833	79.7682	79.343967		
9.1250	83.6753	79.297879		
9.1667	87.2821	79.268463		
9.2083	90.3807	79.251653		
9.2500	92.7994	79.244047		
9.2917	94.4076	79.242880		
9.3333	95.1150	79.245970		
9.3750	94.8711	79.251648		
9.4167	93.6674	79.258678		
9.4583	91.5410	79.266181		
9.5000	88.5801	79.273566		
9.5417	84.9293	79.280457		
9.5833	80.7924	79.286646		
9.6250	76.4287	79.292042		
9.6667	72.1376	79.296633		
9.7083	68.2357	79.300459		
9.7500	65.0251	79.303592		
9.7917	62.7605	79.306116		
9.8333	61.6214	79.308121		

9.8750	61.6938	79.309693		

Table A.2. Estimated spectrums and the downshifted frequency samples from an example AHE calculation.

$\|\hat{Y}_f\|_1$	$\|\hat{Y}_f\|_2$	$\|\hat{Y}_f\|_3$	$\|\hat{Y}_f\|_4$	$\|\hat{Y}_f\|_5$	$\|\hat{Y}_f\|_6$	$\|\hat{Y}_{f0}\|$
0.0000	0.0000	0.0000	0.0000	0.0000	0.0000	289.5450
0.0000	0.0000	0.0000	0.0000	0.0000	0.0000	310.0884
0.0000	0.0000	0.0000	0.0000	0.0000	0.0000	324.5741
0.0000	0.0000	0.0000	0.0000	0.0000	0.0000	324.5043
0.0000	0.0000	0.0000	0.0000	0.0000	0.0000	341.0142
0.0000	0.0000	0.0000	0.0000	0.0000	0.0000	353.6548
0.0000	0.0000	0.0000	0.0000	0.0000	0.0000	289.5450
0.0000	0.0000	0.0000	0.0000	0.0000	0.0000	310.0884
0.0000	0.0000	0.0000	0.0000	0.0000	0.0000	324.5741
0.0000	0.0000	0.0000	0.0000	0.0000	0.0000	324.5043
0.0000	0.0000	0.0000	0.0000	0.0000	0.0000	341.0142
0.0000	0.0000	0.0000	0.0000	0.0000	0.0000	289.5450
0.0000	0.0000	0.0000	0.0000	0.0000	0.0000	310.0884
0.0000	0.0000	0.0000	0.0000	0.0000	0.0000	324.5741
0.0000	0.0000	0.0000	0.0000	0.0000	0.0000	324.5043
0.0000	0.0000	0.0000	0.0000	0.0000	0.0000	289.5450
0.0000	0.0000	0.0000	0.0000	0.0000	0.0000	310.0884
0.0000	0.0000	0.0000	0.0000	0.0000	0.0000	324.5741
0.0000	0.0000	0.0000	0.0000	0.0000	0.0000	289.5450
0.0000	0.0000	0.0000	0.0000	0.0000	0.0000	310.0884
0.0000	0.0000	0.0000	0.0000	0.0000	0.0000	289.5450
0.0000	0.0000	0.0000	0.0000	0.0000	0.0000	
0.0000	0.0000	0.0000	0.0000	0.0000	0.0000	
0.0000	0.0000	0.0000	0.0000	0.0000	0.0000	
0.0000	0.0000	0.0000	0.0000	0.0000	0.0000	
0.0000	0.0000	0.0000	0.0000	0.0000	0.0000	
0.0000	0.0000	0.0000	0.0000	0.0000	0.0000	
0.0000	0.0000	0.0000	0.0000	0.0000	0.0000	
0.0000	0.0000	0.0000	0.0000	0.0000	0.0000	
0.0000	0.0000	0.0000	0.0000	0.0000	0.0000	

0.0000	0.0000	0.0000	0.0000	0.0000	0.0000	
0.0000	0.0000	0.0000	0.0000	0.0000	0.0000	
0.0000	0.0000	0.0000	0.0000	0.0000	0.0000	
0.0000	0.0000	0.0000	0.0000	0.0000	0.0000	
0.0000	0.0000	0.0000	0.0001	0.0000	0.0000	
0.0001	0.0001	0.0001	0.0001	0.0000	0.0000	
0.0001	0.0001	0.0001	0.0001	0.0001	0.0001	
0.0001	0.0001	0.0001	0.0001	0.0001	0.0001	
0.0001	0.0001	0.0001	0.0001	0.0001	0.0001	
0.0001	0.0001	0.0001	0.0001	0.0001	0.0001	
0.0001	0.0001	0.0001	0.0001	0.0001	0.0001	
0.0002	0.0002	0.0002	0.0002	0.0001	0.0001	
0.0002	0.0002	0.0002	0.0002	0.0001	0.0002	
0.0002	0.0002	0.0002	0.0002	0.0002	0.0002	
0.0003	0.0003	0.0003	0.0003	0.0002	0.0002	
0.0003	0.0003	0.0003	0.0003	0.0002	0.0003	
0.0003	0.0004	0.0004	0.0004	0.0003	0.0003	
0.0004	0.0004	0.0004	0.0004	0.0003	0.0003	
0.0005	0.0005	0.0005	0.0005	0.0004	0.0004	
0.0006	0.0006	0.0006	0.0006	0.0004	0.0005	
0.0007	0.0007	0.0007	0.0007	0.0005	0.0006	
0.0008	0.0008	0.0008	0.0008	0.0006	0.0007	
0.0009	0.0009	0.0009	0.0010	0.0007	0.0008	
0.0011	0.0011	0.0011	0.0011	0.0008	0.0009	
0.0012	0.0012	0.0013	0.0013	0.0009	0.0010	
0.0014	0.0014	0.0015	0.0015	0.0011	0.0012	
0.0017	0.0017	0.0017	0.0018	0.0013	0.0014	
0.0020	0.0020	0.0020	0.0021	0.0015	0.0017	
0.0023	0.0023	0.0023	0.0024	0.0017	0.0019	
0.0026	0.0026	0.0027	0.0028	0.0020	0.0022	
0.0031	0.0031	0.0031	0.0033	0.0023	0.0026	
0.0036	0.0035	0.0036	0.0038	0.0027	0.0030	
0.0041	0.0041	0.0042	0.0044	0.0031	0.0035	
0.0048	0.0048	0.0049	0.0051	0.0036	0.0040	
0.0055	0.0055	0.0057	0.0059	0.0042	0.0047	
0.0064	0.0063	0.0065	0.0068	0.0048	0.0054	
0.0074	0.0073	0.0075	0.0078	0.0056	0.0062	
0.0085	0.0084	0.0087	0.0090	0.0064	0.0072	
0.0098	0.0097	0.0100	0.0104	0.0074	0.0083	

0.0112	0.0112	0.0115	0.0119	0.0085	0.0095	
0.0129	0.0128	0.0133	0.0137	0.0098	0.0110	
0.0148	0.0147	0.0152	0.0157	0.0112	0.0126	
0.0170	0.0169	0.0175	0.0181	0.0129	0.0144	
0.0195	0.0193	0.0200	0.0207	0.0148	0.0166	
0.0223	0.0221	0.0229	0.0237	0.0169	0.0190	
0.0256	0.0253	0.0262	0.0271	0.0193	0.0217	
0.0292	0.0289	0.0300	0.0309	0.0221	0.0248	
0.0333	0.0329	0.0342	0.0353	0.0252	0.0283	
0.0380	0.0375	0.0391	0.0402	0.0287	0.0323	
0.0433	0.0427	0.0445	0.0458	0.0327	0.0367	
0.0493	0.0486	0.0506	0.0521	0.0372	0.0418	
0.0560	0.0552	0.0576	0.0592	0.0423	0.0475	
0.0637	0.0627	0.0654	0.0672	0.0480	0.0540	
0.0722	0.0711	0.0742	0.0762	0.0544	0.0613	
0.0819	0.0805	0.0841	0.0863	0.0616	0.0694	
0.0927	0.0910	0.0953	0.0976	0.0697	0.0786	
0.1048	0.1029	0.1078	0.1103	0.0788	0.0889	
0.1185	0.1162	0.1218	0.1246	0.0890	0.1005	
0.1337	0.1310	0.1375	0.1405	0.1004	0.1134	
0.1508	0.1476	0.1551	0.1583	0.1131	0.1279	
0.1698	0.1661	0.1747	0.1782	0.1273	0.1440	
0.1910	0.1867	0.1966	0.2004	0.1431	0.1621	
0.2147	0.2097	0.2210	0.2251	0.1608	0.1821	
0.2411	0.2352	0.2481	0.2525	0.1804	0.2045	
0.2704	0.2635	0.2783	0.2830	0.2022	0.2294	
0.3029	0.2949	0.3119	0.3168	0.2264	0.2570	
0.3390	0.3297	0.3491	0.3542	0.2531	0.2876	
0.3790	0.3682	0.3903	0.3957	0.2828	0.3215	
0.4232	0.4107	0.4359	0.4415	0.3155	0.3590	
0.4721	0.4577	0.4864	0.4920	0.3517	0.4004	
0.5261	0.5094	0.5420	0.5478	0.3916	0.4462	
0.5855	0.5663	0.6034	0.6091	0.4355	0.4966	
0.6510	0.6289	0.6710	0.6766	0.4838	0.5521	
0.7230	0.6975	0.7453	0.7506	0.5368	0.6131	
0.8020	0.7728	0.8270	0.8318	0.5950	0.6801	
0.8886	0.8552	0.9165	0.9208	0.6587	0.7536	
0.9836	0.9453	1.0146	1.0180	0.7284	0.8341	
1.0874	1.0436	1.1219	1.1243	0.8046	0.9221	

1.2007	1.1508	1.2392	1.2401	0.8876	1.0182	
1.3244	1.2675	1.3672	1.3662	0.9781	1.1231	
1.4592	1.3944	1.5066	1.5034	1.0766	1.2373	
1.6057	1.5321	1.6583	1.6524	1.1835	1.3615	
1.7649	1.6813	1.8232	1.8139	1.2995	1.4965	
1.9376	1.8428	2.0021	1.9888	1.4252	1.6429	
2.1247	2.0172	2.1960	2.1779	1.5611	1.8014	
2.3270	2.2055	2.4058	2.3820	1.7080	1.9729	
2.5455	2.4083	2.6325	2.6019	1.8663	2.1581	
2.7812	2.6263	2.8771	2.8386	2.0367	2.3579	
3.0350	2.8605	3.1406	3.0929	2.2200	2.5729	
3.3078	3.1114	3.4240	3.3656	2.4167	2.8041	
3.6008	3.3800	3.7284	3.6576	2.6275	3.0523	
3.9147	3.6669	4.0549	3.9698	2.8530	3.3184	
4.2507	3.9728	4.4044	4.3029	3.0939	3.6030	
4.6096	4.2984	4.7781	4.6578	3.3507	3.9071	
4.9924	4.6444	5.1769	5.0351	3.6241	4.2314	
5.4001	5.0113	5.6018	5.4356	3.9146	4.5767	
5.8334	5.3997	6.0537	5.8599	4.2227	4.9437	
6.2932	5.8099	6.5336	6.3084	4.5489	5.3331	
6.7802	6.2423	7.0423	6.7818	4.8936	5.7456	
7.2951	6.6972	7.5805	7.2802	5.2571	6.1816	
7.8384	7.1746	8.1489	7.8040	5.6398	6.6417	
8.4107	7.6747	8.7482	8.3532	6.0418	7.1262	
9.0122	8.1971	9.3787	8.9278	6.4632	7.6355	
9.6433	8.7417	10.0407	9.5275	6.9040	8.1697	
10.3040	9.3079	10.7346	10.1520	7.3640	8.7289	
10.9941	9.8951	11.4602	10.8006	7.8431	9.3131	
11.7135	10.5023	12.2175	11.4725	8.3408	9.9219	
12.4616	11.1285	13.0060	12.1666	8.8566	10.5549	
13.2377	11.7722	13.8252	12.8817	9.3898	11.2117	
14.0410	12.4320	14.6743	13.6161	9.9396	11.8914	
14.8703	13.1059	15.5523	14.3681	10.5047	12.5930	
15.7241	13.7917	16.4578	15.1353	11.0842	13.3153	
16.6008	14.4870	17.3893	15.9155	11.6764	14.0569	
17.4983	15.1890	18.3448	16.7057	12.2798	14.8161	
18.4144	15.8946	19.3223	17.5029	12.8924	15.5910	
19.3465	16.6005	20.3192	18.3035	13.5123	16.3793	
20.2915	17.3028	21.3327	19.1038	14.1372	17.1787	

21.2463	17.9976	22.3596	19.8996	14.7644	17.9863	
22.2072	18.6803	23.3964	20.6863	15.3914	18.7992	
23.1703	19.3463	24.4393	21.4591	16.0151	19.6141	
24.1314	19.9905	25.4842	22.2127	16.6323	20.4274	
25.0856	20.6074	26.5264	22.9416	17.2398	21.2353	
26.0282	21.1915	27.5612	23.6400	17.8338	22.0337	
26.9539	21.7366	28.5833	24.3016	18.4108	22.8181	
27.8570	22.2367	29.5872	24.9200	18.9667	23.5842	
28.7317	22.6851	30.5673	25.4886	19.4976	24.3270	
29.5719	23.0753	31.5173	26.0004	19.9992	25.0416	
30.3712	23.4004	32.4311	26.4485	20.4674	25.7229	
31.1229	23.6535	33.3021	26.8256	20.8977	26.3655	
31.8205	23.8274	34.1237	27.1247	21.2858	26.9642	
32.4569	23.9151	34.8890	27.3385	21.6275	27.5136	
33.0253	23.9097	35.5912	27.4601	21.9185	28.0082	
33.5187	23.8041	36.2234	27.4825	22.1546	28.4429	
33.9300	23.5917	36.7786	27.3992	22.3319	28.8124	
34.2525	23.2659	37.2501	27.2040	22.4465	29.1117	
34.4793	22.8205	37.6313	26.8914	22.4952	29.3364	
34.6041	22.2498	37.9157	26.4564	22.4747	29.4820	
34.6206	21.5486	38.0973	25.8951	22.3824	29.5449	
34.5229	20.7122	38.1703	25.2047	22.2161	29.5217	
34.3056	19.7366	38.1295	24.3839	21.9742	29.4102	
33.9639	18.6189	37.9702	23.4332	21.6557	29.2087	
33.4935	17.3570	37.6884	22.3557	21.2607	28.9166	
32.8907	15.9501	37.2808	21.1579	20.7897	28.5347	
32.1528	14.3988	36.7449	19.8508	20.2445	28.0650	
31.2778	12.7061	36.0791	18.4521	19.6281	27.5114	
30.2645	10.8780	35.2830	16.9892	18.9446	26.8796	
29.1129	8.9265	34.3571	15.5043	18.1996	26.1778	
27.8239	6.8773	33.3032	14.0619	17.4006	25.4168	
26.3997	4.7996	32.1246	12.7594	16.5569	24.6106	
24.8435	2.9634	30.8259	11.7361	15.6801	23.7769	
23.1597	2.5265	29.4133	11.1672	14.7847	22.9375	
21.3542	4.1955	27.8950	11.2167	13.8882	22.1190	
19.4341	6.6374	26.2809	11.9598	13.0116	21.3524	
17.4077	9.3352	24.5833	13.3476	12.1798	20.6731	
15.2849	12.1657	22.8174	15.2542	11.4215	20.1192	
13.0773	15.0804	21.0016	17.5444	10.7677	19.7295	

10.7979	18.0495	19.1583	20.1064	10.2496	19.5394	
8.4629	21.0483	17.3158	22.8551	9.8933	19.5763	
6.0938	24.0541	15.5101	25.7257	9.7149	19.8555	
3.7325	27.0441	13.7879	28.6670	9.7146	20.3777	
1.5871	29.9952	12.2110	31.6362	9.8760	21.1294	
1.7579	32.8839	10.8594	34.5956	10.1683	22.0851	
3.9373	35.6861	9.8296	37.5111	10.5525	23.2114	
6.2661	38.3774	9.2166	40.3504	10.9868	24.4709	
8.5755	40.9330	9.0738	43.0829	11.4309	25.8251	
10.8240	43.3283	9.3773	45.6788	11.8482	27.2366	
12.9864	45.5386	10.0306	48.1096	12.2065	28.6699	
15.0421	47.5397	10.9093	50.3475	12.4779	30.0926	
16.9724	49.3080	11.8991	52.3658	12.6385	31.4747	
18.7599	50.8208	12.9104	54.1390	12.6685	32.7892	
20.3891	52.0568	13.8771	55.6431	12.5515	34.0117	
21.8457	52.9959	14.7510	56.8555	12.2752	35.1204	
23.1177	53.6200	15.4975	57.7556	11.8313	36.0963	
24.1954	53.9129	16.0916	58.3249	11.2171	36.9227	
25.0718	53.8610	16.5171	58.5474	10.4369	37.5857	
25.7430	53.4532	16.7650	58.4095	9.5062	38.0742	
26.2090	52.6816	16.8337	57.9007	8.4595	38.3799	
26.4741	51.5415	16.7302	57.0137	7.3666	38.4974	
26.5475	50.0318	16.4711	55.7444	6.3667	38.4249	
26.4442	48.1557	16.0852	54.0924	5.7151	38.1637	
26.1859	45.9205	15.6160	52.0611	5.7547	37.7189	
25.8017	43.3388	15.1258	49.6578	6.6667	37.0995	
25.3291	40.4285	14.6973	46.8939	8.3166	36.3189	
24.8145	37.2145	14.4327	43.7848	10.4716	35.3947	
24.3127	33.7306	14.4436	40.3504	12.9616	34.3495	
23.8862	30.0223	14.8302	36.6147	15.6812	33.2107	
23.6008	26.1538	15.6560	32.6061	18.5605	32.0107	
23.5199	22.2220	16.9327	28.3575	21.5466	30.7871	
23.6967	18.3866	18.6242	23.9068	24.5946	29.5816	
24.1655	14.9375	20.6648	19.2981	27.6631	28.4392	
24.9359	12.4126	22.9772	14.5856	30.7121	27.4059	
25.9918	11.5940	25.4841	9.8503	33.7016	26.5253	
27.2948	12.8810	28.1125	5.3042	36.5921	25.8344	
28.7906	15.7602	30.7953	2.6582	39.3435	25.3584	
30.4162	19.4832	33.4702	5.7328	41.9159	25.1066	

32.1051	23.5646	36.0792	10.1283	44.2699	25.0693	
33.7915	27.7351	38.5676	14.5372	46.3664	25.2190	
35.4123	31.8340	40.8838	18.7732	48.1674	25.5128	
36.9087	35.7518	42.9788	22.7521	49.6366	25.8978	
38.2263	39.4053	44.8063	26.4111	50.7394	26.3161	
39.3161	42.7264	46.3228	29.6953	51.4437	26.7097	
40.1343	45.6566	47.4881	32.5546	51.7205	27.0237	
40.6429	48.1446	48.2654	34.9433	51.5440	27.2090	
40.8099	50.1458	48.6215	36.8196	50.8926	27.2237	
40.6105	51.6217	48.5279	38.1470	49.7494	27.0343	
40.0275	52.5397	47.9605	38.8938	48.1022	26.6167	
39.0525	52.8739	46.9005	39.0344	45.9451	25.9578	
37.6880	52.6049	45.3345	38.5491	43.2785	25.0576	
35.9498	51.7206	43.2553	37.4252	40.1102	23.9318	
33.8708	50.2163	40.6617	35.6573	36.4575	22.6173	
31.5079	48.0953	37.5592	33.2472	32.3497	21.1798	
28.9524	45.3696	33.9604	30.2051	27.8341	19.7245	
26.3464	42.0600	29.8850	26.5489	22.9908	18.4098	
23.9073	38.1978	25.3605	22.3056	17.9740	17.4537	
21.9515	33.8261	20.4235	17.5115	13.1497	17.1118	
20.8812	29.0040	15.1235	12.2155	9.5841	17.6045	
21.0718	23.8163	9.5416	6.5008	9.5871	19.0211	
22.6767	18.4029	3.9820	1.3692	13.5181	21.2918	
25.5500	13.0624	3.5964	6.5035	19.2601	24.2489	
29.3784	8.7076	9.4549	13.2278	25.6820	27.7041	
33.8406	7.9908	15.7837	20.1922	32.3656	31.4878	
38.6724	11.8524	22.1883	27.2759	39.1075	35.4569	
43.6669	17.5234	28.5507	34.3829	45.7730	39.4897	
48.6587	23.6690	34.7789	41.4181	52.2527	43.4797	
53.5088	29.8601	40.7852	48.2850	58.4478	47.3308	
58.0954	35.8911	46.4829	54.8852	64.2650	50.9533	
62.3078	41.6209	51.7859	61.1196	69.6144	54.2630	
66.0438	46.9326	56.6090	66.8896	74.4093	57.1796	
69.2077	51.7207	60.8690	72.0975	78.5659	59.6264	
71.7102	55.8874	64.4856	76.6485	82.0045	61.5310	
73.4682	59.3413	67.3825	80.4512	84.6496	62.8248	
74.4052	61.9977	69.4888	83.4192	86.4310	63.4439	
74.4522	63.7793	70.7401	85.4723	87.2845	63.3299	
73.5486	64.6175	71.0801	86.5377	87.1530	62.4302	

71.6431	64.4537	70.4622	86.5513	85.9869	60.6986	
68.6955	63.2414	68.8520	85.4590	83.7449	58.0963	
64.6788	60.9488	66.2298	83.2182	80.3951	54.5921	
59.5822	57.5632	62.5958	79.7997	75.9154	50.1636	
53.4180	53.0983	57.9777	75.1900	70.2939	44.7973	
46.2349	47.6087	52.4462	69.3950	63.5300	38.4896	
38.1537	41.2238	46.1467	62.4472	55.6349	31.2485	
29.4753	34.2313	39.3718	54.4201	46.6327	23.0976	
21.0903	27.3131	32.7343	45.4642	36.5642	14.0985	
16.0138	22.1594	27.5365	35.9095	25.4991	4.6714	
19.4699	21.9192	26.0466	26.6127	13.6205	7.3525	
29.8028	28.1054	30.0234	20.1365	3.8532	18.6288	
43.0900	38.6581	38.6697	21.5321	14.4377	30.8317	
57.8982	51.6281	50.2445	31.0172	28.8481	43.7145	
73.7137	66.0880	63.6123	44.4284	44.1023	57.1728	
90.2735	81.5835	78.1649	59.6873	59.9670	71.1124	
107.392	97.8390	93.5451	76.0195	76.3050	85.4368	
124.914	114.648	109.507	93.0501	92.9899	100.044	
142.691	131.837	125.858	110.534	109.895	114.831	
160.578	149.240	142.417	128.273	126.891	129.686	
178.431	166.700	159.034	146.102	143.847	144.497	
196.109	184.062	175.554	163.844	160.630	159.151	
213.466	201.173	191.829	181.341	177.105	173.532	
230.363	217.883	207.715	198.437	193.140	187.525	
246.660	234.045	223.071	214.979	208.603	201.018	
262.223	249.516	237.763	230.818	223.368	213.900	
276.921	264.158	251.661	245.813	237.312	226.063	
290.630	277.840	264.642	259.828	250.316	237.407	
303.234	290.439	276.590	272.737	262.271	247.835	
314.625	301.842	287.400	284.421	273.075	257.259	
324.706	311.945	296.974	294.775	282.636	265.599	
333.389	320.655	305.225	303.703	290.870	272.781	
340.599	327.894	312.081	311.123	297.708	278.745	
346.273	333.594	317.479	316.967	303.088	283.439	
350.362	337.703	321.370	321.180	306.966	286.821	
352.829	340.184	323.719	323.723	309.306	288.862	
353.654	341.014	324.504	324.574	310.088	289.545	
352.829	340.184	323.719	323.723	309.306	288.862	
350.362	337.703	321.370	321.180	306.966	286.821	

346.273	333.594	317.479	316.967	303.088	283.439	
340.599	327.894	312.081	311.123	297.708	278.745	
333.389	320.655	305.225	303.703	290.870	272.781	
324.706	311.945	296.974	294.775	282.636	265.599	
314.625	301.842	287.400	284.421	273.075	257.25	
303.234	290.439	276.590	272.737	262.271	247.835	
290.630	277.840	264.642	259.828	250.316	237.407	
276.921	264.158	251.661	245.813	237.312	226.063	
262.223	249.516	237.763	230.818	223.368	213.900	
246.660	234.045	223.071	214.979	208.603	201.018	
230.363	217.883	207.715	198.437	193.140	187.525	
213.466	201.173	191.829	181.341	177.105	173.532	
196.109	184.062	175.554	163.844	160.630	159.151	
178.431	166.700	159.034	146.102	143.847	144.497	
160.578	149.240	142.417	128.277	126.891	129.686	
142.691	131.837	125.854	110.534	109.895	114.831	
124.914	114.648	109.507	93.0501	92.9899	100.044	
107.392	97.8390	93.5451	76.0195	76.3050	85.4368	
90.2735	81.5835	78.1649	59.6873	59.9670	71.1124	
73.7137	66.0880	63.6123	44.4284	44.1023	57.1728	
57.8982	51.6281	50.2445	31.0172	28.8481	43.7145	
43.0900	38.6581	38.6697	21.5321	14.4377	30.8317	
29.8028	28.1054	30.0234	20.1365	3.8532	18.6288	
19.4699	21.9192	26.0466	26.6127	13.6205	7.3525	
16.0138	22.1594	27.5365	35.9095	25.4991	4.6714	
21.0903	27.3131	32.7343	45.4642	36.5642	14.0985	
29.4753	34.2313	39.3718	54.4201	46.6327	23.0976	
38.1537	41.2238	46.1467	62.4472	55.6349	31.2485	
46.2349	47.6087	52.4462	69.3950	63.5300	38.4896	
53.4180	53.0983	57.9777	75.1900	70.2939	44.7973	
59.5822	57.5632	62.5958	79.7997	75.9154	50.1636	
64.6788	60.9488	66.2298	83.2182	80.3951	54.5921	
68.6955	63.2414	68.8520	85.4590	83.7449	58.0963	
71.6431	64.4537	70.4622	86.5513	85.9869	60.6986	
73.5486	64.6175	71.0801	86.5377	87.1530	62.4302	
74.4522	63.7793	70.7401	85.4723	87.2845	63.3299	
74.4052	61.9977	69.4888	83.4192	86.4310	63.4439	
73.4682	59.3413	67.3825	80.4512	84.6496	62.8248	
71.7102	55.8874	64.4856	76.6485	82.0045	61.5310	

69.2077	51.7207	60.8690	72.0975	78.5659	59.6264	
66.0438	46.9326	56.6090	66.8896	74.4093	57.1796	
62.3078	41.6209	51.7859	61.1196	69.6144	54.2630	
58.0954	35.8911	46.4829	54.8852	64.2650	50.9533	
53.5088	29.8601	40.7852	48.2850	58.4478	47.3308	
48.6587	23.6690	34.7789	41.4181	52.2527	43.4797	
43.6669	17.5234	28.5507	34.3829	45.7730	39.4897	
38.6724	11.8524	22.1883	27.2759	39.1075	35.4569	
33.8406	7.9908	15.7837	20.1922	32.3656	31.4878	
29.3784	8.7076	9.4549	13.2278	25.6820	27.7041	
25.5500	13.0624	3.5964	6.5035	19.2601	24.2489	
22.6767	18.4029	3.9820	1.3692	13.5181	21.2918	
21.0718	23.8163	9.5416	6.5008	9.5871	19.0211	
20.8812	29.0040	15.1235	12.2155	9.5841	17.6045	
21.9515	33.8261	20.4235	17.5115	13.1497	17.1118	
23.9073	38.1978	25.3605	22.3056	17.9740	17.4537	
26.3464	42.0600	29.8850	26.5489	22.9908	18.4098	
28.9524	45.3696	33.9604	30.2051	27.8341	19.7245	
31.5079	48.0953	37.5592	33.2472	32.3497	21.1798	
33.8708	50.2163	40.6617	35.6573	36.4575	22.6173	
35.9498	51.7206	43.2553	37.4252	40.1102	23.9318	
37.6880	52.6049	45.3345	38.5491	43.2785	25.0576	
39.0525	52.8739	46.9005	39.0344	45.9451	25.9578	
40.0275	52.5397	47.9605	38.8938	48.1022	26.6167	
40.6105	51.6217	48.5279	38.1470	49.7494	27.0343	
40.8099	50.1458	48.6215	36.8196	50.8926	27.2237	
40.6429	48.1446	48.2654	34.9433	51.5440	27.2090	
40.1343	45.6566	47.4881	32.5546	51.7205	27.0237	
39.3161	42.7264	46.3228	29.6953	51.4437	26.7097	
38.2263	39.4053	44.8063	26.4111	50.7394	26.3161	
36.9087	35.7518	42.9788	22.7521	49.6366	25.8978	
35.4123	31.8340	40.8838	18.7732	48.1674	25.5128	
33.7915	27.7351	38.5676	14.5372	46.3664	25.2190	
32.1051	23.5646	36.0792	10.1283	44.2699	25.0693	
30.4162	19.4832	33.4702	5.7328	41.9159	25.1066	
28.7906	15.7602	30.7953	2.6582	39.3435	25.3584	
27.2948	12.8810	28.1125	5.3042	36.5921	25.8344	
25.9918	11.5940	25.4841	9.8503	33.7016	26.5253	
24.9359	12.4126	22.9772	14.5856	30.7121	27.4059	

24.1655	14.9375	20.6648	19.2981	27.6631	28.4392	
23.6967	18.3866	18.6242	23.9068	24.5946	29.5816	
23.5199	22.2220	16.9327	28.3575	21.5466	30.7871	
23.6008	26.1538	15.6560	32.6061	18.5605	32.0107	
23.8862	30.0223	14.8302	36.6147	15.6812	33.2107	
24.3127	33.7306	14.4436	40.3504	12.9616	34.3495	
24.8145	37.2145	14.4327	43.7848	10.4716	35.3947	
25.3291	40.4285	14.6973	46.8939	8.3166	36.3189	
25.8017	43.3388	15.1258	49.6578	6.6667	37.0995	
26.1859	45.9205	15.6160	52.0611	5.7547	37.7189	
26.4442	48.1557	16.0852	54.0924	5.7151	38.1637	
26.5475	50.0318	16.4711	55.7444	6.3667	38.4249	
26.4741	51.5415	16.7302	57.0137	7.3666	38.4974	
26.2090	52.6816	16.8337	57.9007	8.4595	38.3799	
25.7430	53.4532	16.7650	58.4095	9.5062	38.0742	
25.0718	53.8610	16.5171	58.5474	10.4369	37.5857	
24.1954	53.9129	16.0916	58.3249	11.2171	36.9227	
23.1177	53.6200	15.4975	57.7556	11.8313	36.0963	
21.8457	52.9959	14.7510	56.8555	12.2752	35.1204	
20.3891	52.0568	13.8771	55.6431	12.5515	34.0117	
18.7599	50.8208	12.9104	54.1390	12.6685	32.7892	
16.9724	49.3080	11.8991	52.3658	12.6385	31.4747	
15.0421	47.5397	10.9093	50.3475	12.4779	30.0926	
12.9864	45.5386	10.0306	48.1096	12.2065	28.6699	
10.8240	43.3283	9.3773	45.6788	11.8482	27.2366	
8.5755	40.9330	9.0738	43.0829	11.4309	25.8251	
6.2661	38.3774	9.2166	40.3504	10.9868	24.4709	
3.9373	35.6861	9.8296	37.5111	10.5525	23.2114	
1.7579	32.8839	10.8594	34.5956	10.1683	22.0851	
1.5871	29.9952	12.2110	31.6362	9.8760	21.1294	
3.7325	27.0441	13.7879	28.6670	9.7146	20.3777	
6.0938	24.0541	15.5101	25.7257	9.7149	19.8555	
8.4629	21.0483	17.3158	22.8551	9.8933	19.5763	
10.7979	18.0495	19.1583	20.1064	10.2496	19.5394	
13.0773	15.0804	21.0016	17.5444	10.7677	19.7295	
15.2849	12.1657	22.8174	15.2542	11.4215	20.1192	
17.4077	9.3352	24.5833	13.3476	12.1798	20.6731	
19.4341	6.6374	26.2809	11.9598	13.0116	21.3524	
21.3542	4.1955	27.8950	11.2167	13.8882	22.1190	

23.1597	2.5265	29.4133	11.1672	14.7847	22.9375	
24.8435	2.9634	30.8259	11.7361	15.6801	23.7769	
26.3997	4.7996	32.1246	12.7594	16.5569	24.6106	
27.8239	6.8773	33.3032	14.0619	17.4006	25.4168	
29.1129	8.9265	34.3571	15.5043	18.1996	26.1778	
30.2645	10.8780	35.2830	16.9892	18.9446	26.8796	
31.2778	12.7061	36.0791	18.4521	19.6281	27.5114	
32.1528	14.3988	36.7449	19.8508	20.2445	28.0650	
32.8907	15.9501	37.2808	21.1579	20.7897	28.5347	
33.4935	17.3570	37.6884	22.3557	21.2607	28.9166	
33.9639	18.6189	37.9702	23.4332	21.6557	29.2087	
34.3056	19.7366	38.1295	24.3839	21.9742	29.4102	
34.5229	20.7122	38.1703	25.2047	22.2161	29.5217	
34.6206	21.5486	38.0973	25.8951	22.3824	29.5449	
34.6041	22.2498	37.9157	26.4564	22.4747	29.4820	
34.4793	22.8205	37.6313	26.8914	22.4952	29.3364	
34.2525	23.2659	37.2501	27.2040	22.4465	29.1117	
33.9300	23.5917	36.7786	27.3992	22.3319	28.8124	
33.5187	23.8041	36.2234	27.4825	22.1546	28.4429	
33.0253	23.9097	35.5912	27.4601	21.9185	28.0082	
32.4569	23.9151	34.8890	27.3385	21.6275	27.5136	
31.8205	23.8274	34.1237	27.1247	21.2858	26.9642	
31.1229	23.6535	33.3021	26.8256	20.8977	26.3655	
30.3712	23.4004	32.4311	26.4485	20.4674	25.7229	
29.5719	23.0753	31.5173	26.0004	19.9992	25.0416	
28.7317	22.6851	30.5673	25.4886	19.4976	24.3270	
27.8570	22.2367	29.5872	24.9200	18.9667	23.5842	
26.9539	21.7366	28.5833	24.3016	18.4108	22.8181	
26.0282	21.1915	27.5612	23.6400	17.8338	22.0337	
25.0856	20.6074	26.5264	22.9416	17.2398	21.2353	
24.1314	19.9905	25.4842	22.2127	16.6323	20.4274	
23.1703	19.3463	24.4393	21.4591	16.0151	19.6141	
22.2072	18.6803	23.3964	20.6863	15.3914	18.7992	
21.2463	17.9976	22.3596	19.8996	14.7644	17.9863	
20.2915	17.3028	21.3327	19.1038	14.1372	17.1787	
19.3465	16.6005	20.3192	18.3035	13.5123	16.3793	
18.4144	15.8946	19.3223	17.5029	12.8924	15.5910	
17.4983	15.1890	18.3448	16.7057	12.2798	14.8161	
16.6008	14.4870	17.3893	15.9155	11.6764	14.0569	

15.7241	13.7917	16.4578	15.1353	11.0842	13.3153	
14.8703	13.1059	15.5523	14.3681	10.5047	12.5930	
14.0410	12.4320	14.6743	13.6161	9.9396	11.8914	
13.2377	11.7722	13.8252	12.8817	9.3898	11.2117	
12.4616	11.1285	13.0060	12.1666	8.8566	10.5549	
11.7135	10.5023	12.2175	11.4725	8.3408	9.9219	
10.9941	9.8951	11.4602	10.8006	7.8431	9.3131	
10.3040	9.3079	10.7346	10.1520	7.3640	8.7289	
9.6433	8.7417	10.0407	9.5275	6.9040	8.1697	
9.0122	8.1971	9.3787	8.9278	6.4632	7.6355	
8.4107	7.6747	8.7482	8.3532	6.0418	7.1262	
7.8384	7.1746	8.1489	7.8040	5.6398	6.6417	
7.2951	6.6972	7.5805	7.2802	5.2571	6.1816	
6.7802	6.2423	7.0423	6.7818	4.8936	5.7456	
6.2932	5.8099	6.5336	6.3084	4.5489	5.3331	
5.8334	5.3997	6.0537	5.8599	4.2227	4.9437	
5.4001	5.0113	5.6018	5.4356	3.9146	4.5767	
4.9924	4.6444	5.1769	5.0351	3.6241	4.2314	
4.6096	4.2984	4.7781	4.6578	3.3507	3.9071	
4.2507	3.9728	4.4044	4.3029	3.0939	3.6030	
3.9147	3.6669	4.0549	3.9698	2.8530	3.3184	
3.6008	3.3800	3.7284	3.6576	2.6275	3.0523	
3.3078	3.1114	3.4240	3.3656	2.4167	2.8041	
3.0350	2.8605	3.1406	3.0929	2.2200	2.5729	
2.7812	2.6263	2.8771	2.8386	2.0367	2.3579	
2.5455	2.4083	2.6325	2.6019	1.8663	2.1581	
2.3270	2.2055	2.4058	2.3820	1.7080	1.9729	
2.1247	2.0172	2.1960	2.1779	1.5611	1.8014	
1.9376	1.8428	2.0021	1.9888	1.4252	1.6429	
1.7649	1.6813	1.8232	1.8139	1.2995	1.4965	
1.6057	1.5321	1.6583	1.6524	1.1835	1.3615	
1.4592	1.3944	1.5066	1.5034	1.0766	1.2373	
1.3244	1.2675	1.3672	1.3662	0.9781	1.1231	
1.2007	1.1508	1.2392	1.2401	0.8876	1.0182	
1.0874	1.0436	1.1219	1.1243	0.8046	0.9221	
0.9836	0.9453	1.0146	1.0180	0.7284	0.8341	
0.8886	0.8552	0.9165	0.9208	0.6587	0.7536	
0.8020	0.7728	0.8270	0.8318	0.5950	0.6801	
0.7230	0.6975	0.7453	0.7506	0.5368	0.6131	

0.6510	0.6289	0.6710	0.6766	0.4838	0.5521	
0.5855	0.5663	0.6034	0.6091	0.4355	0.4966	
0.5261	0.5094	0.5420	0.5478	0.3916	0.4462	
0.4721	0.4577	0.4864	0.4920	0.3517	0.4004	
0.4232	0.4107	0.4359	0.4415	0.3155	0.3590	
0.3790	0.3682	0.3903	0.3957	0.2828	0.3215	
0.3390	0.3297	0.3491	0.3542	0.2531	0.2876	
0.3029	0.2949	0.3119	0.3168	0.2264	0.2570	
0.2704	0.2635	0.2783	0.2830	0.2022	0.2294	
0.2411	0.2352	0.2481	0.2525	0.1804	0.2045	
0.2147	0.2097	0.2210	0.2251	0.1608	0.1821	
0.1910	0.1867	0.1966	0.2004	0.1431	0.1621	
0.1698	0.1661	0.1747	0.1782	0.1273	0.1440	
0.1508	0.1476	0.1551	0.1583	0.1131	0.1279	
0.1337	0.1310	0.1375	0.1405	0.1004	0.1134	
0.1185	0.1162	0.1218	0.1246	0.0890	0.1005	
0.1048	0.1029	0.1078	0.1103	0.0788	0.0889	
0.0927	0.0910	0.0953	0.0976	0.0697	0.0786	
0.0819	0.0805	0.0841	0.0863	0.0616	0.0694	
0.0722	0.0711	0.0742	0.0762	0.0544	0.0613	
0.0637	0.0627	0.0654	0.0672	0.0480	0.0540	
0.0560	0.0552	0.0576	0.0592	0.0423	0.0475	
0.0493	0.0486	0.0506	0.0521	0.0372	0.0418	
0.0433	0.0427	0.0445	0.0458	0.0327	0.0367	
0.0380	0.0375	0.0391	0.0402	0.0287	0.0323	
0.0333	0.0329	0.0342	0.0353	0.0252	0.0283	
0.0292	0.0289	0.0300	0.0309	0.0221	0.0248	
0.0256	0.0253	0.0262	0.0271	0.0193	0.0217	
0.0223	0.0221	0.0229	0.0237	0.0169	0.0190	
0.0195	0.0193	0.0200	0.0207	0.0148	0.0166	
0.0170	0.0169	0.0175	0.0181	0.0129	0.0144	
0.0148	0.0147	0.0152	0.0157	0.0112	0.0126	
0.0129	0.0128	0.0133	0.0137	0.0098	0.0110	
0.0112	0.0112	0.0115	0.0119	0.0085	0.0095	
0.0098	0.0097	0.0100	0.0104	0.0074	0.0083	
0.0085	0.0084	0.0087	0.0090	0.0064	0.0072	
0.0074	0.0073	0.0075	0.0078	0.0056	0.0062	
0.0064	0.0063	0.0065	0.0068	0.0048	0.0054	
0.0055	0.0055	0.0057	0.0059	0.0042	0.0047	

0.0048	0.0048	0.0049	0.0051	0.0036	0.0040	
0.0041	0.0041	0.0042	0.0044	0.0031	0.0035	
0.0036	0.0035	0.0036	0.0038	0.0027	0.0030	
0.0031	0.0031	0.0031	0.0033	0.0023	0.0026	
0.0026	0.0026	0.0027	0.0028	0.0020	0.0022	
0.0023	0.0023	0.0023	0.0024	0.0017	0.0019	
0.0020	0.0020	0.0020	0.0021	0.0015	0.0017	
0.0017	0.0017	0.0017	0.0018	0.0013	0.0014	
0.0014	0.0014	0.0015	0.0015	0.0011	0.0012	
0.0012	0.0012	0.0013	0.0013	0.0009	0.0010	
0.0011	0.0011	0.0011	0.0011	0.0008	0.0009	
0.0009	0.0009	0.0009	0.0010	0.0007	0.0008	
0.0008	0.0008	0.0008	0.0008	0.0006	0.0007	
0.0007	0.0007	0.0007	0.0007	0.0005	0.0006	
0.0006	0.0006	0.0006	0.0006	0.0004	0.0005	
0.0005	0.0005	0.0005	0.0005	0.0004	0.0004	
0.0004	0.0004	0.0004	0.0004	0.0003	0.0003	
0.0003	0.0004	0.0004	0.0004	0.0003	0.0003	
0.0003	0.0003	0.0003	0.0003	0.0002	0.0003	
0.0003	0.0003	0.0003	0.0003	0.0002	0.0002	
0.0002	0.0002	0.0002	0.0002	0.0002	0.0002	
0.0002	0.0002	0.0002	0.0002	0.0001	0.0002	
0.0002	0.0002	0.0002	0.0002	0.0001	0.0001	
0.0001	0.0001	0.0001	0.0001	0.0001	0.0001	
0.0001	0.0001	0.0001	0.0001	0.0001	0.0001	
0.0001	0.0001	0.0001	0.0001	0.0001	0.0001	
0.0001	0.0001	0.0001	0.0001	0.0001	0.0001	
0.0001	0.0001	0.0001	0.0001	0.0001	0.0001	
0.0001	0.0001	0.0001	0.0001	0.0000	0.0000	
0.0000	0.0000	0.0000	0.0001	0.0000	0.0000	
0.0000	0.0000	0.0000	0.0000	0.0000	0.0000	
0.0000	0.0000	0.0000	0.0000	0.0000	0.0000	
0.0000	0.0000	0.0000	0.0000	0.0000	0.0000	
0.0000	0.0000	0.0000	0.0000	0.0000	0.0000	
0.0000	0.0000	0.0000	0.0000	0.0000	0.0000	
0.0000	0.0000	0.0000	0.0000	0.0000	0.0000	
0.0000	0.0000	0.0000	0.0000	0.0000	0.0000	
0.0000	0.0000	0.0000	0.0000	0.0000	0.0000	
0.0000	0.0000	0.0000	0.0000	0.0000	0.0000	

0.0000	0.0000	0.0000	0.0000	0.0000	0.0000	
0.0000	0.0000	0.0000	0.0000	0.0000	0.0000	
0.0000	0.0000	0.0000	0.0000	0.0000	0.0000	
0.0000	0.0000	0.0000	0.0000	0.0000	0.0000	
0.0000	0.0000	0.0000	0.0000	0.0000	0.0000	
0.0000	0.0000	0.0000	0.0000	0.0000	0.0000	
0.0000	0.0000	0.0000	0.0000	0.0000	0.0000	
0.0000	0.0000	0.0000	0.0000	0.0000	0.0000	
0.0000	0.0000	0.0000	0.0000	0.0000	0.0000	
0.0000	0.0000	0.0000	0.0000	0.0000	0.0000	
0.0000	0.0000	0.0000	0.0000	0.0000	0.0000	
0.0000	0.0000	0.0000	0.0000	0.0000	0.0000	
0.0000	0.0000	0.0000	0.0000	0.0000	0.0000	
0.0000	0.0000	0.0000	0.0000	0.0000	0.0000	
0.0000	0.0000	0.0000	0.0000	0.0000	0.0000	
0.0000	0.0000	0.0000	0.0000	0.0000	0.0000	
0.0000	0.0000	0.0000	0.0000	0.0000	0.0000	
0.0000	0.0000	0.0000	0.0000	0.0000	0.0000	
0.0000	0.0000	0.0000	0.0000	0.0000	0.0000	
0.0000	0.0000	0.0000	0.0000	0.0000	0.0000	
0.0000	0.0000	0.0000	0.0000	0.0000	0.0000	
0.0000	0.0000	0.0000	0.0000	0.0000	0.0000	
0.0000	0.0000	0.0000	0.0000	0.0000	0.0000	
0.0000	0.0000	0.0000	0.0000	0.0000	0.0000	
0.0000	0.0000	0.0000	0.0000	0.0000	0.0000	
0.0000	0.0000	0.0000	0.0000	0.0000	0.0000	

APPENDIX D

YULE-WALKER SUBROUTINE

```
function [dfac,freq,H_hat,ff,a_hat,y_hat] = YW(y,v,order,fs)
%
dt = 1/fs;
y = detrend(y,'constant');



M = order;

%Lag_m = M;
r = [];

R = xcorr(y,y,M,'biased');

N = length(y);
r=zeros(M+1,1);
for i = 0 : M,
   r(i+1)=y(1:N-i)'*y(i+1:N)/N;
end

a_hat = levinson(r,M);
H_hat = freqz(1,a_hat);

ff = (0:1:length(H_hat)-1)*(1/(2*dt*length(H_hat)));

%lp = [1 a_hat];
lp = a_hat;
rLP = roots(lp);  % calculate the roots of the lp.


dfac = log(abs(rLP))/dt;
a = imag(rLP);
b = real(rLP);
freq = atan(a./b)/(2*pi*dt);

y_hat = zeros(1,(2*length(v)+order));
end
```